Performance Enhancement and Load Reduction on Wind Turbines Using Inflow Measurements

Kragh, Knud Abildgaard

Publication date:
2013

Document Version
Publisher's PDF, also known as Version of record

Performance Enhancement and Load Reduction on Wind Turbines Using Inflow Measurements

DTU Vindenergi
Report 2013

Knud Abildgaard Kragh

DTU Wind Energy PhD-0014 (EN)

ISBN: 978-87-92896-37-7

June 2013

DTU Vindenergi
Institut for Vindenergi

Author: Knud Abildgaard Kragh
Title: Performance enhancement and load reduction on wind turbines using inflow measurements

June 2013

Pages:175
Tables: 3
References: 43

Technical University of Denmark

www.vindenergi.dtu.dk

Performance enhancement and load reduction on wind turbines using inflow measurements

Knud Abildgaard Kragh

Roskilde 2013

Technical University of Denmark
Department of Wind Energy
Building 118, DK-4000 Roskilde, Denmark
Phone +45 4677 50853
info@vindenergi.dtu.dk
www.vindenergi.dtu.dk

Summary

Wind energy is being applied at a larger and larger scale worldwide, and is one of the technologies eligible for accommodating the increasing demand for renewable energy. However, wind energy is still not competitive compared to technologies that are based on fossil energy sources. Therefore, much wind energy research is focused on decreasing the cost of the energy that can be produced from the wind. The cost of energy can for example be decreased by ensuring that wind turbines are operated in a way that ensures that the maximum amount of energy is extracted, and that the turbines are not loaded excessively.

The operation of a wind turbine is governed by a number of controllers that are based on a series of sensors and actuators. Classical wind turbine control utilizes sensors for measuring turbine parameters such as rotor speed, power and shaft torque, as well as actuators for applying generator torque and collective pitch angle changes. Thus, classical wind turbine control schemes are based on measurements of the effects of the inflow on the turbine. Therefore, the reactions of the control system to the inflow changes are inherently delayed compared to the actual inflow changes. Because of the inherent delay of the control system, the ability of the system to react promptly to inflow changes is limited.

Control schemes that are based on inflow measurements have been developed to overcome the limitations of the classical wind turbine control system. By measuring the inflow directly, actuation can be initiated instantly as the inflow changes. If the inflow is measured upstream of the turbine, actuation can be initiated prior to the occurrence of a wind speed change at the turbine. Hereby, even the actuator delay can be compensated for. Upstream inflow measurements could for example be acquired using "Light Detection and Ranging".

In this thesis, the potentials for improving the power production and decreasing the load variations of horizontal axis upwind turbines by applying inflow measurement based control are assessed. The potential for increasing the power output through improved yaw alignment is studied by analyzing operational data from different turbines, and through experiments with a modified yaw controller. The results demonstrate that there is no significant potential for increased power output through improved yaw alignment for well calibrated turbines. The potential for increasing the power output through pitch control is studied through optimization of collective and individual pitch actuation. The results show that there is a potential for increasing the power output through individual pitch control. However, the increased power output is penalized by increased load variations.

The load variations on a wind turbine can be alleviated using either yaw or pitch actuation. A method is presented for alleviating load variations using yaw control, and it is shown how the method can be efficiently applied for decreasing the load variations that are caused by a vertical wind shear. The potential of reducing the load variations using both inflow measurement based collective and individual pitch control is studied through simulations. The results demonstrate that tower and blade load variations can be efficiently alleviated in situations with large scale inflow variations using collective pitch control. For individual pitch control, it is demonstrated that control based on upstream inflow measurements can lead to great load reductions in certain situations. However, it is also shown that the potential load variation reductions are sensitive to uncertainties relating to the estimated inflow.

This thesis is comprised of a collection of scientific papers that covers the various results presented in this summary.

Resumé

Vindenergi installeres i stadig større omfang på verdensplan og er en af de teknologier, der skal være med til at tilfredsstille den stigende efterspørgelse på bæredygtig energi. Vindenergi er dog stadig ikke konkurrencedygtig i forhold til teknologier, der er baseret på fossile energikilder. Derfor er en stor del af vindenergiforskningen fokuseret på at nedbringe prisen på at producere energi fra vind. Prisen for den producerede energi kan f.eks. reduceres ved at sikre, at vindmøller styres således, at der altid produceres den højest mulige effekt, og at møllen ikke belastes unødigt.

Klassisk vindmøllestyring er baseret på målinger af rotorhastighed og effekt, samt regulering af generatormoment og den kollektive pitchvinkel. Da kun effekterne af indstrømningsfeltet på møllen måles, vil styringen reagere med en forsinkelse sammenlignet med ændringer i indstrømningsfeltet. Denne forsinkelse begrænser systemets mulighed for at maksimere energiproduktionen og begrænse lastvariationerne.

For at eliminere begrænsningerne ved klassisk vindmøllestyring er der udviklet styringsalgoritmer, som er baseret på målinger af indstrømningsfeltet. Ved at måle indstrømningsfeltet direkte kan styringen reagere øjeblikkeligt i takt med at indstrømningsfeltet forandres. Hvis indstrømningsfeltet måles opstrøms for møllen, kan aktuering påbegyndes inden indstrømningsfeltet ændrer sig. Herved kan der kompenseres for forsinkelser i aktuatorerne. Indstrømningsfeltet kunne f.eks. måles ved brug af "Light Detection and Ranging".

I denne afhandling undersøges potentialet for at forøge energiproduktionen og reducere lastvariationerne på en vindmølle ved brug af målinger af indstrømningsfeltet. Potentialet for at øge energiproduktionen ved forbedret krøjestyring undersøges

gennem analyse af driftsdata og gennem eksperimenter med en modificeret krøjestyring på en testmølle. Resultaterne viser, at potentialet er meget begrænset for en velkalibreret mølle. Potentialet for forøget energiproduktion ved pitchstyring er undersøgt gennem optimeringsstudier af både individuel og kollektiv pitchstyring. Resultaterne viser, at der er et potentiale for at forøge energiproduktionen ved individuel pitchstyring. Den forøgede energiproduktion medfører dog forøgede lastvariationer.

Lastvariationer på en vindmølle kan reduceres gennem både pitch- og krøjestyring. En metode er introduceret, som ved brug af krøjestyring kan reducere de lastvariationer, der skyldes en vertikal vindhastighedsgradient. Potentialet for lastreduktion ved brug af både kollektiv og individuel pitchstyring baseret på målinger af indstrømningsfeltet er undersøgt gennem simuleringer. Resultaterne viser, at tårn- og bladlastvariationer, som skyldes middelændringer i indstrømningsfeltet, kan reduceres ved brug af kollektiv pitchstyring. For individuel pitchstyring er det vist, at styring baseret på målinger af indstrømningsfeltet kan lede til store lastreduktioner. Det er dog også vist, at lastreduktionerne er følsomme over for usikkerheder relateret til estimeringen af indstrømningsfeltet.

Denne afhandling indeholder et antal videnskabelige artikler, der beskriver de introducerede resultater.

Preface

This thesis was prepared at the department of wind energy at the Technical University of Denmark during the period from Marts 2010 to February 2013 in partial fulfillment of the requirements for acquiring the Ph.D. degree in engineering. The work has been supervised by Senior Scientist Morten H. Hansen, and co-supervised by Senior Scientist Torben J. Larsen and Professor Torben Mikkelsen all from the department of Wind Energy at DTU. The project has been founded by DTU Wind Energy and by the HTF project entitled *Integration of wind LIDAR's in wind turbines for improved productivity and control* (HTF number 049-2009-3). The thesis consists of a summary report and a collection of seven research papers written during the period 2010–2013, and elsewhere published.

Roskilde, February 2013

Knud Abildgaard Kragh

Papers included in the thesis

[A] Knud A. Kragh, Morten H. Hansen and Torben Mikkelsen Precision and Shortcomings of Yaw Error Estimation Using Spinner-based Light Detection and Ranging. *Wind Energy*, 2012.

[B] Knud A. Kragh and Morten H. Hansen Potential of Power Gain with Improved Yaw Alignment. *Wind Energy*, (Submitted).

[C] Knud A. Kragh, Paul A. Fleming and Andrew Scholbrock Increased Power Capture by Rotor Speed Dependent Yaw Control of Wind Turbines. *Journal of Solar Energy Engineering*, (Accepted).

[D] Knud A. Kragh and Morten H. Hansen Load Alleviation of Wind Turbines by Yaw Misalignment. *Wind Energy*, (Accepted).

[E] Knud A. Kragh, Morten H. Hansen and Lars C. Henriksen Sensor Comparison Study for Load Alleviating Wind Turbine Pitch Control. *Wind Energy*, (Submitted).

[F] Knud A. Kragh and Morten H. Hansen Individual Pitch Control Based on Local and Upstream Inflow Measurements. *50th AIAA Aerospace Sciences Meeting including the New Horizons Forum and Aerospace Exposition*, 2012.

[G] Knud A. Kragh, Lars C. Henriksen and Morten H. Hansen On the Potential of Pitch Control for Increased Power Capture and Load Alleviation. *In the Proceedings of The Science of Making Torque From Wind*, 2012.

Acknowledgements

I am grateful to all of my supervisors for their invaluable advise and our discussions regarding both wind turbine modeling, measurement technologies and control design. I also wish to thank my colleagues at DTU Wind Energy for always taking time to help out, especially Lars C. Henriksen for his valuable inputs regarding control design and numerical optimization.

Furthermore, I wish to thank Alan Wright and Paul A. Fleming from the National Renewable Energy Laboratory in Boulder, Colorado, for their hospitality during my stay there. I gained at lot of knowledge and experience during the visit, and I am glad that we have been able to publish results together and continue our collaboration.

Finally, I wish to thank my wife Line for her invaluable and consistent support during the Ph.D. studies.

Contents

Nomenclature

$\bar{\Omega}$	Average steady state rotor speed.
$\bar{V_0}$	Average free wind speed.
$\bar{V_0}$	The estimated transport velocity of the LiDAR measurements.
ΔM_{ff}	Range of steady state tower bottom fore-aft bending moment variations.
ΔM_{in}	Range of steady state blade root in-plane bending moment variations.
ΔM_{out}	Range of steady state blade root out-of-plane bending moment variations.
ΔM_{ss}	Range of steady state tower bottom side-side bending moment variations.
ΔM_{tilt}	Range of steady state tilt moment variations.
ΔM_{yaw}	Range of steady state yaw moment variations.
ΔT_d	Time shift of preview time.
δ	Estimation error of LiDAR measurement transport velocity.
λ	Tip speed ration.
λ^*	Optimal tip speed ratio of the rotor.
Ω	Rotor speed.
ψ	Rotor azimuth angle.
ψ_i	Azimuth angle of blade i.

ρ Density of the air.

τ Preview time.

$\mathbf{u}$ Vector containing optimization variables.

θ_a Azimuth angle of LiDAR sensor beam.

θ_c Cone angle of LiDAR sensor beam (angle between rotor axis and LiDAR sensor beam).

θ_p^i Pitch angle of blade i.

θ_E Yaw error.

θ_p Pitch angle.

$\tilde{\tau}$ Preview time with uncertainty.

$\tilde{M}_{out}$ High-pass filtered blade root out-of-plane bending moment.

$\tilde{P}$ Power available from the wind when a yaw error is present.

$\tilde{T}_d$ Transport time of LiDAR measurements with estimation uncertainty.

$\widetilde{\Delta M_{out}}$ Range of steady state blade root out-of-plane bending variations normalized with range at zero yaw error.

A_r Rotor area.

C_p Power coefficient.

C_p^{max} Maximum power coefficient of the rotor.

F_L Focal distance of LiDAR sensor.

F_L^n n'th focal distance of LiDAR sensor (for pulsed LiDAR sensor).

F_s Sampling frequency.

I Turbulence intensity.

k Gain of generator torque controller.

L_p Distance from the LiDAR sensor measurement pattern to the rotor.

M_{ff} Tower bottom fore-aft bending moment.

M_{in} Blade root in-plane bending moment.

M_{out} Blade root out-of-plane bending moment.

M_{ss} Tower bottom side-side bending moment.

M_{tilt} Tilting moment.

M_{yaw} Yawing moment.

P Power output of the turbine.

P_r Rated power of the turbine.

$P_{loss}(\theta_E)$ Power loss due a yaw error.

P_{max} Maximum available power from the wind.

Q_g Generator torque.

R Radius of the rotor.

T Integration time.

t Time.

T_d Time from the LiDAR sensor measures a wind speed till it reaches the rotor.

V_0 Free wind speed.

$V_L(\theta_a, \theta_c, F_L)$ Lidar wind speed measurement as a function of, azimuth angle, cone angle, and focal distance.

V_p Wind speed perpendicular to the rotor.

Chapter 1

Introduction

One of the defining factors for the design of a wind turbine is the load variations that the turbine should be able to endure during its life time. These load variations depend on the inflow to the turbine, in particular the variations of the inflow. The magnitude of the inflow variations in the area that is swept by the rotor of a wind turbine increases with increasing rotor size. Thus, the potential load variations increase in magnitude with increasing rotor size. The increasing load variations can either be absorbed by increasing the strength of the turbine, and thereby increasing the cost of the turbine, or by introducing intelligent operation of the turbine through control schemes that reduce load variations. Another defining factor for the design is the ability of the turbine to extract the maximum amount of energy from the wind. The power capturing capabilities of a turbine is determined by the aerodynamic design of the rotor, and the control systems ability to keep the turbine at an optimal operating state. Hence, the control system is vital to the performance of a wind turbine.

Classical wind turbine control is limited to speed and power/torque regulation, and has limited abilities to alleviate the varying loads and maximize the power production. Therefore, a need for controllers that enable load alleviation and power maximization is emerging as the size of wind turbines is increasing to accommodate the increasing demand of renewable energy. Such controllers can be based on various sensors and control concepts. This thesis is focused on assessing the potential of inflow measurement based control for load alleviation

and increased power capture of horizontal axis upwind turbines.

This chapter contains a brief introduction to classical control of horizontal axis upwind turbines, an overview of the state of the art of wind turbine control, an overview of the potential benefits of inflow measurement based control, and a description of the scope of the thesis.

1.1 Classical Wind Turbine Control

The control system of a wind turbine consists of three main components that are each responsible for different tasks related to the operation of a wind turbine: a supervisory controller, a safety system, and the closed loop controllers.

The *supervisory controller* is responsible for the overall operation of the turbine, and for bringing the turbine from one operational state to another. For example, it is the responsibility of the supervisory controller to bring the turbine from a standby to a power producing operational state, when the wind speed increases from below to above the cut-in wind speed. This transition involves a controlled start-up of the turbine that includes powering up the actuators, disengaging the shaft brake, pitching to a certain value, waiting for the rotor speed to increase etc. The supervisory controller is also responsible for shutting down the turbine and bringing it to a safe state in case of an abnormal event such as extreme winds, loss of electrical power, or other types of failures that can be detected by the controller.

The role of the *safety system* is to take over, and ensure a safe operation of the wind turbine when the supervisory controller is incapable of doing so. Thus, the safety system acts as a redundant system that takes over in case of failure of the main system. The safety system is designed to be independent of the main control system, fail-safe, highly reliable, and based on hard-wired circuits.

The objective of the *closed loop controllers* depends on the operational state of the wind turbine, which can be divided into two operational domains: below and above the rated wind speed. The rated wind speed is the wind speed at which the rotor produces an aerodynamic torque that matches the rated torque of the generator. At below rated wind speeds, the objective of the closed loop controllers is to maximize the power output, while the objective is to keep the power or generator torque constant and limit the rotor speed at above rated wind speeds.

Different strategies can be applied for achieving the objectives of the closed loop

controllers, but the most common strategy of modern turbines is variable speed and pitch to feather control. The following description applies to this type of turbine. For information related to other types of turbines c.f. [1].

The control of a variable speed and pitch regulated turbine involves yaw, collective pitch, and generator torque actuation. *Yaw actuation* is applied to ensure that the rotor is perpendicular to the mean wind direction at all times. Yaw control usually relies on feed-back from a measurement of the inflow direction relative to the rotor axis. Such a measurement is usually acquired using a transducer that is located atop of the nacelle. Due to the large forces that are required for changing the yaw direction, the yaw controller is usually a dead-band controller that only applies actuation when the turbine has been misaligned for a certain amount of time. Hence, the yaw controller is usually a slow acting system. An example of a yaw controller is given in Appendix C.

Collective pitch and *generator torque actuation* are applied for regulating the rotor speed. For below rated operation, the objective of the speed regulation is to ensure that the rotor speed is kept at the value that yields the highest possible power output. The maximum power output is achieved by ensuring that the turbine operates at the optimal pitch angle and tip speed ratio. The pitch is kept constant at its optimal value (fine pitch) for below rated operation, whereas the tip speed ratio is kept at its optimal value by regulating the generator torque and hereby the rotor speed. The generator torque can i.e. be specified by the following control law [1]:

$$Q_g = k\Omega^2, \qquad \text{where} \qquad k = \frac{1}{2}\rho\pi R^5 \frac{C_p^{max}}{\lambda^*}, \tag{1.1}$$

ρ is the density of the air, R is the radius of the rotor, C_p^{max} is the maximum power coefficient, and λ^* is the optimal tip speed ratio. Thus, the gain of the torque controller can be calculated from the performance characteristics of the rotor.

At above rated wind speeds, the role of the speed controller is to regulate the rotor speed to yield either constant power or constant torque. The rotor speed can be efficiently regulated by changing the aerodynamic torque through pitching of the turbine blades. The above rated rotor speed control is traditionally implemented as proportion-integral-derivative (PID) control of the collective pitch angle. More elaborate descriptions of classical control schemes for wind turbines can be found in various publications, i.e. [1, 2].

1.2 State of the Art Wind Turbine Control

The traditional wind turbine control strategy does not guarantee optimal power capture nor does it ensure that the load variations on the turbine are minimized. Increasing the power capture and alleviation of the varying loads on turbines are active research topics. In the following, the state of the art of power maximization and load alleviation using pitch and yaw control is presented.

1.2.1 Emerging Sensor Technologies

Recently developed control schemes for wind turbines have transpired on the basis of innovations within different measurement technologies. Especially technologies for measuring the inflow to a turbine, such as pitot tubes, advanced anemometers and LiDAR sensors, have lead to new control concepts.

Pitot tubes can be used for measuring the local inflow to a blade section. The application of pitot tubes on wind turbine blades was successfully demonstrated in the DANAERO experiment [3]. Measuring the local inflow allows for fast detection of inflow disturbances because the wind disturbance is only filtered by the inflow dynamics before it is measured.

Improved on-turbine wind speed and direction measurements have also been developed. For example, the spinner anemometer that relies on three sonic anemometers that are placed on the spinner. Using the measurements from the anemometers and careful calibration based on computational fluid dynamics (CFD) the inflow speed and direction can be estimated [4].

Finally, numerous studies have shown that light detection and ranging (LiDAR) sensors can be used for measuring the inflow to a turbine [5, 6, 7, 8, 9, 10], and control based on LiDAR sensors is a very active research area. Two types of LiDAR sensors have been suggested for inflow estimation: pulsed and continuous wave LiDAR. The fundamental differences between a pulsed and a continuous wave LiDAR sensor are described in [11], and can be summarized as:

- A continuous wave LiDAR sensor emits a focused and continuous laser beam, and measures the returning light in short intervals. A pulsed LiDAR sensor emits short pulses of laser light and measures the returning light at different times after the emission time, which corresponds to measuring the wind speed at different distances (ranges) in front of the LiDAR sensor.

- A continuous wave LiDAR sensor is generally capable of providing a much higher sampling speed than a pulsed LiDAR sensor.
- The averaging volume of a continuous wave LiDAR sensor depends on the focal distance, whereas the averaging volume of a pulsed LiDAR sensor is constant.
- A continuous wave LiDAR sensor only measures the wind speed at one distance in front of the lens. A pulsed LiDAR sensor samples wind speeds at different distances in front of the lens simultaneously.

The LiDAR sensor setups that have been suggested for wind turbine control applications vary, but the general concepts of the LiDAR sensors for wind turbine control are illustrated in Figure 1.1. With the pulsed LiDAR sensor, measurements are sampled from scaled versions of the scanning pattern at multiple distances upwind of the LiDAR sensor. The continuous wave LiDAR sensor only provides measurements from a scan pattern at one distance. Both types of LiDAR sensors provide a preview of the incoming wind speeds, which might prove useful in wind turbine control systems.

1.2.2 Power Maximizing Control

A primary condition for maximizing the power output of a horizontal axis wind turbine is that the rotor is positioned perpendicular to the mean wind direction, which is the responsibility of the yaw controller. In recent studies, inflow sensors have been used for characterizing the performance of the yaw alignment system

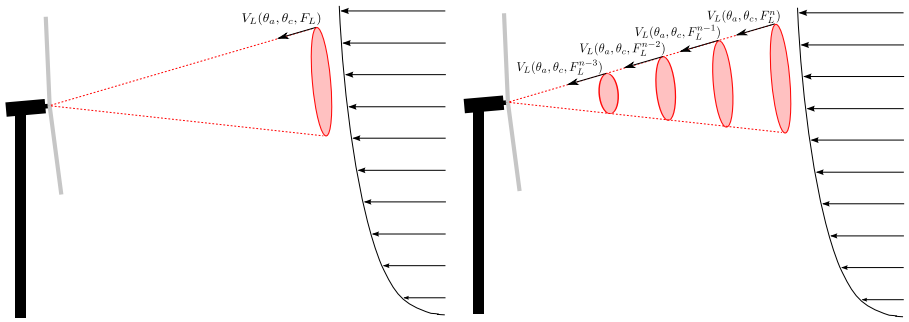

Figure 1.1: Illustration of LiDAR sensor setups for wind turbine control applications. a) Continuous wave LiDAR sensor, b) Pulsed LiDAR sensor.

of different turbines. In [7, 8, 12], measurements from a spinner mounted continuous wave LiDAR sensor are used to estimate the yaw error of an operating onshore 2 MW turbine. The results indicate that this particular turbine is operating with a mean yaw error that is varying around approximately 10 deg. In [4], a spinner anemometer is used for estimating the yaw error of a 3.6 MW onshore turbine. The results show that the turbine is operating with a mean yaw error around 10 deg in the measured wind speed range, and that the variance of the yaw error is dependent on the wind speed. In [13], a nacelle mounted pulsed LiDAR sensor is used for estimating the yaw error of a well calibrated onshore prototype turbine. The mean yaw error of this particular turbine is close to zero. In [6], the mean yaw error of several turbines are measured using LiDAR sensor systems, and mean yaw errors from 12-15 deg are observed.

Different control schemes have been suggested for eliminating the yaw error that is observed for some turbines. In [6], it is suggested to use measurements from a simple LiDAR sensor as input to the yaw control system. It is shown through experiments that the yaw error of different turbines can be kept close to zero, and the power production thereby is increased. In [4], the use of a spinner anemometer is suggested for yaw control.

Pitch and torque control can also be applied for maximizing the power output of a turbine. In [14], three different improvements of the conventional control scheme are suggested; simple gain modification, optimally tracking rotor control, and adaptive control. Power improvements of 0.5%-1% are shown through simulation studies for the simple gain modification, and for the optimally tracking rotor control algorithm. However, power improvements of 5%-14% are observed from an experiment with the adaptive controller implemented on a 600 kW turbine. In [15], simulation studies show that the power output of a turbine that is operating with a conventional speed controller can be significantly increased by using a nonlinear dynamic state feedback controller with estimation of wind speed and aerodynamic torque. The results show that a power increased of 18% can be achieved by applying the nonlinear dynamic state feedback controller compared to a baseline controller. In [13], the prospects of power optimization by LiDAR sensor assisted torque control are investigated. A method for direct speed control is suggested that is based on adding a feed-forward term to the standard $k\Omega^2$ indirect speed controller. Simulation results show that the method enables efficient tracking of the optimal tip-speed ratio, but the resulting power increase is small.

1.2.3 Load Alleviation

Alleviation of load variations can be achieved using yaw, generator torque, pitch or aerodynamic control surface (flaps, microtaps etc) actuation. This thesis only covers yaw and pitch actuation. A review of control based on aerodynamic control surface actuation can be found in [16].

Pitch control can be divided into two categories: collective pitch and individual pitch control. *Collective pitch control* can be used for alleviating thrust variations that cause load variations on both the blades and the tower. In [17], it is suggested to use measurements of the tower top accelerations as input to a feed-back collective pitch controller, and a feed-back tower damping scheme is tested experimentally in [18]. The experimental results show that the load variations can be significantly reduced by applying the tower damping. The tower top accelerations are the results of the wind speed variations. Because of the dynamics of the turbine, the measured accelerations have a phase delay compared to the wind speed variations. Therefore, control schemes that are based on feed-back of acceleration measurements have an inherent time delay. Using feed-forward of the incoming inflow to the collective pitch control has the potential of drastically decreasing the oscillations and loads. In [18], a feed-forward collective pitch control scheme is suggested that efficiently alleviates load variations that are caused by mean wind speed changes. The performance of a preview collective pitch controller based on measurement from a nacelle mounted pulsed LiDAR sensor is demonstrated experimentally in [9]. It is shown that the low frequent load variations are decreased by the preview controller. In [19], a collective pitch feed-forward approach is tested in combination with individual pitch through simulations. Fatigue load reductions of 5-15% are observed compared to a feed-back only controller. Advanced model predictive controllers have also been developed for load alleviating collective pitch control [20]. The results show load reductions up to 50% for extreme gusts and 30% for lifetime fatigue loads without negative impact on overall energy production

Individual pitch control offers the possibility of reducing the load variations that are caused by the inflow variations within the rotor plane. Several control schemes have been suggested that are based on the Coleman or l-q transform of e.g. blade root bending load measurements, [21, 22, 23]. Experimental results presented in [18] show that the once-per-revolution (1P) blade loads can be efficiently decreased using a cyclic pitch control design based on the Coleman transform. A different approach is suggested in [24], using measurements of the local inflow to a section of the blade as input to an individual pitch controller. Simulated results show that the inflow based controller yields a better alleviation of the extreme loads than a cyclic pitch controller based on blade root bending moments. Using preview measurements for individual pitch control

have also been suggested in several studies. In [25], it is shown that using LiDAR measurements as inputs to a disturbance accommodating controller yields larger load reductions than when structural measurements are applied. In [19], an individual pitch gain-scheduled shaped compensator is tested with perfect upstream inflow measurements as input. The results show that the tower and blade load variations can be decreased using the suggested controller if a preview of three to five seconds is available. In [26], a cyclic pitch design based on preview measurements from a spinner mounted LiDAR is suggested and the simulated performance of the suggested controller is compared to two feed-back only controllers. The comparison shows that the suggested preview controller yields slightly larger load reductions than the baseline controllers. In [27], a model predictive controller is implemented based on simulated LiDAR measurements. Simulations show significant load reductions compared to a baseline individual pitch controller. In [28], simulations show that the advantages of using preview control based on LiDAR measurements diminish if non-perfect LiDAR measurements are used as input.

1.3 Motivation

Feed-back only control systems are based on sensors that either measure the response of the turbine to a disturbance, such as a wind speed change, or the wind speed behind the rotor. Thus, the conventional measurement suite is only able to measure the effect of a disturbance. Therefore, feed-back control is inherently delayed by the aero- and structural dynamics by which the disturbance is filtered before it is measured by the sensors. Furthermore, the reaction to the disturbance is delayed by the actuator dynamics. Inflow measurements have the potential of eliminating the delay in the measurement system, thus, allowing direct measurements of the disturbances. If the inflow is measured upstream of the turbine, the preview of the inflow can even aid in compensating for the delay that is caused by the actuator dynamics. Thus, including measurements of the inflow in the control system can potentially improve the performance of the turbine by increasing the power output and reducing the loads. This has also been indicated in different studies, see the previous section. Some of the potential benefits of applying inflow measurement based control are listed below.

- Supervisory control
  - A system for measuring the wind speed and direction upstream of the turbine would enable detection of a sudden rise in wind speed from below cut-in to above cut-in before the wind speed change reaches

the turbine. Hereby, start-up of the wind turbine can be initiated earlier to ensure an earlier start of energy extraction.

  - A system for measuring the wind speed and direction upstream of the turbine would enable detection of an extreme inflow change before the inflow change reaches the turbine. Hereby, the extreme loads can be lowered by bringing the turbine to a safe state prior to the occurrence of the extreme event at the turbine.

- Closed loop control

  - Upstream measurements of the inflow directions could be applied in the yaw control system to ensure that the turbine operates with optimal yaw alignment, which could lead to optimal conditions for power extraction and reduce the load variations.
  - Preview knowledge of the incoming mean/rotor effective wind speed combined with feed-forward collective pitch control could lead to increased power capture by optimal Cp-tracking.
  - Preview knowledge of the incoming mean/rotor effective wind speed combined with feed-forward collective pitch control could lead to reduced tower motion and load variations.
  - Detailed knowledge of the inflow field combined with individual pitch control could lead to individual pitch actuation that is optimized for maximizing the power capture.
  - Detailed knowledge of the inflow field combined with individual pitch control could lead to decreased load variations in situations with azimuth dependent inflow.

Many of the existing studies on inflow measurement based control are focused on the development of one specific controller that is based on one specific technology, and aimed at one specific task (maximizing power, minimizing specific load variations etc). Thus, only the potential benefits of that particular application are explored. In this thesis the overall potential of inflow measurement based control is assessed by exploring the potential of load alleviation and power maximization based on different types of inflow measurements.

1.4 This Thesis

The objective of this thesis is to study the potential benefits and challenges of applying inflow measurements in wind turbine control systems. The study is limited to assessing the potential of improving the yaw and pitch control. The

potential benefits of applying inflow measurements in a wind turbine control system are divided into two categories:

1. Increased power production
2. Decreased load variations

Each benefit can be achieved using either improved pitch or yaw control. At below rated wind speeds, the focus is on increased power production, whereas the focus is on decreasing the load variations at above rated wind speeds. The thesis contains a summary of the results that were achieved during the thesis work, as well as overall discussions of the results and results that have be published by others. The scientific results of the thesis work are documented in the research papers that are included in Appendix A - G.

The main contributions of this thesis are:

- A method for estimating the yaw error of a wind turbine using measurements from a spinner mounted LiDAR. Presented in Appendix A
- A study of the yaw tracking performance of an operating offshore turbine during a three year period. Presented in Appendix B
- A method for improving the yaw tracking performance of a turbine using the conventional transducers. Presented in Appendix C
- A method for decreasing blade load variations through yaw control. Presented in Appendix D
- Suggestions for control schemes based on measurements from different types of inflow sensors. Presented in Appendix E and F
- An optimization study for assessing the potential of increased turbine performance through pitch and torque actuation independent of control design. Presented in Appendix G
- A summary of the uncertainties of applying inflow measurement based control of wind turbines

The thesis is divided into two main chapters that summarize the achieved results. First, the potential of increasing the power production is discussed, then the potential of decreasing the load variations is discussed. After the main chapters, the thesis contains a discussion of the achieved results, and conclusions relating to the potential of including inflow measurements in the wind turbine control systems, as well as suggestions for further work.

Chapter 2

Increased Power Production

To assess the potential of increasing the power production of a wind turbine by introducing inflow measurements and more sophisticated control systems, it is useful to understand the potential causes of power loss. The potential causes of power loss of a traditional wind turbine control system are the topic of the first section of this chapter. The potential of improving the power capture through yaw and pitch control, respectively, are the topics of the remaining two sections of the chapter. The focus of this chapter is solely on below rated operation, because the power output cannot be increased for a turbine that is operating above the rated wind speed.

2.1 Causes of Power Loss

The power output of a wind turbine that is operating in a uniform inflow is defined as [1, 29]:

$$P = \frac{1}{2}\rho A_r V_p^3 C_p(\lambda, \theta_p), \tag{2.1}$$

where ρ is the density of the air, A_r is the swept area of the rotor, V_p is the wind speed perpendicular to the rotor, C_p is the power coefficient, λ is the tip speed ratio, and θ_p is the collective pitch angle. In uniform inflow, a wind turbine is producing its maximum power when V_p is equal to the free wind speed V_0, and

$$C_p = \max_{\lambda,\theta_p}(C_p(\lambda,\theta_p)). \tag{2.2}$$

Hence, power loss can be caused by operation where $V_p < V_0$ and $C_p(\lambda,\theta_p) < \max_{\lambda,\theta_p}(C_p(\lambda,\theta_p))$.

If the rotor axis of a turbine is not aligned with the free wind direction, the wind speed perpendicular to the rotor plane is reduced to:

$$V_p = V_0 \cos(\theta_E), \tag{2.3}$$

where θ_E is the magnitude of the misalignment, which is referred to as the yaw error of the turbine. Hence, the maximum amount of power that can be extracted by a turbine that is operating with a yaw error θ_E is reduced to:

$$\tilde{P} = \frac{1}{2}\rho A_r (V_0 \cos(\theta_E))^3 C_p(\lambda,\theta_p). \tag{2.4}$$

Thus, the extractable power is reduced by a factor of $\cos^3(\theta_E)$. Experimental results, however, suggest that the actual reduction is slightly less [30, 31], due to changes in the induced velocities of the yawed wake.

The power coefficient of a wind turbine depends on the aerodynamic design, and the shape of the C_p-surface differs from turbine to turbine. For illustration, the C_p-surface of the NREL 5 MW reference turbine is shown in Figure 2.1. The C_p is calculated using blade element momentum (BEM) theory, and assuming that the turbine is stiff and that the inflow to the turbine is uniform and perpendicular to the rotor.

From Figure 2.1, it is evident that the maximum power coefficient for this particular turbine is achieved when the turbine is operating at a pitch angle of $\theta = -0.9$ deg and a tip speed ratio of $\lambda = 7.8$. Thus, optimal power extraction

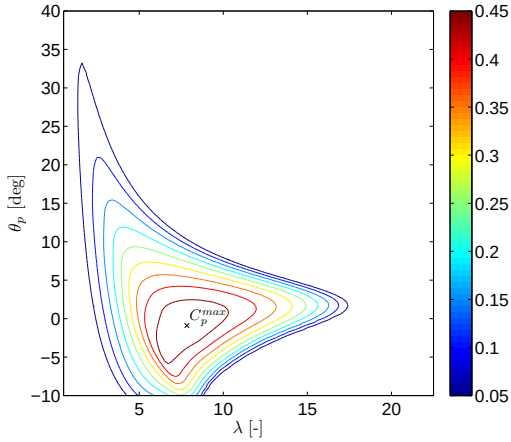

Figure 2.1: Contour plot for the power coefficient of the NREL 5 MW reference turbine as a function of the collective pitch angle and the tip speed ration. The figure was generated using blade element momentum theory [29] and assuming stationary and uniform inflow, and no turbine flexibility.

is achieved if the pitch and tip speed ratio is kept at these values for a stationary uniform inflow. However, the inflow to a turbine is neither stationary nor uniform; it changes with time and is non-uniform due to wind shear, yaw error, turbulence, etc. Thus, continuous regulation is required for maintaining optimal power extraction.

Power is potentially lost when the wind speed changes because the rotor speed only changes slowly to maintain the optimal tip speed ration and that the pitch traditionally is kept constant. Furthermore, the optimal tip speed ratio, which is tracked, is calculated for a uniform inflow. The optimal operating pitch and tip speed ratio of a turbine that is operating in a non-uniform inflow might be different from those estimated for a uniform inflow. They might even be azimuth dependent. Hereby, a turbine that operates with only collectively regulated pitch angles in a non-uniform inflow is likely to be operating sub-optimally. Consequently, power is lost because of the assumption of uniform inflow in the estimation of the optimal pitch and tip speed ratio.

The causes of power loss that were introduced above can be eliminated through improved wind turbine control. In the following, the potential of increasing the power production of wind turbines by minimizing the yaw error and by applying optimal pitch control is assessed.

2.2 Improving the Power Capture by Improved Yaw Alignment

The potential of improving the power capture of a wind turbine by improving the yaw alignment through inflow measurements depends on both the performance of the current yaw alignment system, and the ability of the inflow measurement system to estimate the inflow direction. Therefore, both the current performance of a conventional yaw alignment system, and the capabilities of an inflow measurement system have been explored The results are summarized in the following.

2.2.1 Current Performance of Yaw Alignment Systems for Horizontal Axis Turbines

The yaw performance of an offshore 2.3 MW turbine was assessed by analyzing a multiyear dataset containing turbine data and measurements from an upstream meteorological mast (met mast). The estimated mean yaw errors and root mean square (RMS) variations around the means are shown in Figure 2.2 as a function of the mean wind speed. The results show that the studied turbine is operating with a mean yaw error that varies from approximately -1 deg to 2 deg depending on the mean wind speed. The RMS variation of the yaw error also depends on the wind speed and is below 5 deg for wind speeds above 5 m/s. Details regarding the estimation of the yaw errors can be found in Appendix B.

Furthermore, a study of the yaw error of an experimental variable speed, and pitch regulated turbine (CART3 [32, 33]) have been carried out by analyzing all available data for the turbine and estimating the yaw error using measurements from an upwind met mast. In Figure 2.3, the estimated yaw errors are shown as a function of rotor speed. It is seen that the mean yaw error varies from approximately 0 deg at standstill to approximately 15 deg at the rated rotational speed. Thus, it appears that the wind direction measurements from the nacelle mounted transducer are affected by the flow distortions that are caused by the rotor, when the turbine is operating.

Based on the yaw performance that was observed for the CART3 turbine, a correction scheme was implemented that corrects for the rotor speed dependent wind direction measurement error. The updated controller was tested, and the performances of the current and improved yaw controller are compared in Figure 2.4. The yaw error has clearly decreased, and the mean yaw error is close to zero when the updated controller is applied. The details of the study can be

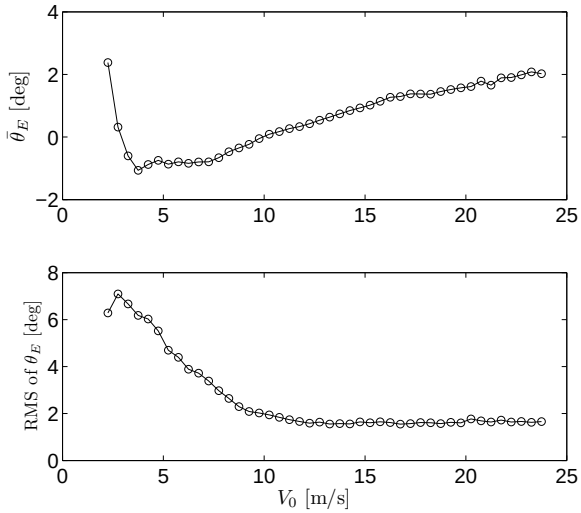

Figure 2.2: Mean yaw errors and RMS variations around the means of the offshore 2.3MW turbine that was studier in Appendix B as a function of wind speed. The yaw error is estimated using turbine data and met mast measurements

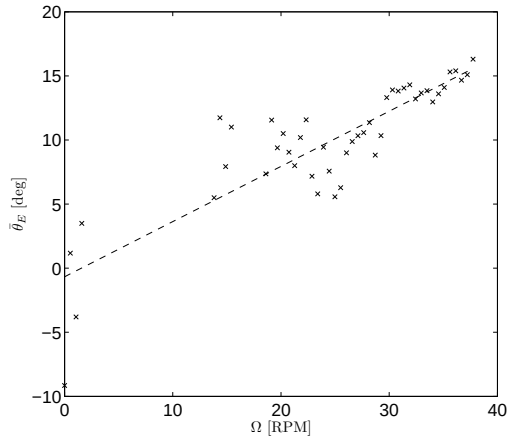

Figure 2.3: Mean yaw errors of the CART3 research turbine as a function of rotor speed. The dashed line represents a linear fit to the data. The yaw errors are estimated from turbine and met mast measurements. See Appendix C for details.

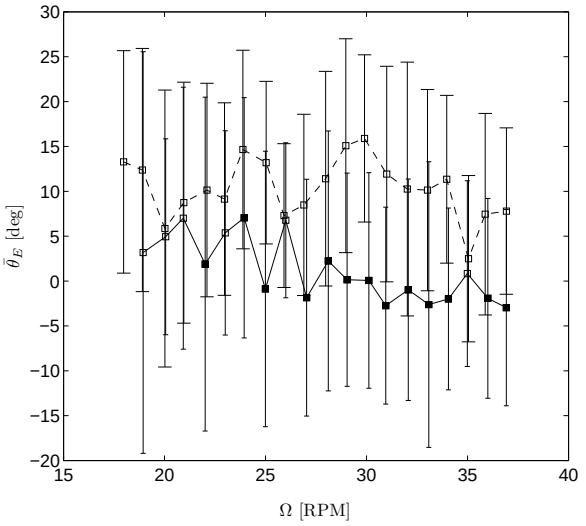

Figure 2.4: Medians of 1-minute average yaw errors of the CART3 turbine binned according to rotor speed. The yaw errors are shown for the original yaw controller (− − −) and the updated yaw controller (—). The whiskers indicate the standard deviation of the yaw errors in each bin. Narrow whiskers are for the corrected controller, whereas wide whiskers are for the uncorrected controller. Solid squares indicate that the value of the corrected controller is significantly lower than the corresponding value of the uncorrected controller—at a level of significance of 95% using the t-distribution. For details c.f. Appendix C.

found in Appendix C.

Finally, the yaw errors of an onshore 2 MW turbine have been estimated using measurements from a spinner mounted LiDAR sensor. In Figure 2.5, the estimated yaw error of the turbine is shown, and it appears that the turbine is operating with a mean yaw error around 10 deg, see Appendix A.

In summary, the presented results indicate that it is not uncommon for a turbine to be operating with yaw errors that can potentially lead to significant power losses. However, the results also show that using the traditional transducers and yaw control schemes, the yaw error can be kept close to zero. The yaw performances of the studied turbines and turbines that have been studied by others are summarized in Table 2.1.

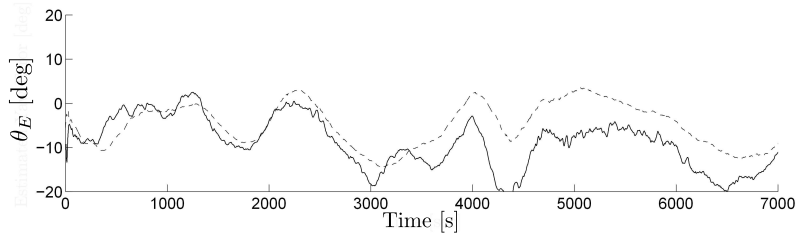

Figure 2.5: Yaw error as a function of time of the 2 MW onshore turbine that was studied in Appendix A, estimated using measurements from a spinner mounted LiDAR sensor (—) and met mast measurements (– – –).

2.2.2 Improving Yaw Error Estimation by Upstream Inflow Measurements

In the previous section it was shown that is not uncommon for a turbine to be misaligned with the mean wind direction. The yaw errors are caused by deficiencies of the current yaw controller or measurement system. The primary input to the yaw controller of modern wind turbines is a wind direction measurement from a sensor, which is usually mounted on the nacelle behind the rotor. This measurement gives rise to two main uncertainties relating to the estimated inflow direction:

1. The swirl of the wake will effectively change the wind direction that is measured by the nacelle mounted transducer. Thus, the direction of the distorted flow behind the rotor is not the same as the direction of the undistorted flow upstream of the rotor. This effect is shown numerically in [34], and is indicated by experimental results in [4], Appendix B and C, where it is observed that the magnitude of the yaw error depends on wind speed and rotor speed.

2. The measurements from the nacelle mounted transducer are only point measurements. For large rotors, the wind direction is not necessarily uniform in the entire rotor plane, but may vary due to i.e. wind veer. Therefore, a single point measurement might not be the best way to estimate the effective wind direction that is acting on the rotor.

Because of the uncertainties that are associated with the current wind direction measurement, a number of alternatives for estimating the effective inflow direction have been suggested. An approach for improving the wind direction estimate is to use measurements from a LiDAR sensor mounted in or on the

nacelle that measures the wind speeds in a pattern at a distance upwind of the turbine. Using a spinner mounted LiDAR sensor, measurements are sampled in the undisturbed flow and distributed across the rotor plane. Thus, both of the uncertainties of the traditional nacelle based wind direction measurement are eliminated. In Appendix A, the ability to estimate the yaw error based on measurements from three different scan types is investigated through simulation. It is found that the best estimate of the yaw error is achieved with a circular scan with a cone angle of 30 deg. The precision of the yaw error estimates depends on both turbulence intensity and wind speed, see Figure 2.6. However, the median error of the estimates is below 3 deg in the tested range of wind speeds and turbulence intensities. Thus, it appears that a precise estimate of the yaw error can be achieved by using LiDAR sensors.

Another possible sensor for estimating the yaw error is a blade mounted pitot tube. Using a blade mounted pitot tube, the flow direction in the entire rotor plane can be estimated as the blade rotates. The inflow direction could also be estimated using a spinner anemometer [4]. However, this measurement still only supplies a point measurement, and eliminates only one of the two uncertainties of the current system. Finally, it might also be possible to estimate the yaw error from the blade root bending moments. Neither of these methods are studied in detail in this thesis. However, in the following section the potential of improving the power yield by completely eliminating the yaw error is investigated. Hence, an upper limit is provided for the effect of improving the yaw alignment using

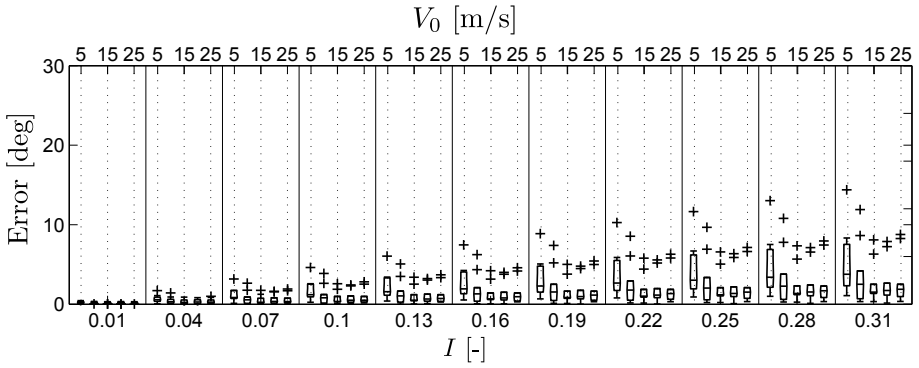

Figure 2.6: Mean error of yaw error estimates calculated from simulated continuous wave LiDAR measurements from a circular scan with a cone angle of 30 deg and a focal length of 100 m as a function of turbulence intensity and mean wind speed. The centerlines of the box-plots are the medians of the simulation results, whereas the upper and lower lines represent the 75th and 25th percentiles. The whiskers represents $\pm 2.7\sigma$. Points outside the $\pm 2.7\sigma$ range are considered outliers and are marked by '+', c.f. Appendix A for details.

any sensor beyond what is achievable with conventional sensors.

2.2.3 The Potential of Increased Power Capture by Improved Yaw Alignment

Based on the yaw tracking performance that was observed for the studied turbines it appears that the yaw tracking performance can be improved in three ways:

1. By reducing the mean yaw error
2. By eliminating the wind speed and rotor speed dependence of the yaw error
3. By reducing the variation of the yaw error

A rough estimate of the potential of reducing the mean yaw error can be given if it is assumed that the power loss due to a yaw error is proportional to $(1 - \cos(\theta_E)^3)$, as in Equation (2.4), and that the yaw error decreases the power in the entire wind speed range. The potential power loss is then:

$$P_{loss}(\theta_E) = 1 - \cos(\theta_E)^3. \tag{2.5}$$

Table 2.1 shows the mean yaw error of a number of turbines studied in the literature as well as the potential of improving the power output by eliminating the observed mean yaw error estimated using Equation (2.5). As expected, there is a large potential for improving the power output by eliminating the observed mean yaw error for turbines that are operating with large mean yaw errors, whereas the potential is small for the well calibrated turbines. Thus, it appears that a significant part of the power loss can be regained through calibration. It should be noted that the estimated potentials that are indicated in Table 2.1 are upper limits, because the estimates are based on the assumption that the yaw error induces power loss in the entire wind speed range. In reality, the yaw error induces no power loss at above rated wind speeds.

The potential of improving the power output by removing the wind speed and rotor speed dependence of the yaw error. In [4] and in Appendix B, it was shown that the gradient of the mean yaw error is small, and the difference between the

mean yaw error at low wind speeds and at the rated wind speed is small ($< 2-3$ deg). If it is assumed that the average mean yaw error in the below rated wind speed range can be reduce to zero through static calibration, the mean yaw error of the turbines studied in [4] and Appendix B will vary in magnitude between 1-1.5 deg. Such a variation corresponds to a power loss that varies between 0 and 0.1% in the below rated wind speed range according to Equation 2.5. In Appendix C, the rotor speed dependence is seen to cause a mean yaw error variation in the below rated domain of approximately 5 deg. With good static calibration of the turbine, this variation corresponds to a power loss that will vary between 0% and 0.3% according to Equation (2.5).

It is shown in [4] and in Appendix B that the RMS variation of the yaw error is below approximately 4 deg for below rated wind speeds. Thus, the potential power increase by decreasing the yaw error variation is expected to be less than $P_{loss}(4) = 0.7\%$, because even with inflow measurements from a LiDAR sensor, the estimated inflow direction is associated with some uncertainty.

The potentials that are estimated above for the three types of improvements are based on rough assumptions and only on the yaw performance. In Appendix B, a detailed analysis is made of the potential power improvements of an operating turbine that takes into account the measured yearly wind speed distribution. The analysis shows that for this particular turbine; only approximately 0.2% power is loss due to the observed yaw error distribution. Thus, the potential of improving the power yield by introducing all three improvements and completely eliminate the yaw error is $< 0.2\%$ for this particular turbine.

In summary, it appears that the potential of improving the power output by improved yaw alignment is only significant for badly calibrated turbines, and that more detailed inflow measurements will not enable significant power increases for well calibrated turbines. It should be noted, however, that the presented results are from turbines that are operating in non-complex inflow conditions. It is possible that the potential is larger for turbines that are operating in more complex inflow conditions, e.g. in mountainous regions or in wakes of other turbines. However, more complex inflow is also likely to decrease the performance of the inflow estimation as discussed in Appendix A. Additional studies could be aimed at assessing the optimal yaw position for power production of turbines that are operating in complex inflow, e.g. in wakes.

Turbine	Mean yaw error [deg]	P_{loss} [%]	Reference
Onshore 2 MW	10	4.5	[7, 8, 35, 12] and Appendix A
Onshore 3.6 MW	10	4.5	[4]
Onshore 5 MW	≈ 0	≈ 0	[13]
Vestas V-82	15	9.9	[6]
Nordex N60	13	7.5	[6]
Vestas V-82	15	9.9	[6]
Other 2 MW	15	9.9	[6]
Other $>$ 2 MW	12	6.4	[6]
Offshore 2.3 MW	≈ 0	≈ 0	Appendix B
CART3	10	4.5	Appendix C

Table 2.1: Summary of the documented mean yaw error of different turbines and the potential for improving the power production by eliminating the mean yaw error assuming that Equation 2.4 is valid, and that the power is decreased in the entire operating range by the yaw error.

2.3 Improving Power Capture by Pitching

In Appendix G, the potential of increasing the power output through feed-forward collective pitch, individual pitch and generator torque actuation is assessed through numerical optimization, and hereby independent of control design. Two types of inflows are tested: uniform inflow with mean wind speed step changes and half wake inflow.

The uniform inflow with mean wind speed step changes represents an extreme situation that is not seen in real operating conditions. This type of inflow is chosen because it represents a severe challenge for a turbine control system. Thus, the results represent a first attempt of estimating the maximum potential of applying power maximization using feed-forward collective pitch and generator torque control in a situation with rapid mean wind speed changes. Such a control scheme could for example be based on preview of the inflow provided by measurements from a spinner mounted LiDAR sensor. Two types of optimizations are performed for the uniform inflow:

1. Constant collective pitch is applied and the generator torque is regulated according to the standard speed control law that is defined in Equation (1.1). The optimization variables are the constant collective pitch angle and the constant k. The result of this optimization yields a standard speed controller that is optimized for capturing power in case of a wind

speed change. Thus, this is a best case of what can be accomplished with traditional speed control.

2. Collective pitch and generator torque are prescribed by two linear interpolations that are each described by 20 points distributed around the wind speed change. The optimization variables are the collective pitch and generator torque values in the 20 optimization points. Hereby, the optimization yields the optimal pitch and torque trajectory for maximizing the power capture in case of a wind speed change.

The optimization problem is given as:

$$\max_{\mathbf{u}} \frac{1}{T} \int_{t}^{t+T} P(t)dt \tag{2.6}$$

where $\mathbf{u} = (\theta_p, k)$ and $\mathbf{u} = (\theta_p(t_i), Q_g(t_i)), i = 1...20$ for the two optimization cases, t_i is time of the i'th input sample. The results of the optimizations are presented in Figure 2.7. For the case with optimized pitch and generator torque, the actuations are applied slightly before the wind speed change occurs. However, it is seen that the actuations have limited effect on the power output, and the observed increase in integrated power output is negligible compared to the case of the optimized speed controller (0.04% power increase). Thus, a preview of the inflow for collective pitch control appears to have very limited potential for improving the power capture compared to using feed-back control. It might appear counter intuitive that the preview of the inflow leads to no significant power increase. But, this can be explained by the shape of the C_p-surface. In the simulation study, a model of the NREL 5 MW reference turbine is used, and the peak of the C_p-surface for this particular turbine is very flat, see Figure 2.1. Hence, perturbations around the optimal operating position yields only small power decreases. It is possible that the advantages of applying preview measurement would be greater for a turbine that is designed with a steeper slope of the C_p-surface.

The half wake inflow is an extreme situation where the wind speed is significantly higher in one half of the rotor plane than in the other. This inflow is an idealization of what is expected for a turbine in a wind farm. In a real wind farm, the wake would meander and not remain constant in one half-plane [36]. Two types of optimizations are performed to assess the potential of increasing the power yield of a turbine that is operating in the wake of another turbine:

1. The same optimization as for the uniform inflow, where the collective pitch angle θ_p and the feed-back gain k are optimized.

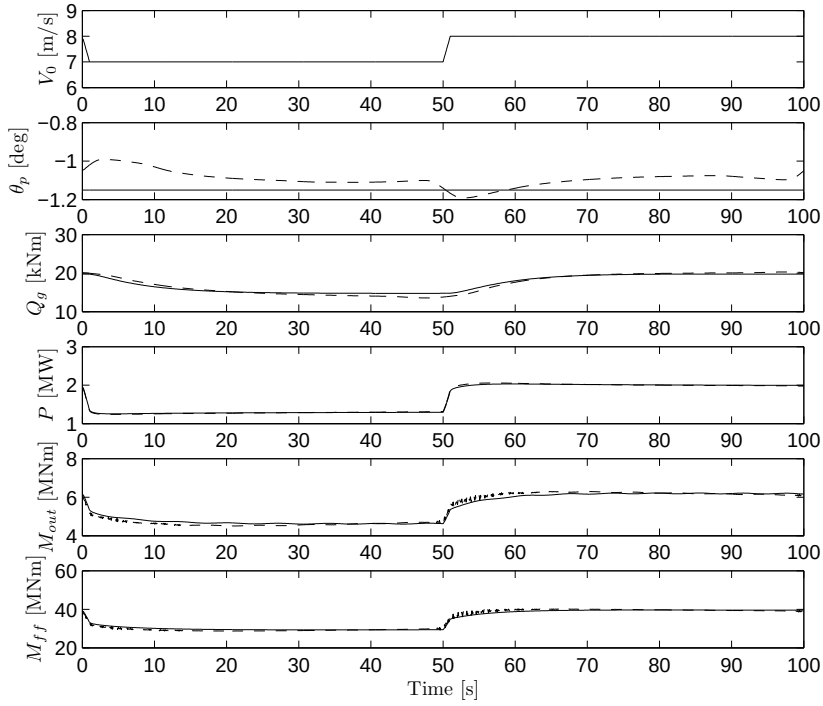

Figure 2.7: Results of power maximization through pitch and torque control at below rated wind speeds and step changes of the collective wind speed for a stiff version of the NREL 5 MW reference turbine. Results are shown for the case of optimized constant pitch and gain factor (—), and for the case of optimized periodic pitch and generator torque actuation (− − −). From the top and down: Free wind speed, pitch angle, generator torque, power output, blade root out-of-plane bending moment, and tower bottom fore-aft bending moment, c.f. Appendix G for details.

2. The generator torque is controlled using the standard speed control law. An azimuth dependent pitch signal that is defined from two reference pitch values and the azimuthal position of the two reference pitch values (the phase) is superimposed to the collective pitch signal that is generated by the speed controller. The pitch values at the intermediate azimuth angles are obtained by interpolation between the two reference pitch values using a cubic spline. Thus, the optimization variables are k and the values and positions of the two reference pitch points $\theta_p^i(\psi_1)$ and $\theta_p(\psi_2)$.

The optimization problem is given as:

$$\max_{\mathbf{u}} \frac{1}{2\pi} \int_{-\pi}^{\pi} P(\psi_i) \frac{\bar{\Omega}}{\Omega(\psi_i)} d\psi_i \tag{2.7}$$

where $\mathbf{u} = (\theta_p, k)$ and $\mathbf{u} = (\theta_p^i(\psi_1), \theta_p(\psi_2), k)$ are the optimization variables for the two optimizations, $\theta_p(\psi_i)$ is the pitch angle at the azimuth angle ψ_i, $P(\psi_i)$ is the obtained azimuth angle dependent power output, $\bar{\Omega}$ is the average steady state rotor speed and $\Omega(\psi_i)$ is the azimuth angle dependent rotor speed. The results of the power maximization are presented in Figure 2.8. It is seen that by applying the optimized cyclic pitch signal, the power output is raised compared to when only k and the collective pitch angle are optimized. With the optimized cyclic pitch signal, the power integrated over one period is increased approximately 3.6%. However, the increased power output is penalized by increased load variations. Especially, the blade root load variations are increased.

2.4 Summary

The results that are presented in the current literature and the results that are achieved in the present work lead to the following summary relating to increased power production through inflow measurements:

- Turbines with poorly calibrated yaw alignment systems are not uncommon. For such turbines there is a potential for increasing the power yield by improving the yaw alignment
- Well calibrated turbines are able to align the rotor axis close to the mean wind direction using only the existing measurement systems
- The potential of increasing the power output of a well calibrated turbine by means of inflow measurement based yaw control is small
- The potential of increasing the power output by feed-forward of the mean wind speed to the control system is small
- There is a theoretical potential for improving the power performance through feed-forward individual pitch control in situations with azimuth dependent inflow. However, the results are based on a simplified model and further validation is needed

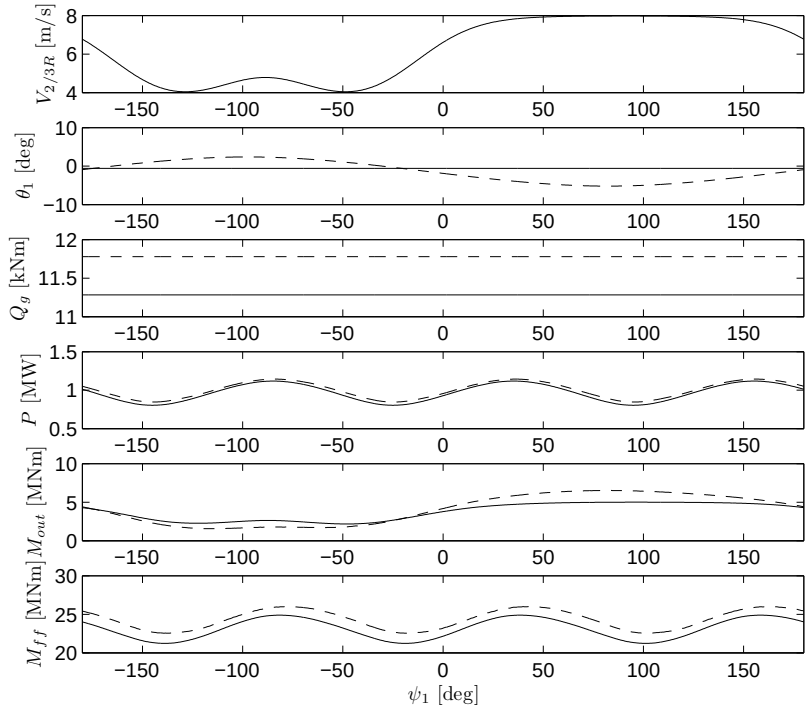

Figure 2.8: Results of power maximization at below rated wind speeds in half-wake operation for a stiff version of the NREL 5 MW reference turbine. Results are shown for the case of optimized constant pitch and gain factor (—), and for the case of optimized gain factor and pitch values for cyclic pitch (− − −). From the top and down: free wind speed at the two-thirds radius of the rotor, pitch angle, generator torque, power output, blade root out-of-plane bending moment, and tower bottom fore-aft bending moment, c.f. Appendix G for details.

The identified potentials are all under the assumption that valid and accurate inflow measurements are available. The uncertainties of using inflow measurements as input to wind turbine control systems are discussed in Chapter 4.

Chapter 3

Reducing Load Variations

To understand how inflow measurements can be used for alleviation of load variations, it is useful to understand the causes of load variations on a wind turbine. Therefore, this chapter contains an introduction to the causes of load variations on horizontal axis wind turbines. The potential of applying inflow measurement based pitch and yaw control for load variation alleviation is assessed in the subsequent sections.

3.1 Causes of Load Variations

The load variations on a horizontal axis wind turbine are caused by the instationary inflow to the turbine, which is the sum of different phenomena inducing different types of loads on the turbine. The phenomena that typically constitute the inflow to a turbine are illustrated in Figure 3.1. The effects of the different inflow phenomena are summarized below.

- The mean wind speed is a primary parameter of the inflow. Generally, the mean wind speed changes slowly with large scale turbulent structures, and causes thrust variations on the entire rotor resulting in blade and tower

load variations. Rapid mean wind speed variations might also occur, and these are referred to as gusts

- Vertical wind shear is the wind speed gradient along the vertical direction, and is a result of the surface roughness and the viscosity of the air. The blades of a turbine that is operating in a vertical wind shear will be exposed to an inflow that varies with the rotational frequency of the rotor. Thus, a vertical wind shear causes once per revolution (1P) blade load variations and 3P load variations on the tower (for a 3-bladed turbine)
- Yaw error occurs when the turbine yaw controller is not able to track the mean inflow direction. The blades of a turbine that is operating with a yaw error will experience 1P varying inflow conditions, which leads to 1P blade load and 3P tower load variations (for a 3-bladed turbine). The effect of wind shear and yaw error is discussed in more detail in Appendix D
- Horizontal wind shear causes load variations that are similar to those of a vertical wind shear, but shifted 90 deg in phase
- Up or down flow can be observed in areas with complex terrain. The induced blade load variations are similar to those caused by yaw error but shifted 90 deg in phase
- Wakes from upstream turbines are a major concern for wind turbines that are operating in a wind farm. Wakes are localized areas of low wind speed that changes location as the wake meanders [36], and cause abrupt tower and blade load variations
- The tower is blocking the flow in the area upstream of the tower. Therefore, there is a localized wind speed drop just upstream of the tower (tower shadow) that causes sudden blade load variations

The phenomena that are described above are all changing slowly with time. On top of the slow changing mean effects is a stochastic small scale variation (turbulence), which induces rapid load variations.

Different control schemes can be applied for alleviating the effect of each of the inflow phenomena. Torque and collective pitch actuation can be used for varying the thrust exerted on the rotor. Thus, torque and collective pitch actuation can be used for alleviating the effects of mean wind speed variations. Yaw control can be used to minimize the yaw error, and thereby the cyclic load variations due to a yaw error. Individual pitch can be applied for alleviating the effects of the azimuth dependent wind speed/direction variations (wind shear, yaw error, up/down flow, wake, and tower shadow). Localized control surface devices, such as flaps, can be applied to alleviate the effect of small scale and fast changing

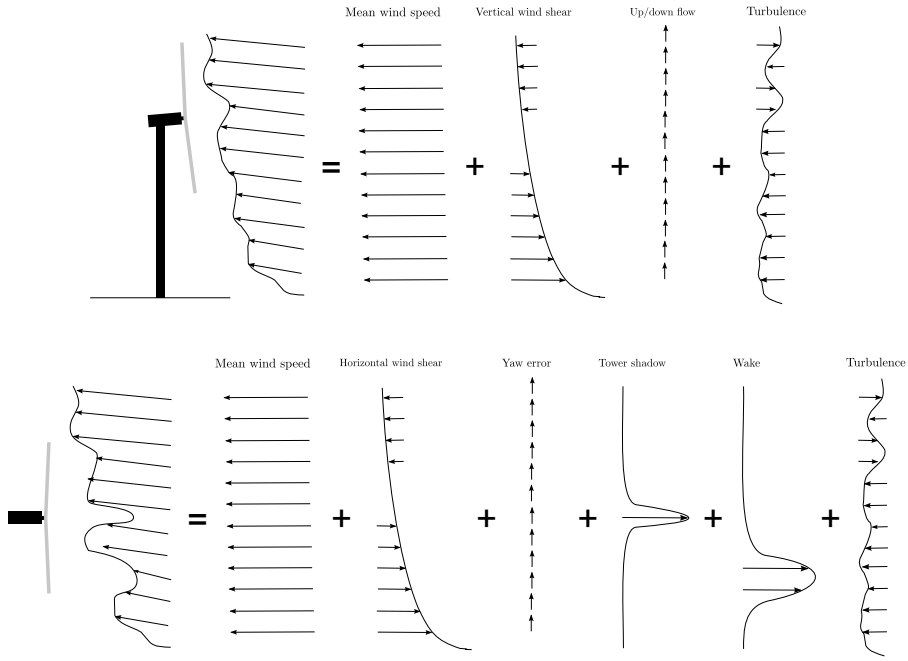

Figure 3.1: Illustration of the different inflow phenomena that constitute the inflow to a wind turbine. Top: Turbine seen from the side. Bottom: Turbine seen from the top.

turbulence, as well as the large scale azimuth dependent inflow. In the following, an assessment is given of the load alleviating capabilities of both yaw and pitch control based on inflow measurements.

3.2 Alleviating Load Variations by Yaw Control

The majority of the recent research on load alleviating control for wind turbines is focused on pitch control or flap control. However, the load variations that are caused by a vertical wind shear can also be reduced by introducing an intentional yaw error, which is shown in Appendix D.

For a known shape of the vertical shear, a wind speed dependent yaw error angle can be applied to alleviate the wind shear induced load variations. In real applications, the wind shear varies with the atmospheric stability. Therefore, the yaw error angle must be calculated from an estimate of the wind shear

shape, e.g. found using measurements from a spinner mounted LiDAR sensor. Alternatively, the yaw angle can be estimated from blade load measurements. Four methods for estimating the optimal yaw error angle for load alleviation are suggested, see Appendix D. Three of the methods are based on numerical minimization of the blade root bending moment, local thrust force, and angle of attack variations, respectively, and one is based on an analytic expression. For illustration, the optimal yaw error angles for the NREL 5 MW reference turbine are estimated as a function of wind speed using the four suggested methods, see Figure 3.2. The sign of the optimal yaw error angle is different for wind speeds below and above the rated wind speed. The sign change is caused by the different local inflow conditions that characterize operation at below and above the rated wind speed for a pitch regulated turbine. Below and around the rated wind speed, there is a significant mean lift generated on the blade. Consequently, the effect of the relative wind speed variations on the blade thrust force variation is most significant at these wind speeds. The most significant reduction of the thrust force variations due to the vertical wind shear is therefore achieved by increasing the relative velocity in the bottom part of the rotor while decreasing it at the top. Such adjustments of the relative velocity can be achieved by introducing a positive yaw error (wind from the right when see from the rotor).

At above rated wind speeds, the lift coefficient is close to zero along the outer part of the blade, making the variation of the relative velocity less significant. Hence, at above rated wind speeds, the minimum blade load variations are achieved by reducing the angle of attack variations to a mean value close to zero deg. Such a smoothening of the angle of attack variations in a situation with wind shear is achieved by introducing a negative yaw error. Finally, it is evident from Figure 3.2 that the minimization of the angle of attack variations and the simplified analytic estimation only agree with the more complex estimations at well above rated wind speeds.

To validate the theoretically estimated optimal yaw error angles, a number of HAWC2 [37] simulations where performed with two different types of wind shear, varying wind speed, and varying yaw error angle. The optimal yaw error was identified as the yaw error that yields the least steady state blade root bending moment variations. The results are presented in Figure 3.3 where both the optimal yaw error and the resulting blade load variations are shown. The load variations have been normalized such that:

$$\widetilde{\Delta M_{out}} = \frac{\Delta M_{out}(V_0, \theta_E)}{\Delta M_{out}(V_0, 0)} \tag{3.1}$$

where $\Delta M_{out}(V_0, \theta_E)$ is the range of the steady state blade root out-of-plane

bending moment variations as a function of free wind speed and yaw error. In the remainder of this section $\widetilde{(\cdot)}$ indicates that the result $(\cdot)$ has been normalized with $(\cdot)$ at zero yaw error. It is seen that the theoretical expectations and the simulation results compares well, and that the optimal yaw error yields significant reductions of the blade load variations.

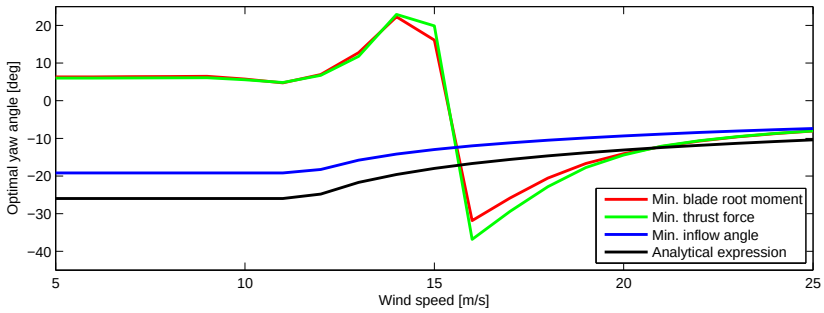

Figure 3.2: Four predictions of the optimal yaw error angle of the NREL 5 MW reference turbine based on the minimization problems that are derived in Appendix D. A positive yaw error corresponds to inflow coming from the right, when seen from the turbine.

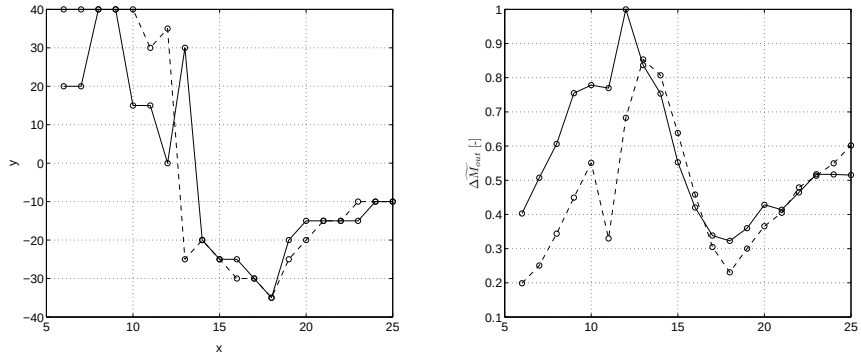

(a) (b)

Figure 3.3: Results of HAWC2 simulations of the NREL 5 MW reference turbine with varying wind speed and yaw error angle for the power law wind shear with an exponent of 0.2 (—), and the linear wind shear with a slope of 0.05 s^{-1} (– – –). a) Optimal yaw error angle for alleviating blade root out-of-plane bending moment variations as a function of wind speed. b) Normalized load range with the optimal yaw error angle applied as a function of wind speed. See Appendix D for details

In turbulent inflow, the identified optimal yaw error is different from the results that are presented in Figure 3.3. The load variation reductions are less and depend on the turbulence level. The results of the simulations in turbulent inflow are summarized in Table 3.1 that shows that the blade load reductions, which are achievable through yaw error, are penalized by increased tower loads.

In summary, the results show that it is possible to decrease the blade load variations that are caused by wind shear by yaw control. However, the blade load reductions are penalized by increased tower loads. Therefore, a full design load case must be performed and the results related to a cost model to assess if the increased tower loads are justified by the blade load reductions.

3.3 Alleviating Load Variations by Pitching

In the previous section, it was demonstrated how yaw control can be used for alleviating load variations that are caused by vertical wind shear. However, as seen in Figure 3.1, the vertical wind shear is only one of several phenomena that induce loads on a wind turbine. The effects of the remaining slow changing phenomena can be reduced by regulating the aerodynamic torque and thrust through pitch actuation. Pitch control can be divided in two categories: collective pitch and individual pitch. In the following, the two types of actuation are covered separately.

	Turbulence Intensities				
	18%	13.5%	9%	4.5%	0%
$\widetilde{\theta_m^{opt}}$ [deg]	-15	-15	-20	-20	-25
$\widetilde{DEL(M_{out})}$ [%]	97.5	94.0	88.8	80.6	60.6
$\widetilde{DEL(M_{in})}$ [%]	96.7	97.3	97.2	97.7	98.0
$\widetilde{DEL(M_{tilt})}$ [%]	97.5	98	99	103.3	127.1
$\widetilde{DEL(M_{yaw})}$ [%]	103.5	103.7	105.3	107.5	134.7
$\widetilde{DEL(M_{ff})}$ [%]	106.3	102.7	108.6	106.7	154.9
$\widetilde{DEL(M_{ss})}$ [%]	110.2	95.5	101.6	87.9	122.9

Table 3.1: Identified optimal yaw misalignment angles and estimated normalized 1 Hz damage equivalent loads at the optimal yaw misalignment angle at four turbulence intensities. For the blade loads it is assumed that the slope of the Wohler curve is $m = 10$ and for the remaining loads $m = 3$.

3.3.1 Collective Pitch

In Appendix G, the potential of alleviating extreme load variations by collective pitch is assessed through numerical optimization. Using numerical optimization, it is possible to estimate the optimal actuation trajectory for load alleviation independent of the control design. A stiff version of the NREL 5 MW turbine was simulated in conditions where the inflow consists of a series of wind speed steps. The wind speed steps were chosen because they represent the most extreme case that can be encountered by a turbine, thus, a worst case scenario. The collective pitch signal was optimized by varying the pitch value specified in 20 points distributed around the wind speed step. The applied pitch signals were linear interpolations between the optimization points, and the optimization problem was defined as:

$$\min_{\mathbf{u}} \frac{1}{T} \int_{t}^{t+T} |P(t) - P_r| + |\tilde{M}_{out}| dt \tag{3.2}$$

where P_r is the rated power of the turbine, $\tilde{M}_{out}$ is the high-pass filtered blade root out-of-plane bending moment signal, $\mathbf{u} = \theta(t_i)$, and $i = 1...20$ is the vector containing the optimization variables. The results of the optimization are compared to the results of a simulation with a standard collective pitch rotor speed controller in Figure 3.4. In the optimized case, the pitch actuation is applied prior to the wind speed change. Hereby, the extreme load variations are reduced. Thus, the results suggest that collective pitch feed-forward control can reduce the loads on a wind turbine compared to feed-back only control in situations with extreme wind speed changes. This result is consistent with the conclusions of related studies, i.e. [9, 38]. In [9], experimental results show that collective feed-forward pitch control can also alleviate the fatigue loads of a turbine.

3.3.2 Individual Pitch

In Appendix F, an individual pitch control scheme for alleviating load variations is suggested. The idea of the control scheme is to minimize the variation of the sectional thrust force at one discrete radial position on the blades, thus, basing the controller on inflow measurements. The controller is tested through simulations with two types of inflow measurements as input: on-blade measurements of angle of attack and relative velocity, and upstream inflow measurements from a simulated LiDAR sensor. The controller is implemented as a feed-forward controller and is tested with and without preview of the inflow. For the on-blade measurement, the preview is available for each blade from the measurements

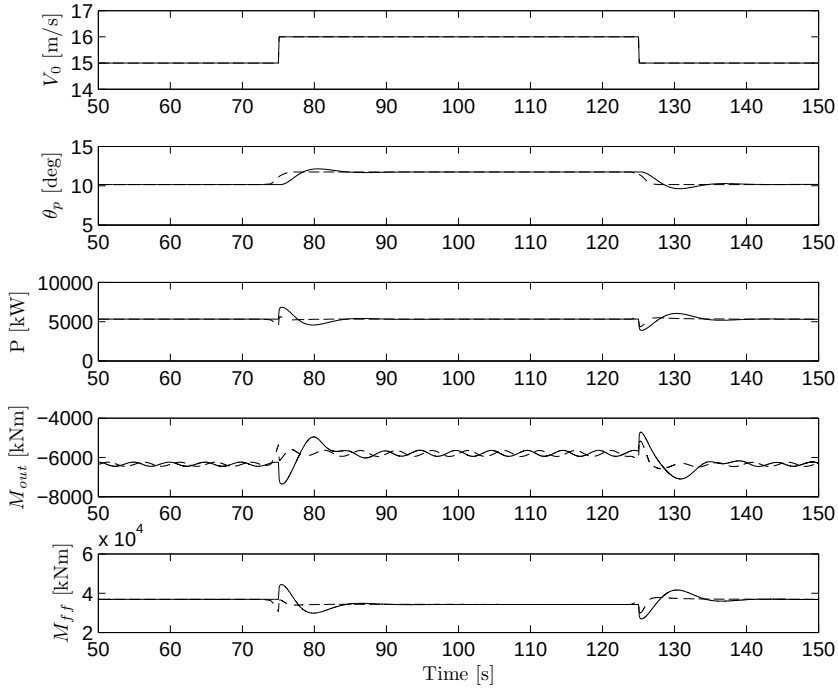

Figure 3.4: Results of load variation minimization through collective pitch control of the NREL 5 MW reference turbine at above rated wind speeds and step changes of the mean wind speed. Results are presented for standard collective pitch control (—), and for optimized periodic pitch values (− − −). From the top and down: free wind speed, pitch angle, power output, blade root out-of-plane bending moment, and tower bottom fore-aft bending moment. See Appendix G for details.

from the blade leading in the rotation. The simulation results show that the best performance is achieved with the on-blade measurements, see Figure 3.5. Thus, it appears that the uncertainties of estimating the local inflow from upstream measurements, and the fact that the relative movement of the blade is not captured by the upstream measurement have a negative effect on the performance of the controller.

In Appendix E, the influence of different measurement types on the controller performance is further investigated by using a baseline cyclic pitch control design. Three different measurement types are tested through simulations with the baseline controller: blade root out-of-plane bending moment, on-blade in-

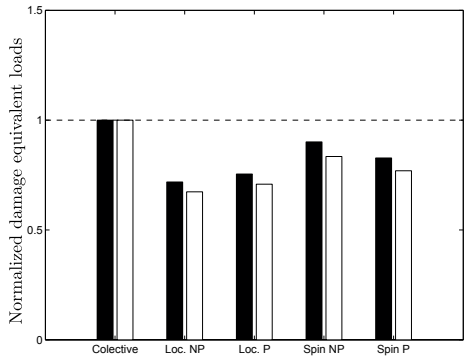

Figure 3.5: Out-of-plane damage equivalent blade root load variations for collective pitch control and two types of inflow measurement based individual pitch control with and without preview of the inflow simulated on a model of a 2 MW onshore turbine. The loads are normalized with the loads of the collective pitch controller. Black: Class A wind conditions. White: Class C wind conditions. NP: No preview, P: Preview, Loc: controller based on on-blade inflow measurements, Spin: controller based on measurements from a spinner mounted LIDAR sensor. See Appendix F for details.

flow measurements, and simulated upstream LiDAR measurements. The baseline cyclic pitch controller is based on the Coleman transformation of loads that are estimated from the different types of measurements, and is similar to the one suggested in [21]. For the blade root out-of-plane bending moment measurement based controller, the raw bending moment signal is used as input to the controller. For the inflow measurement based controllers, the thrust force at a radial section is estimated from the measurements and used as input to the controller. The controller that is based on upstream inflow measurements is designed to apply a preview of the inflow that enables the controller to apply actuation before an inflow change reaches the turbine.

The results show that controllers that are based on either blade root bending moment or on-blade inflow measurements outperform the LiDAR sensor based controller for stationary inflow conditions (constant wind shear, no turbulence). Thus, the preview does not provide any advantages. However, the controller based on the upstream inflow measurements leads to larger load reductions than any of the no-preview measurement based controllers for situations with extreme wind shear. Thus, for fast changing inflow conditions, there is an advantage of applying the preview controller. Furthermore, for the extreme wind shear case, it is seen that the controller that is based on on-blade inflow measurements performs better than the controller that is based on the blade root bending moments. The results of the simulations with deterministic inflow are summarized in Figure 3.6 that shows the blade load reductions as a function of

the applied preview time. It is evident that the performance of the controller based on upstream inflow measurements is sensitive to the preview time. If the preview time is changed $\Delta T_d = \pm 0.1$s from the optimal preview time, the extreme load range is equal to that of the local inflow measurement based controller. A preview time change of $\Delta T_d = \pm 0.3$s yields a load range equal to that of the blade root bending moment based controller, and $\Delta T_d = \pm 1$s yields a load range equal to that of the collective pitch controller.

The results that are presented in Figure 3.6 relies on the assumption that the speed at which a measured wind speed travels towards the turbine is known. Hereby, the time from a wind speed is measured until it reaches the turbine can be calculated as:

$$T_d = \frac{L_p}{V_0}, \tag{3.3}$$

where L_p is the distance from the measurement point to the rotor. In reality, the true transport velocity of a measured wind speed is not known precisely and

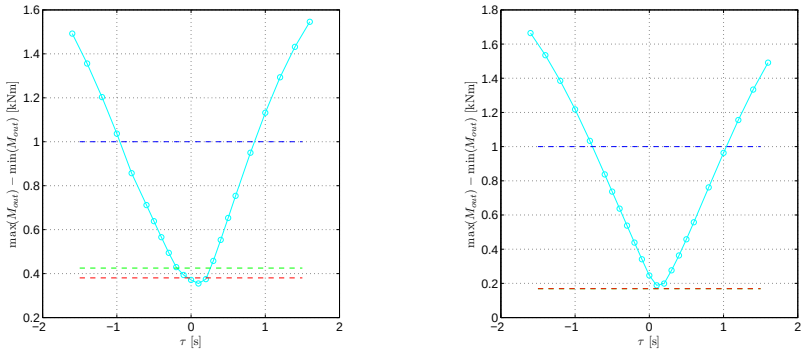

(a) (b)

Figure 3.6: Results of simulations of the NREL 5 MW reference turbine with three different measurements applied for cyclic pitch control in situations with an IEC extreme wind shear (a) and a standard IEC wind shear (b). Range of the extreme load variations that are caused by the wind shear as a function of preview time of the LiDAR based cyclic pitch (cyan), collective pitch controller (blue), M_{out} based cyclic pitch (green), and cyclic pitch based on on-blade inflow measurements (red). The results have been normalized with the moment range observed when the baseline collective pitch controller is applied. See Appendix E for details.

a more realistic estimate of the transport time is:

$$\tilde{T}_d = \frac{L_p}{\bar{V}_0 + \delta}, \tag{3.4}$$

where δ is the estimation error of the transport velocity, and $\bar{V}_0$ is the estimated transport velocity. The estimation error effectively changes the preview time because the wind speeds that are expected to reach the rotor are shifted in time. Thereby, the effective preview time is:

$$\tilde{\tau} = \tau + \Delta T_d, \quad \text{where} \quad \Delta T_d = T_d - \tilde{T}_d. \tag{3.5}$$

Using Equation (3.4) and (3.5), the estimation error of the transport velocity δ corresponding to a given preview time disturbance ΔT_d can be estimated as:

$$\delta = \frac{-L_p}{\Delta T_d - \frac{L_p}{\bar{V}_0}} - \bar{V}_0. \tag{3.6}$$

In Figure 3.7 the estimation error δ is plotted as a function of preview time shift ΔT_d for a mean wind speed of 15 m/s. It is seen that the LiDAR sensor based controller only outperforms the local inflow measurement based controller if the transport velocity error is $-0.2 \leq \delta \leq 0.2$ m/s. To outperform the controller based on the blade root bending moment measurements, the transport velocity error should be $-0.6 \leq \delta \leq 0.7$ m/s. Finally, the error should be $-2.0 \leq \delta \leq 2.6$ m/s for the LiDAR sensor based cyclic pitch controller to outperform the collective pitch controller. In addition to the uncertainties relating to the transport time, the evolution of the inflow from the upstream measurement section to the turbine causes uncertainties relating to the measured wind speed.

In turbulent inflow, the results show that similar load variation reductions are achieved using either blade root bending moment measurements or local inflow measurements. The LiDAR sensor based controller yields smaller load reductions than either of the other controllers, see Table 3.2.

The majority of the studies on inflow measurement based control are focused on applying one particular control strategy and compares the results of the applied controller to the performance of a simpler baseline controller. In Appendix G, the potential of individual pitch control is investigated independent of control design through numerical optimization. The pitch actuation is optimized for a deterministic inflow with wind shear and tower shadow, and is performed with

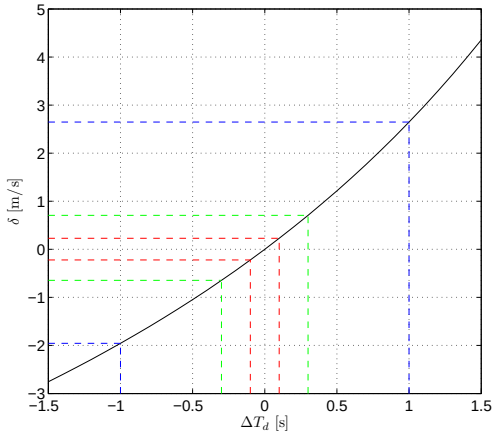

Figure 3.7: Transport velocity error as a function of preview time shift (black) for the IEC extreme wind shear. The six horizontal lines indicates the error that decreases the performance of the LiDAR sensor based cyclic pitch controller to the levels of the inflow based IPC (red), blade root bending moment IPC (green), and collective pitch controller (blue), respectively. See Appendix E for details.

	Collective pitch	M_{out} cyclic pitch	Inflow cyclic pitch	LiDAR cyclic pitch
M_{out}	100%	85.1%	85.8%	90.7%
M_{ff}	100%	103%	108%	110%

Table 3.2: Damage equivalent blade root out-of-plane bending and tower bottom fore-aft bending load variations for the NREL 5 MW reference turbine when collective pitch controller and cyclic pitch control based on different types of measurements are applied. The results have all been normalized with the damage equivalent loads of the collective pitch controller. See Appendix E for details.

an increasing number of optimization variables. The optimization problem is given as:

$$\min_{\mathbf{u}} \sqrt{\frac{1}{TF_s - 1} \sum_{i=1}^{TF_s} (M_{out,i} - \bar{M}_{out})^2} \tag{3.7}$$

where $\mathbf{u} = \theta(\psi_i), i = 1...n$, $\theta(\psi_i)$ is a vector containing discrete pitch angles for the n azimuthally distributed optimization points, and ψ_i is the azimuth angle

of the i'th optimization point. Thus, both the pitch value and its azimuthal position are optimized. The pitch signal that is applied in the simulations is a cubic spline interpolation of the optimization points. In Equation (3.7), T is the steady state simulation time, F_s is the sampling frequency, $M_{out,i}$ is the blade root out-of-plane bending moment at time step i of one of the blades, and $\bar{M}_{out}$ is the mean steady state blade root out-of-plane bending moment. The results of the optimization are shown in Figures 3.8 and 3.9 that show the power and load variations, and the steady state pitch actuation, respectively. For all the optimizations, the power output is unaffected. The blade load variations for the two azimuthal optimization points are similar to those of the simple cyclic pitch controller. This is expected because the two pitch optimization points only allow for a 1P varying pitch signal. With additional optimization points, the optimized pitch signal that tries to alleviate the loads caused by the tower shadow, and the blade load variations are further decreased. Inspecting the tower bottom load variations, it is seen that these are smallest when four optimization points are applied. Thus, it appears that applying the complex pitch signal is not beneficial.

3.4 Summary

The results that have been presented for inflow measurement based control for load variation alleviation show that there is indeed a potential for reducing the loads using inflow measurements. The results are summarized below.

- The blade load variations that are caused by the vertical wind shear can be reduced by introducing the suggested yaw misalignment control.
- The load variations on the turbine that are caused by mean wind speed variations can effectively be reduced by feed-forward control based on preview of the inflow, e.g. available from a LiDAR sensor.
- The load variations that are caused by smaller scale effects such as wind shear can be reduced by individual pitch control based on either load or inflow measurements.
- The potential of reducing the load variations using inflow measurements and individual pitch control beyond what is possible with conventional sensors is limited, even when perfect measurements are assumed.
- The performance of individual pitch controllers based on upstream inflow measurements is very sensitive to preview time disturbances. Even small

disturbance will diminish the benefits of using preview measurement in the control system.

- For alleviating load variations that are caused by changing in-plane inflow conditions, such as extreme wind shear, on-blade measurements could potentially of increase load alleviation beyond what is possible with load measurements.

Thus, the primary benefits of applying load variation alleviating control based on inflow measurements are associated with collective pitch control based on preview measurements of the inflow. A similar conclusion is reached in [38]. The conclusion is further supported by the uncertainties relating to measurements from a spinner mounted LiDAR sensor, which are discussed in the following section.

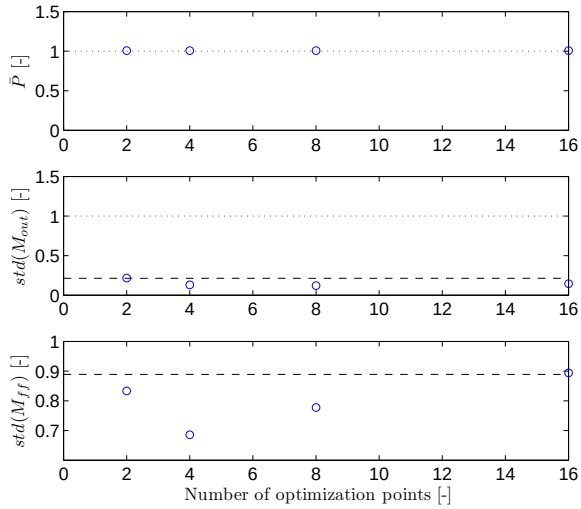

Figure 3.8: Results of load variation minimization by individual pitch control of a stiff version of the NREL 5 MW reference turbine at above rated wind speed (15 m/s and power law vertical wind shear). From the top and down: mean steady state power output, steady state standard deviation of the blade root out-of-plane bending moment, and steady state standard deviation of the tower bottom fore-aft bending moment. All results have been normalized with the results of a simulation with a standard collective pitch controller applied. Results obtained with a simple cyclic pitch controller are shown for comparison (– – –). See Appendix G for details.

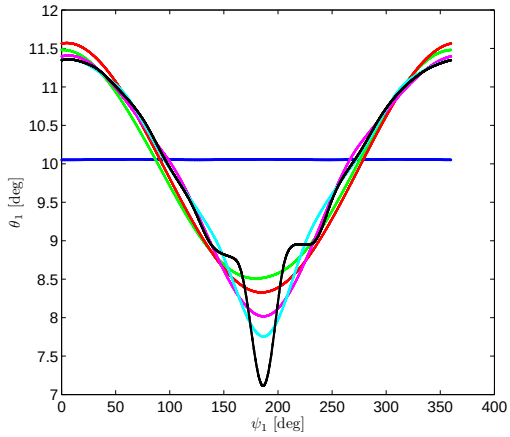

Figure 3.9: The optimized steady state pitch signals for a stiff version of the NREL 5 MW reference turbine. Blue: collective pitch control, green: simple cyclic pitch control, red: 2 optimized pitch angles, magenta: 4 optimized pitch angles, cyan: 8 optimized pitch angles, and black: 16 optimized pitch angles. See Appendix G for details.

Chapter 4

Discussion

In the introduction, potential benefits of applying inflow measurement based control were suggested. Each of the suggested benefits are now discussed on basis of the results that have been presented in this thesis.

4.1 The Potential of Improving the Supervisory Control System

It was suggested to apply upstream inflow measurements to ensure that the turbine is producing power as soon as possible when the wind speed increases from below to above the cut-in wind speed. The typical range of a LiDAR sensor that is used for wind turbine control is approximately equivalent to the rotor diameter. Hence, for a 100 m diameter rotor the preview time is 20 s at a wind speed of 5 m/s. Thus, power production could potentially be initiated 20 s faster than with the conventional sensor if the turbine is equipped with a LiDAR sensor. However, the benefits of initiating the power production 20 s prior to what is possible with the existing system are small because 20 s is a very short period of time compared to the time between cut-in and cut-out.

Furthermore, it was suggested that measurements from a LiDAR sensor can

be used for detecting extreme inflow changes before they arrive at the turbine. Hereby, the turbine can be brought to a safe state, and the extreme load variations that are caused by the inflow event can be eliminated. If the extreme loads can be eliminated, the design loads can be lowered and a turbine can potentially be designed with a lower material consumption. Several results in the literature have demonstrated the benefits of using upstream inflow measurements for alleviating extreme loads during operation. Thus, there is indeed a potential for avoiding extreme loads if the extreme event can be detected by a LiDAR sensor. However, the availability of the measurements from the LiDAR sensor depends and the environment. Some conditions such as heavy rain, snow, dry air, etc, might incapacitate the LiDAR sensor. Thus, the potential benefits of using a LiDAR sensor to avoid extreme loads might diminish, because the design loads can only be lowered if it can be guaranteed that the extreme loads are eliminated. To completely clarify the potential of using LiDAR sensors to avoid extreme loads, the performance of LiDAR sensors in various environments should be thoroughly investigated.

4.2 The Potential of Improving the Closed Loop Controllers

An often mentioned benefit of using inflow measurements in turbine control systems, in particular LiDAR sensors, is the possibility to increase the power capture through improved yaw alignment. The results that have been presented in this thesis show that in non-complex inflow, the inflow direction can be precisely estimated using a spinner mounted LiDAR sensor. However, it is often neglected that the potential benefits of applying LiDAR sensors for yaw control should be assessed by comparing the abilities of the LiDAR sensor to the performance of a well calibrated system. The results that are presented in this thesis and other studies demonstrate that the yaw error of a well calibrated system that is based on conventional sensors is small, and comparable in magnitude to what is expected for a system that is based on a LiDAR sensor. Thus, the primary benefit of LiDAR sensors for yaw alignment is as temporarily mounted sensors for calibration of the existing system. For turbines that are operating in complex inflow it is possible that the effective yaw direction is not the one that can be measured by a traditional sensor mounted on the nacelle. The effective yaw direction might rather be some sort of average of the wind directions in the entire rotor plane. Thus, it is possible that measurements of the flow direction across the entire rotor plane could lead to improved performance. Such measurements could potentially be acquired using a LiDAR sensor. However, it has been shown that LiDAR measurements from a simple scanning pattern in complex inflow are associated with significant uncertainties. Thus, more ad-

vance scanning techniques and algorithms must be developed to apply LiDAR measurements for improved yaw control in complex inflow.

It was suggested that the power capture can be increased by using preview measurements of the inflow for feed-forward collective pitch control aimed at power maximization at below rated wind speeds. However, the results presented in this thesis and results presented by others show that the benefits are small, even in case of rapid wind changes. Thus, the required additional collective pitch actuation cannot be justified by the benefits. In contrast to collective pitch control, it was shown that the power capture can be increased by introducing individual pitch for power maximization at below rated wind speeds with azimuth dependent inflow. The results showed that the required pitch actuation is in-phase with the inflow variation. Thus, it might also be possible to apply individual pitch control based on feed-back from on-turbine sensors and achieve a power increase that is similar to what can be achieved with preview measurements in theory. Using feed-back measurements instead of upstream inflow measurements has the benefit of being independent of Taylor's Hypothesis of frozen turbulence. Therefore, feed-back measurements might lead to better performance in real applications. Controllers for individual pitch control that are based on upstream inflow measurements are expected to be particularly sensitive to the validity of the assumption of frozen turbulence because the controllers are reacting to smaller scale inflow phenomena than the collective pitch controller. Further work could be aimed at assessing the performance difference of using upstream and on-turbine measurements for the power maximizing individual pitch controller.

Results of this thesis and studies by others have shown that feed-forward collective pitch control based on upstream inflow measurement from LiDAR sensors mounted on turbines can effectively decrease both the blade and the tower load variations. Collective pitch control reacts on large scale wind speed changes that are likely to fulfill the assumption of frozen turbulence. Therefore, the benefits of preview collective pitch control demonstrated through simulations are expected to be transferable to real situations, which has also been indicated in experimental studies by others.

Finally, it was suggested to use preview control for individual pitch control for load variation alleviation. The results that have been presented in this thesis and results presented by others indicate that a potential exists for reducing the load variations by applying preview individual pitch control compared to feedback individual pitch control, when frozen turbulence is assumed. However, the real inflow to a wind turbine is not frozen, but evolves. The smaller the scale of the turbulence, the less stationary it is. Individual pitch control is aimed at turbulence scales that are smaller than the rotor diameter. Therefore, it is questionable if the inflow that is measured upstream of the rotor remains

when the measured wind speed reaches the rotor. To overcome the turbulence evolution uncertainties, advanced scanning patterns and model based predictors of the wind speed could be implemented. However, this would complicate the control system, and the estimation would never be perfect.

In this thesis, the potential of using inflow measurements for wind turbine control is assessed under the assumption of 100 % availability of the sensors, which is a bold assumption. Thus, the results represent best case scenarios. To make definite conclusions on the value of inflow measurements for wind turbine control, the measurement availability under different environmental conditions must be further investigated.

4.3 The Limitations and Uncertainties of Inflow Measurement Based Control

The greatest potential benefits of inflow measurement based control were demonstrated for the controllers that exploit preview information, which is available from upstream measurements, i.e. from a LiDAR sensor. However, LiDAR measurements are associated with some uncertainties. These uncertainties can be summarized as:

1. The LiDAR sensor measures wind speeds at a distance upstream of the turbine, and it is assumed that the measured wind speeds travel unchanged towards the turbine with the mean wind speed (Taylor's hypothesis of frozen turbulence). Under this assumption, the wind speeds that are measured upstream reach the turbine with a time delay that is defined as:

$$T_d = \frac{L_p}{V_0}, \tag{4.1}$$

   where L_p is the distance from the LiDAR sensor measurement pattern to the rotor, and V_0 is free wind speed. If Taylor's hypothesis is not valid, the measured wind speeds will arrive disturbed and possibly delayed at the turbine.

2. The LiDAR measurement is a weighted average of the wind speeds in the focal volume. Thus, the frequency content of the inflow that can be resolved using a LiDAR sensor depends on the focal volume.

3. The LiDAR sensor provides an estimate of the wind speed parallel to the measurement beam at a distance in front of the lens. Assumptions regarding the inflow must be made to estimate the axial inflow speed to

the turbine from the wind speed that is measured by the LiDAR sensor. If it is assumed that the flow is perpendicular to the rotor, the axial wind speed can then be estimated as:

$$\tilde{V}_0(\theta_a) = \frac{V_L(\theta_a, \theta_c, F_L)}{cos(\theta_c)}, \tag{4.2}$$

where θ_a is the azimuth angle of the LiDAR beam, θ_c is the cone angle of the LiDAR beam, and F_L is the focal length. Thus, if the true inflow to the turbine is not perpendicular to the turbine or known, the estimation will be erroneous.

4. The LiDAR sensor only provides measurements of the upstream wind speed in conditions where a sufficient amount of airborne particles are present, e.g. very dry conditions might cause low measurement availability.

5. Atmospheric conditions that limits the visibility might cause low measurement availability.

The first of the listed uncertainties is likely to be the most crucial of the uncertainties. The advantages of the preview controllers will diminish if the wind speeds that are measured upstream are not coherent with the wind speeds that reach the turbine. The validity of Taylor's hypothesis for wind turbine applications is investigated through measurements in [39]. It is shown that the hypothesis is valid with a 90% accuracy for eddy length scales in the order of two rotor diameters. In [40], the implications of evolving wind fields for wind turbine control based on circular scan upstream LiDAR measurements are investigated through simulations. It is found that the optimal focal distance is approximately twice the radius of the circular scan. Thus, it appears that the upstream measurements are only valid for slow varying large scale effects. Even if Taylor's hypothesis holds, the transport velocity of the measured wind speeds should be estimated from the measured wind speeds. The measured wind speeds are expected to be associated with uncertainties that will give rise to uncertainties relating to the estimated transport velocity. If the transport velocity is not known exactly, the preview time that is specified for the feed-forward controller cannot be achieved. The influence of preview time disturbances on an individual pitch feed-forward controller was investigated in Appendix E. It was demonstrated that the performance of the controller is sensitive to preview time disturbances.

The implications of the second and third uncertainty are investigated in [41] and in Appendix A. In [41], simulations are used to establish optimal preview distances and cone angles for minimizing the error of the LiDAR measurement. It is shown that cone angles larger than 45 deg should be avoided, and that

for a circular scan with a radius of 75% of the rotor radius of the NREL 5MW reference turbine, the optimal focal distance is approximately 100 meters. The implications of the third uncertainty are also discussed in Appendix A, and it is argued that it is not possible to distinguish between horizontal wind shear and yaw error, and up-flow or down-flow and vertical wind shear when using measurement from a spinner mounted LiDAR. A solution to uncertainty number 3 is suggested in [42] where a more complicated scanning approach is suggested. This approach, however, have not been tested experimentally.

The fourth and fifth uncertainty have not been discussed much in recent literature. However, an implication of these uncertainties is that a LiDAR sensor system cannot be the primary system for estimating the inflow direction. Rather, it can serve as an additional system for improving the performance in situations where the conditions allow for reliable LiDAR measurements.

The inflow could also be estimated using other types of sensors, e.g. blade mounted pitot types [3, 43] and spinner anemometer [4]. Using inflow measurements from blade mounted pitot tubes, the uncertainty of the evolving turbulence is eliminated while maintaining spatially distributed inflow measurements because the flow is measured at the rotating blade. However, no preview is available using pitot tubes. The measurement availability of a pitot tube is not as sensitive to the atmospheric conditions as the LiDAR sensor because it does not rely on optical measurements. However, the holes of the pitot tube may get clocked by dust or ice, and hereby be incapable of providing measurements. Pitot tubes, however, are widely used for a variety of tasks and de-clocking systems have successfully been applied.

A spinner anemometer also provides measurements of the inflow, and is not sensitive to turbulence evolution. However, a spinner anemometer only provides a point measurement of the wind speed and direction Therefore it is mainly useful for yaw alignment, and collective pitch control.

Chapter 5

Conclusions

In this thesis, the potential benefits of inflow measurement based control for increased power production and load variation alleviation have been assessed. The assessment has been based on results that are documented in the existing literature, and on the results that were produced during the thesis work.

The results have shown that poor yaw alignment is not uncommon for operating turbines. Hence, there is a potential for increasing the power capture by improving the yaw alignment. It has been shown that the inflow direction can be accurately estimated using inflow measurements, and that improved yaw alignment is achievable through inflow measurements. However, it has also been demonstrated that the yaw alignment can be considerably improved through calibration of the existing system. Thus, it is concluded that, for the studied turbines the primary benefit of inflow measurements for improved yaw alignment is as temporarily mounted instruments for calibration of the existing system. It should be noted that the presented results relate to turbines that are operating in non-complex inflow.

Through numerical optimization, it has been demonstrated that the potential of increasing the power capture through collective feed-forward pitch control is limited. In contrast, it has been demonstrated that the power output can be increased by applying individual pitch control for power maximization in situations with azimuth dependent inflow. The results demonstrated that the power

output of a turbine that is operating in an idealized half-wake can be increased through independent pitch control compared to collective pitch control.

It has been shown that the blade load variations that are caused by a vertical wind shear can be alleviated by introducing a yaw misalignment angle that depends on the wind speed and the shape of the wind shear. The results have shown that the blade load variations can be alleviated without increasing the yaw actuation rate, but are penalized by increased tower load variations.

The potentials of load variation alleviation through both inflow measurement based collective and individual pitch control have been assessed. Optimization results have shown that there are significant benefits of applying upstream measurements for load alleviating collective pitch control.

For inflow measurement based individual pitch control, simulation results have shown that preview individual pitch control can lead to decreased load variations compared to a control scheme without preview. However, the benefits of applying preview individual pitch control have been shown to be very sensitive to uncertainties relating the estimated inflow.

In summary, it is concluded that, for the studied turbines, inflow measurement based wind turbine pitch and yaw control can lead to the following benefits:

- Increased power capture through elimination of static yaw error at below rated wind speeds
- Increased power capture through individual pitch control at below rated wind speeds
- Decreased load variations through intentional yaw misalignment at above rated wind speeds
- Decreased load variations through preview collective pitch control

Chapter 6

Ongoing and Future Work

The results that have been presented in this thesis have highlighted some of the uncertainties that are associated with inflow measurement based wind turbine control. These uncertainties should be further investigated before inflow measurements can be integrated at a commercial stage in wind turbine control systems. A major issue that could be investigated in further studies is the reliability and availability of inflow measurements in different environments. Furthermore, more advanced scanning patterns and inflow estimation methods should be developed for the LiDAR sensor to eliminate the uncertainties relating to the turbulence evolution and the estimation of the axial velocity from the projected velocity. Also, control methods based on other types of inflow sensors such as pitot tubes and blade mounted LiDARs etc. should be further developed. Finally, the identified potential benefits of applying inflow measurement based control should be confirmed by experiments with active control applied to an operating turbine.

Ongoing research is focused on carrying out field test with a LiDAR sensor mounted in the spinner of the CART3 research turbine at NREL, Colorado USA. Tests will be carried out with LiDAR measurements as input to both a collective and an individual pitch controller, and for wind shear and yaw error estimation. Furthermore, research continuous relating to better inflow estimation and more advanced LiDAR scanning patterns.

Bibliography

[1] T. Burton, D. Sharpe, N. Jenkins, and E. Bossanyi. *Wind Energy Handbook*. John Wiley & Sons, Ltd, 2001.

[2] J.H. Laks, L.Y. Pao, and A.D. Wright. Control of wind turbines: Past, present, and future. In *proceedings of American Control Conference*, pages 2096 –2103, St. Louis, June 2009.

[3] Helge Aagaard Madsen, Christian Bak, Uwe Schmidt Paulsen, Mac Gaunaa, Peter Fuglsang, Jonas Romblad, Niels A. Olesen, Peder Enevoldsen, Jesper Laursen, and Leo Jensen. The dan-aero mw experiments. final report. Risø Report Risø-R-1726(EN), Risø, 2010.

[4] T. F. Pedersen, L. Vita, N. N. Sørensen, and P Enevoldsen. Operational experiences with a spinner anemometer on a mw size wind turbine. In *Proceedings of EWEC*, Brussels, April 2008.

[5] M. Harris, D. J. Bryce, A. S. Coffey, D. A. Smith, J. Birkemeyer, and U. Knopf. Advance measurement of gusts by laser anemometry. *Journal of Wind Engineering and Industrial Aerodynamics*, 95(12):1637 – 1647, 2007.

[6] E. Dakin, M. Priyavadan, and A Hopkins. Catching the wind, an update on improved yaw alignment. In *Proceedings of EWEA*, Brussels, March 2011.

[7] T. Mikkelsen, K. Hansen, N. Angelou, M. Sjöholm, M. Harris, P. Hadley, R Scullion, G. Ellis, and G. Vives. Lidar measurements from a rotating spinner. In *proceedings of EWEC*, Warzaw, April 2010.

[8] N. Angelou, T. Mikkelsen, K. H. Hansen, M. Sjöholm, and M. Harris. Lidar wind speed measurements from a rotating spinner (spinnerex 2009). Risø-r-1741(en), Risø-DTU, August 2010.

[9] David Schlipf. Field testing of feedforward collective pitch control on the cart2 using a nacelle-based lidar scanner. In *Proceedings of The Science of Making Torque from Wind*, Oldenburg, October 2012.

[10] A Rettenmeier, D Schlipf, I Wurth, P W Cheng, A Wright, P Fleming, A Scholbrock, and P Veers. Power performance measurements of the nrel cart-2-wind turbine using a nacelle-based lidar scanner. In *In Proceedings of ISARS2012*, Boulder, USA, June 2012.

[11] A. Pena and C. B. Hasager. Remote sensing for wind energy. Risø-i-3068(en), Risø-DTU, May 2010.

[12] T. Mikkelsen, N. Angelou, K. Hansen, M. Sjöholm, M. Harris, C. Slinger, P. Hadley, R. Scullion, G. Ellis, and G. Vives. A spinner-integrated wind lidar for enhanced wind turbine control. *Wind Energy*, pages n/a–n/a, 2012.

[13] D Schlipf, S Kapp, J Anger, O Bischoff, M Hofsaß, A Rettenmeier, and Martin Kuehn. Prospects of optimization of energy production by lidar assisted control of wind turbines. In *Proceedings of EWEA*, Brussels, March 2011.

[14] K E Johnson, L J Fingersh, M J Balas, and L Y Pao. Methods for increasing region 2 power capture on a variable-speed wind turbine. *Journal of Solar Energy Engineering*, 126:1092–1100, 2004.

[15] B Boukhezzar, H Siguerdidjane, and M Maureen Hand. Nonlinear control of variable-speed wind turbines for generator torque limiting and power optimization. *Journal of Solar Energy Engineering*, 128:516–530, 2006.

[16] TK Barlas and GAM van Kuik. Review of state of the art in smart rotor control research for wind turbines. *Progress in Aerospace Sciences*, 46(1):1–27, 2010.

[17] E. A. Bossanyi. Wind turbine control for load reduction. *Wind Energy*, 6(3):229–244, 2003.

[18] E. Bossanyi, B. Savini, M. Iribas, M. Hau, B. Fischer, D. Schlipf, T. van Engelen, M. Rossetti, and C. E. Carcangiu. Advanced controller research for multi-mw wind turbines in the upwind project. *Wind Energy*, 15:119–145, 2012.

[19] Fiona Dunne, Lucy Y. Pao, Alan D. Wright, Bonnie Jonkman, and Neil Kelley. Adding feed forward blade pitch control to standard feedback controllers for load mitigation in wind turbines. *Mechatronics*, 21(4):682–690, 2011.

[20] D. Schlipf, D.J. Schlipf, and M. Kühn. Nonlinear model predictive control of wind turbines using lidar. *Wind Energy*, 2012.

[21] E. A. Bossanyi. Individual blade pitch control for load reduction. *Wind Energy*, 6:119–128, 2003.

[22] E. A. Bossanyi. Further load reductions with individual pitch control. *Wind Energy*, 8:481–485, 2005.

[23] T G van Engelen and E L van der Hooft. Individual pitch control inventory. Technical Report ECN-C-03-138, ECN, 2005.

[24] TJ Larsen, HA Madsen, and K Thomsen. Active load reduction using individual pitch, based on local blade flow measurements. *Wind Energy*, 8:67–80, 2005.

[25] M Hand, A Wright, L Fingersh, , and M Harris. Advanced wind turbine controllers attenuate loads when upwind velocity measurements are inputs. In *In Proceedings of the 44th AIAA Aerospace Sciences Meeting and Exhibit. January*, 2006, Reno.

[26] David Schlipf, Simone Schuler, Patrick Grau, Frank Allgöwer, and Martin Kuehn. Look-ahead cyclic pitch control using lidar. In *Proceedings of The Science of Making Torque from Wind*, Heraklion, June 2010.

[27] J Laks, L Y Pao, E Simley, A Wright, N Kelley, and B Jonkman. Model predictive control using preview measurements from lidar. In *Proceedings of 49th AIAA Aerospace Sciences Meeting including the New Horizons Forum and Aerospace Exposition, Orlando, Florida, January*, 2011.

[28] Jason Laks, Lucy Pao, Alan Wright, Neil Kelley, and Bonnie Jonkman. The use of preview wind measurements for blade pitch control. *Mechatronics*, 21(4):668–681, 2011.

[29] M. O. L. Hansen. *Aerodynamics of Wind Turbines.* James & James, 2000.

[30] H. A. Madsen, N. N. Sørensen, and S. Schreck. Yaw aerodynamics analyzed with three codes in comparison with experiment. In *41st Aerospace Sciences Meeting and Exhibit*, Reno, January 2003.

[31] B Noura, I Dobrev, R Dizene, F Massouh, and S Khelladi. Experimental study of yawed inflow around wind turbine rotor. In *Proceedings of the Institution of Mechanical Engineers, Part A: Journal of Power and Energy*, 2012, 226: 664–676.

[32] A.D. Wright, P.A. Fleming, and J.-W. van Wingerden. Refinement and tests of an advanced controller to mitigate fatigue loads in the controls advanced research turbine. In *Proceedings of 49th AIAA Aerospace Sciences*

Meeting including the New Horizons Forum and Aerospace Exposition, Orlando, January 2011.

[33] P. A. Fleming, A. D. Wright, L. J. Fingersh, and J.-W. van Wingerden. Resonant vibrations resulting from the reengineering of a constant-speed 2-bladed turbine to a variable-speed 3-bladed turbine. In *Proceedings of 49th AIAA Aerospace Sciences Meeting including the New Horizons Forum and Aerospace Exposition*, Orlando, January 2011.

[34] F. Zahle and N.N. Sørensen. Characterization of the unsteady flow in the nacelle region of a modern wind turbine. *Wind Energy*, 14(2):271–283, 2011.

[35] K. A. Kragh, M. H. Hansen, and T. Mikkelsen. Precision and shortcomings of yaw error estimation using spinner based lidar. *Wind Energy*, 2012.

[36] Gunner C. Larsen, Helge Aa. Madsen, Ferhat Bingöl, Jakob Mann, Søren Ott, Jens N. Sørensen, Valery Okulov, Niels Troldborg, Morten Nielsen, Kenneth Thomsen, Torben J. Larsen, , and Robert Mikkelsen. Dynamic wake meandering modeling. Technical Report Risø-R-1607(EN), Risø, 2007.

[37] T. J. Larsen. How 2 hawc2, the user's manual. Risø-r-1597(ver. 3-9)(en), Risø-DTU, September 2009.

[38] E A Bossanyi, A Kumar, and O Hugues-Salas. Wind turbine control applications of turbine-mounted lidar. In *Proceedings of The Science of Making Torque from Wind*, Oldenburg, October 2012.

[39] D Schlipf, D Trabucchi, O Bischoff, M. Hofsäß, J Mann, T Mikkelsen, A Rettenmeier, J J Trujillo, and M Kühn. Testing of frozen turbulence hypothesis for wind turbine applications with a scanning lidar system. In *Proceedings of International Symposium for the Advancement of Boundary Layer Remote Sensing*, 28 - 30 June, 2012, Paris.

[40] E Simley, L Y Pao, N Kelley, B Jonkman, and R Frehlich. Lidar wind speed measurements of evolving wind fields. In *Proceedings of the 50th AIAA Aerospace Sciences Meeting Including the New Horizons Forum and Aerospace Exposition*, Nashville, January 2012.

[41] E. Simley, L.Y. Pao, R. Frehlich, B. Jonkman, and N. Kelley. Analysis of wind speed measurements using continuous wave lidar for wind turbine control. In *Proceedings of the 49th AIAA Aerospace Sciences Meeting Including the New Horizons Forum and Aerospace Exposition*, Orlando, January 2011.

[42] Stefan Kapp. A five-parameter wind field estimation method based on spherical upwind lidar measurements. In *Proceedings of The Science of Making Torque from Wind 2012*, Oldenburg, October 2012.

[43] H A Madsen and A Fischer. Wind shear and turbulence characteristics from inflow measurements on the rotating blade of a wind turbine rotor. In *Procedings of EWEC*, Marseille, March 2009.

Appendix A

Precision and Shortcomings of Yaw Error Estimation Using Spinner-based Light Detection and Ranging

WIND ENERGY
Wind Energ. (2012)
Published online in Wiley Online Library (wileyonlinelibrary.com). DOI: 10.1002/we.1492

RESEARCH ARTICLE

Precision and shortcomings of yaw error estimation using spinner-based light detection and ranging

Knud A. Kragh, Morten H. Hansen and Torben Mikkelsen

DTU Wind Energy, Technical University of Denmark, Frederiksborgvej 399, 4000 Roskilde, Denmark

ABSTRACT

When extracting energy from the wind using horizontal axis wind turbines, the ability to align the rotor axis with the mean wind direction is crucial. In previous work, a method for estimating the yaw error based on measurements from a spinner mounted light detection and ranging (LIDAR) device was developed and tested. In this study, the simulation parameter space is extended to include higher levels of turbulence intensity. Furthermore, the method is applied to experimental data and compared with met-mast data corrected for a calibration error that was not discovered during previous work. Finally, the shortcomings of using a spinner mounted LIDAR for yaw error estimation are discussed. The extended simulation study shows that with the applied method, the yaw error can be estimated with a precision of a few degrees, even in highly turbulent flows. Applying the method to experimental data reveals an average yaw error of approximately 9° during a period of 2 h, and good correlation is seen between LIDAR-based estimates and met-mast data. The final discussion suggests a number of challenges of the method when applied to measurements in complex flow. Copyright © 2012 John Wiley & Sons, Ltd.

KEYWORDS

wind turbine; LIDAR; yaw error; simulation; experimental

Correspondence

Knud A. Kragh, DTU Wind Energy, Technical University of Denmark, Frederiksborgvej 399, 4000 Roskilde, Denmark.
E-mail: knkr@risoe.dtu.dk

Received 17 March 2011; Revised 30 September 2011; Accepted 13 December 2011

NOMENCLATURE

A	Beam radius
A_r	Projected area of the rotor
$F(\Delta)$	Weighting function
F_s	Sampling frequency of the LIDAR
F_L	Rotational frequency of the LIDAR
H	Hub height
h	Measurement height (height of focal point)
L_f	Focus length
M_x	Blade root bending moment
n	Measurement points per revolution
n_f	Fraction of rotational speeds for the 2D scan pattern
n_s	Number of scans used in running average
$P(h)$	Polynomial fitted to axial velocities
$P_\mathrm{max}^\mathrm{wind}$	Maximum available energy in the wind
P_loss	Energy loss due to yaw error
T_i	Turbulence intensity
T_av	Averaging time
V_0	Free wind speed
V_ax	Axial wind speed

$\bar{V}_{ax}$ Time averaged axial wind speed
$\tilde{V}_L$ LIDAR measurement corrected for the effect of wind shear
$\bar{\tilde{V}}_L$ Time averaged LIDAR measurement corrected for the effect of wind shear
V_{rel} Relative inflow speed
V_{xy} Wind speed in the XY-plane
$\bar{V}_{xy}$ Time averaged wind speed in the XY-plane
α Angle of attack
β Power law exponent
Γ Raleigh length
Δ Distance from focal point
θ_{Err} Estimated yaw error
θ_L Azimuthal angle of the LIDAR
θ_m Measurement angle (cone angle)
θ_{rot} Angular rotation of the wind field
θ_{xy} Measurement angle in the XY-plane
λ Laser wavelength
ξ_{yaw} True yaw error
ρ Density of the air
ϕ_{sh} Shear correction factor
$\bar{\phi}_{sh}$ Time averaged shear correction factor

1. INTRODUCTION

This paper is an extended and updated version of Kragh *et al.*[1] and contains a larger simulation study, experimental results corrected for an undiscovered calibration error, further analysis of the experimental data and a discussion on the shortcomings of using a spinner mounted light detection and ranging (LIDAR) for yaw error estimation.

The ability to align the rotor axis with the mean wind direction is crucial when extracting energy from the wind using horizontal axis wind turbines. This alignment is referred to as the yaw alignment, and the rotational movement of the nacelle around the axis of the tower is the yaw of the turbine. The present trend in yaw alignment control of wind turbines is based on using wind direction measurements from transducers placed atop the nacelle. Hence, the yaw alignment is estimated from the distorted flow behind the rotor plane. The objective of this study is to develop a method for use in yaw alignment control based on recent advances in inflow measurement technology.

Since today's yaw alignment is mainly based on indirect measurements of the incoming wind flow, e.g. wind vanes atop the nacelle, it is expected that the turbine will exhibit some yaw misalignment. With the use of LIDAR technology for measuring the inflow wind speed, it has been demonstrated that it is not uncommon for a wind turbine in normal operation to exhibit a yaw misalignment of 10°.[2]

For a perfectly aligned wind turbine, the theoretical maximum available amount of energy in the wind, P_{max}^{wind}, is defined as follows:[3,4]

$$P_{max}^{wind} = \frac{1}{2}\rho A_r V_0^3 \tag{1}$$

where ρ is the density of the air, A_r is the projected area of the rotor and V_0 is the free wind speed. If the turbine is misaligned by an angle of ξ_{yaw}, the wind speed perpendicular to the rotor plane is reduced to $V_p = V_0 \cos(\xi_{yaw})$. Hence, the available energy is reduced by a factor of $\cos^3(\xi_{yaw})$ (cf. Figure 1(a)). Figure 1(b) shows the theoretical energy loss in percent as a function of the yaw error. From the figure, it is obvious that even for small yaw errors, a considerable amount of energy is lost; for example, at $\xi_{yaw} = 10°$, approximately 5% of the available energy is lost. Therefore, improved yaw alignment could have a considerable impact on the turbine power output. Furthermore, the yaw error gives rise to secondary effects; the blades will have varying angles of attack causing dynamic loadings and suboptimal operation.

Wind LIDARs are laser-based devices for measuring the velocity of airborne submicroparticles in the atmosphere. In the planetary boundary layer, these consist of dust, smoke, pollen, and so on. These small particles are carried with the wind at the instantaneous wind velocity. Thus, the measured velocities of the particles are estimates of the true wind velocity. The velocity of the particles is estimated by analyzing the backscatter signature of a laser pointed in the desired measurement direction.[5,6] The advantage of the wind LIDAR measurement method compared with traditional ways of measuring wind velocity is that with the wind LIDAR, it is possible to place the transducer in a fixed position and scan a desired pattern a distance in front of the transducer. It should be noted that the measured velocity is the velocity projected along the LIDAR beam. No information regarding the instantaneous wind direction of the flow can be extracted from a single beam LIDAR measurement.

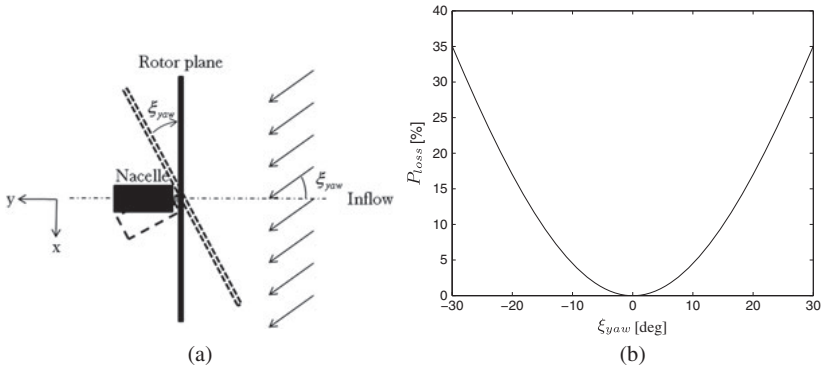

Figure 1. (a) Illustration of yaw misalignment. (b) Power loss in percent as a function of the yaw error, ξ_{yaw}, $P_{\text{loss}} = 1 - \cos^3(\xi_{\text{yaw}})$.

Since inflow estimation is a major concern in relation to modern turbine control, it is appealing to apply LIDARs for direct measurements of the inflow. Methods for using LIDAR inflow measurements for pitch control are suggested in Laks *et al.*[7] and Dunne *et al.*[8] In Laks *et al.*,[7] model predictive control based on LIDAR measurement is applied, whereas three different control strategies are tested in Dunne *et al.*:[8] non-causal series expansion, preview control and optimized finite impulse response filter. Yaw error estimation based on LIDAR measurements is briefly introduced in Mikkelsen *et al.*[2] The experimental capabilities of the LIDAR technology used for inflow measurements have been demonstrated in Mikkelsen *et al.*,[2] Angelou *et al.*[9] and Harris *et al.*[10] in which continuous wave LIDARs were used and mounted in and on the nacelle.

In the present study, simulations are performed using the aeroelastic code developed at Risø-DTU, HAWC2.[11] The turbulence is simulated using Cartesian boxes with Mann turbulence.[12] The wind turbine model used for simulations in this study is of a turbine with a hub height of 59 m and a rated power of 2 MW. A model of a hub mounted LIDAR is implemented in the aeroelastic code and will mimic a continuous wave LIDAR. However, for yaw error estimation in general, a pulsed LIDAR should be equally applicable. The experimental data used in the present study are from a study made by T. Mikkelsen *et al.*[2] in which a LIDAR was mounted in the spinner of a 2 MW turbine.

The paper is organized as follows. First, the implementation of the LIDAR and three different scan patterns in HAWC2 is presented, and then the yaw error estimation method is introduced, followed by simulation and experimental results. Finally, the shortcomings of the introduced method is discussed.

2. LIGHT DETECTION AND RANGING MODEL AND SCAN PATTERNS

The measurements obtained with a continuous wave LIDAR consists of a weighted average of the wind velocity along the measurement beam. The weighting function can be approximated by the Lorentzian function:[13]

$$F(\Delta) = \frac{\Gamma/\pi}{\Delta^2 + \Gamma^2} \tag{2}$$

where Δ is the distance from the focus point along the beam and Γ can be approximated as follows:

$$\Gamma = \frac{\lambda L_{\text{f}}^2}{\pi A^2} \tag{3}$$

where λ is the laser wavelength, L_{f} is the focus length and A is the beam radius at the output lens. In this study, a 1.55 μm laser with a focus length of 100 m and a beam radius of 20 mm is used in the simulations.

The LIDAR model is designed to enable three different scan patterns. Figures 2–4 illustrate the three types of scans. The circular scan pattern shown in Figure 2 is the most simple and can be realized using a single prism for rotating the laser beam around the rotor axis at a given angle. The scan patterns shown in Figures 3 and 4 require a more complex scanner head mechanism, e.g. two steerable prisms.

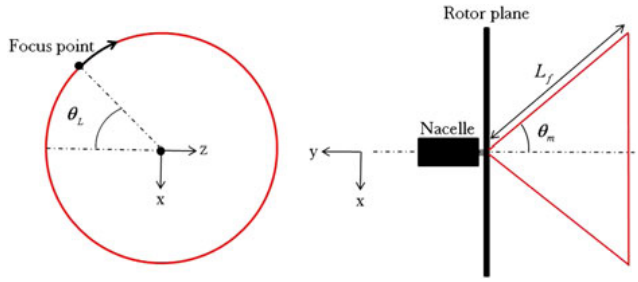

Figure 2. Circular scan pattern, $\dot{\theta}_m = 0$ and $\dot{\theta}_L \neq 0$. Right: top view; Left: view in the direction of the wind.

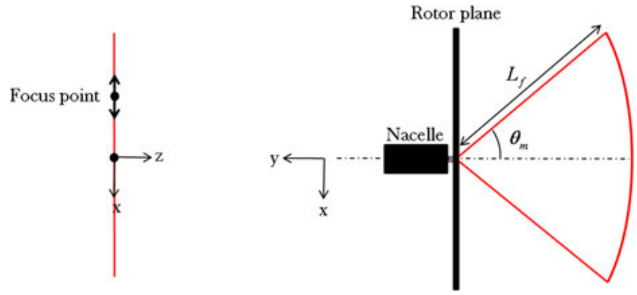

Figure 3. Linear scan pattern, $\dot{\theta}_m \neq 0$ and $\dot{\theta}_L = 0$. Right: top view; Left: view in the direction of the wind.

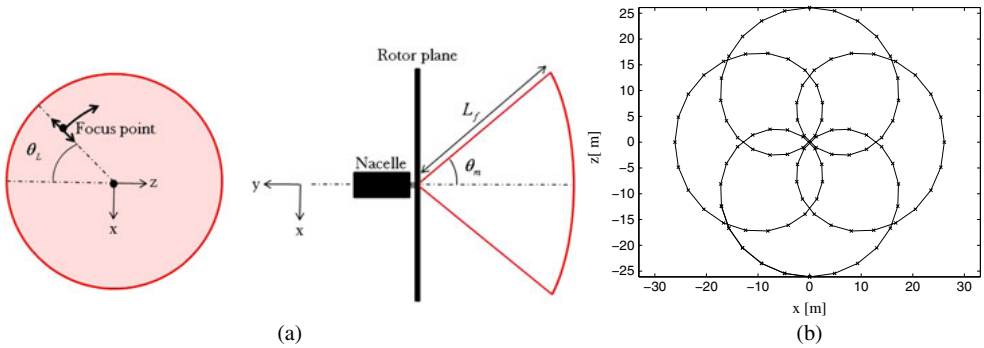

Figure 4. 2D scan pattern. (a) $\dot{\theta}_m \neq 0$ and $\dot{\theta}_L \neq 0$. Right: top view; Left: view in the direction of the wind. (b) 2D scan pattern with $n_f = 5$; the *x*-axis and *z*-axis correspond to the coordinate system defined in Figure 4(a).

For the circular scan pattern, the position of the focus point in the nacelle coordinate system is as follows:

$$(x, y, z) = (-L_f \sin(\theta_m) \sin(\theta_L), -L_f \sin(\theta_m), -L_f \sin(\theta_m) \sin(\theta_L)) \tag{4}$$

where θ_m is constant and θ_L varies at a predefined constant rate $\dot{\theta}_L$. The linear scan pattern is defined as follows:

$$(x, y, z) = (-L_f \sin(\theta_m), -L_f \cos(\theta_m), 0) \tag{5}$$

where θ_m varies at a predefined rate $\dot{\theta}_m$. Finally, a scan pattern composed of two circular scan patterns added together is defined. This pattern will be referred to as the 2D scan pattern. Letting one of the scan patterns rotate n_f times as faster

than the other, measurement points are distributed on a curved surface in front of the turbine. The sum of the measurement angles of the two circular scans yields the total measurement angle span of the curved surface. In the remainder of the study, the measurement angles of the two scan patterns contributing to the 2D pattern are assumed to be equal, and only the sum will be used for characterizing the scan. The scan speed of the 2D scan pattern refers to the azimuthal speed of the slowest of the two scan patterns. In Figure 4(b), an example of a 2D scan pattern with $n_f = 5$ is given. This pattern is used in the remainder of the study.

The three scan types implemented in the HAWC2 code provides n measurements of the line of sight component of the wind, $V_L^i(\theta_m^i, \theta_L^i)$, $i = 1, \ldots, n$, per scan period. The number of measurement points per revolution, n, is defined as follows:

$$n = \frac{F_s}{F_L} \tag{6}$$

where F_s is the sampling frequency of the LIDAR and F_L is the rotational frequency of the LIDAR system (the number of scan periods completed per second).

It is important to notice that it is assumed that the measurements are independent of the aerosol density, since such dependency is not modeled in the turbulence box. Hence, all simulated measurements are ideal measurements. Furthermore, it is assumed that the measurements are not affected by backscatter from other objects than the aerosols. In reality, the measurements might be affected by distant obstacles, such as threes, the ground, snow, rain, and so on.

3. ESTIMATION METHOD

The yaw error is estimated by projecting the line of sight wind speeds into the XY-plane (the horizontal plane at hub height) and then finding the direction of maximum speed. The wind speeds projected into the XY-plane, V_{xy}, are obtained as a function of the in-plane measurement angle, θ_{xy}. For the linear scan, V_{xy} and θ_{xy} correspond to the actual measurements and measurement angles, whereas for the circular and 2D scan, transformations of the measurements are needed. The transformations are given as follows:

$$V_{xy}^i = \frac{V_L^i(\theta_m^i, \theta_L^i)}{\cos(\theta_m^i \cos(\theta_L^i)))}, \quad \theta_{xy}^i = \theta_m^i \sin(\theta_L^i) \tag{7}$$

where V_L^i is the ith wind measurement in the scan pattern and θ_m^i and θ_L^i are the corresponding measurement and azimuthal angles, $i \in [1 : n]$. In a deterministic wind field with no wind shear, the yaw error, θ_{Err}, is then estimated as follows:

$$\theta_{Err} = \arg\max(V_{xy}(\theta_{xy})) \tag{8}$$

3.1. Correction for wind shear

Equation (8) is valid for the linear scan pattern in wind flows both with and without wind shear. However, applying equation (8) directly to the transformed measurements obtained using either the circular or the 2D scan pattern in situations with a vertical wind shear will result in erroneous results. The results will be biased because the measured wind speeds will be a function of both θ_{xy} and the height at which the measurements are sampled. This bias is corrected for by estimating the wind shear relative to the wind speed measured at hub height and removing the effect of the estimated wind shear from the measured wind speeds. The correction factor, $\phi_{sh}(h)$, that will remove the effect of the wind shear is found by relating the vertical wind profile in front of the turbine to the axial wind speed measured at hub height. The wind profile is in this study found by fitting a polynomial, $p(h)$, to the axial wind speeds estimated using the LIDAR measurements. The function, $p(h)$, is a function of the measurement heights. The axial wind speeds are estimated as follows:

$$V_{ax}^i = \frac{V_L^i}{\cos(\theta_m^i)} \tag{9}$$

The measurement height of a particular measurement point, i, relative to the hub is given as follows:

$$h^i = L_f \sin(\theta_m^i) \cos(\theta_L^i) \tag{10}$$

The correction factors are then given as function of measurement height as follows:

$$\phi_{sh}(h) = \frac{p(H)}{p(h)} \tag{11}$$

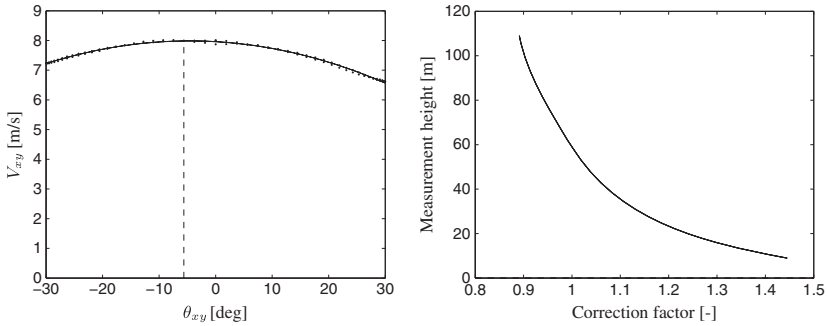

Figure 5. (a) $V_{\mathrm{xy}}(\theta_{\mathrm{m}})$ from the circular scan, corrected for wind shear (power law $\beta = 0.2$); wind speed: 8 m s^{-1}, no turbulence. $-\cdot-$: $V_{\mathrm{xy}}(\theta_{\mathrm{m}})$; $---$: Estimated yaw error. (b) Curve-fitted correction factor, $\phi(h)$.

where H is the hub height. The LIDAR measurements corrected for the wind shear are then given as follows:

$$\tilde{V}_{\mathrm{L}}^{i} = \phi_{\mathrm{sh}}(h^{i}) V_{\mathrm{L}}^{i} \tag{12}$$

Hence, the wind shear is estimated in terms of the wind speed at hub height, and applying equation (12) yields hub height equivalent wind speeds. In Figure 5(b), an example of the curve-fitted correction factors for a power law prescribed wind shear is given. Figure 5(a) shows an example of the described yaw error estimation procedure applied to simulated measurements from a turbine operating in -5° yaw error and with a power law wind shear. The figure shows $V_{\mathrm{xy}}(\theta_{\mathrm{m}})$ calculated using $\tilde{V}_{\mathrm{L}}$, and it is seen that the largest velocity is observed at approximately $\theta_{\mathrm{xy}} = -5^{\circ}$ corresponding to the applied yaw error.

3.2. Averaging in turbulent wind fields

The previously described approach will estimate the yaw error instantaneously in deterministic wind flows. However, in turbulent flows, the measurements will be scattered. Hence, temporal averaging is necessary for both the wind shear and yaw error estimation. The temporal averaging is implemented in the following way: a time-limited running averaging is performed at each measurement point in the scan pattern:

$$\bar{V}_{\mathrm{L}}^{i} = \frac{\sum_{j=1}^{n_{\mathrm{s}}} \tilde{V}_{\mathrm{L}}^{i,j}}{n_{\mathrm{s}}} \tag{13}$$

where n_{s} is the number of scans used in the running average. The values of $\bar{V}_{\mathrm{L}}^{i}$ are transformed to $\bar{V}_{\mathrm{xy}}$ and $\bar{V}_{\mathrm{ax}}$ using equations (7) and (9). The wind shear correction $\bar{\phi}_{\mathrm{sh}}$ is found using $\bar{V}_{\mathrm{ax}}$. The correction is applied to $\bar{V}_{\mathrm{L}}$, and a second-order polynomial is least squared fitted to the corrected values of $\bar{V}_{\mathrm{xy}}$. Finally, the yaw error is estimated as the position of the maximum of the fitted polynomial. The application of the fitted polynomial reduces effects of outliers that are not fully removed by the running average.

For the presented method, it should be noted that the maximum yaw error that can be estimated using the presented method corresponds approximately to the measurement angle, θ_{m}. Since the estimation is based on curve fitting, it might be possible to estimate yaw errors slightly larger than the measurement angle. Furthermore, it should be noted that the averaging defined in equation (13) requires that the measurements are taken in the exact same azimuthal positions during each scanning revolution. In an experimental setting, this is not realistic. Therefore, for experimental results, the measurements have to be binned prior to the averaging. The number of scans, n_{s}, uses in the averaging depends on the desired averaging time, which is investigated in the results section.

4. SIMULATION RESULTS

In Kragh *et al.*,[1] different factors effect on the yaw error estimates was investigated using a 2^{k} factorial simulation design.[14] It was shown that only a subset of the tested factors had significant effect on the yaw error estimates. The significant parameters are given in Table I.

Table I. Factors identified as being significant for the yaw error estimation from Kragh *et al.*[1] T_i, V_0, T_{av}, θ_m and ξ_{yaw} are abbreviations for turbulence intensity, wind speed, averaging time, measurement angle and true yaw error, respectively.

Linear scan	Circular scan	2D scan
T_i	T_i	T_i
V_0, T_{av}	θ_m	V_0, T_{av}
T_{av}	T_{av}	V_0
V_0	V_0	T_{av}
θ_m	θ_m, T_{av}	θ_m
ξ_{yaw}, V_0, θ_m, T_{av}	V_0, θ_m	V_0, θ_m, T_{av}
		ξ_{yaw}, θ_m
		ξ_{yaw}, V_0, T_{av}

Table II. Parameters and parameter space for the extended simulation study.

Parameter	Parameter space	Unit
T_i	[0.01 0.04 0.07 0.1 0.13 0.16 0.19 0.22 0.25 0.28 0.31]	—
V_0	[5 10 15 20 25]	m s^{-1}
θ_m	[15 30]	degrees
ξ_{yaw}	[5 10 15]	degrees
T_{av}	600	seconds

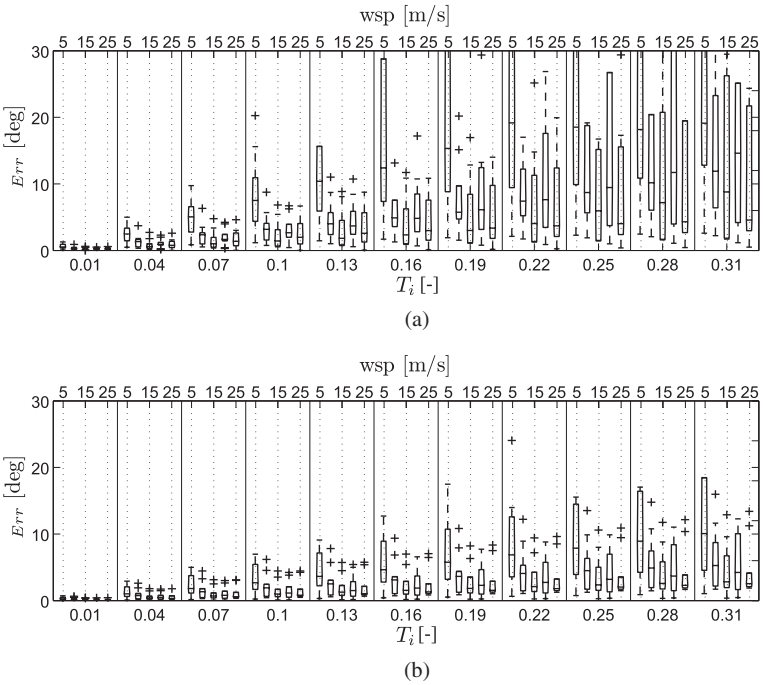

Figure 6. Precision of yaw error estimates using the linear scan pattern, $\xi_{yaw} = 10°$. (a) $\theta_m = 15$; (b) $\theta_m = 30$.

From Table I, it is seen that the significant main factors are T_i, V_0, T_av and θ_m, whereas ξ_yaw is only significant in interaction with one or more of the significant main factors. From Table I, it is also seen that the wind shear does not have any significant effect. Hence, the estimation and correction of the wind shear is reliable. It is also seen that the sampling and scanning frequencies are insignificant. In the remainder of this study, a LIDAR sampling frequency of 50 Hz and a scanning frequency of 0.5 Hz are used. Furthermore, the wind shear exponent is set to $\beta = 0.2$. The conclusions in this section are of course only valid for the applied parameter space.

The influence of the parameters identified as being significant was explored in Kragh *et al.*[1] by expanding the parameter space. The parameter space is now further expanded to include higher levels of turbulence. The parameter space for the present set of simulations is given in Table II. The simulations are carried out using 12 different seed numbers for generating the turbulence boxes. Hence, the simulation series is replicated 12 times.

The results of the simulations are given in Figures 6–8. The figures show box-plots of the precision of the yaw error estimates, $|\xi_\mathrm{yaw} - \theta_\mathrm{Err}|$, obtained using each of the three scan patterns. The precision is shown as function of both turbulence intensity and wind speed. The parameter study and these simulations have shown that ξ_yaw has little influence of the results; therefore, only results from simulations where $\xi_\mathrm{yaw} = 10°$ are presented. The centerlines of the box-plots are the medians of the simulation results, whereas the upper and lower lines represent the 75th and 25th percentiles. The whiskers represents $\pm 2.7\sigma$. Points outside the $\pm 2.7\sigma$ range are considered outliers and are marked by '+'.

Figure 6 shows that for the linear scan, there is a noticeable difference in the precision of the estimates obtained using either the small or large measurement angle. For the narrow measurement angle, it is seen that when the turbulence intensity rises above 0.07, the variance of the precision of the estimates grows rapidly. Especially for the low wind speed cases, the precision of the yaw error estimates becomes poor at increasing turbulence intensity. The reason for this is that at low wind speeds, the $V_\mathrm{xy}(\theta_\mathrm{xy})$ curve is more flat than at high wind speeds. Hence, the estimation of the yaw error is more sensitive. With the use of the large measurement angle, the variances of the precision of the estimates decrease; at the highest level of turbulence intensity, the median precision is below 6°, except for the low wind speed case.

The results for the 2D scan pattern, shown in Figure 7, show the same tendency as with the linear scan; for the narrow measurement angle, the yaw error estimates become unreliable at high levels of turbulence intensity and at low wind

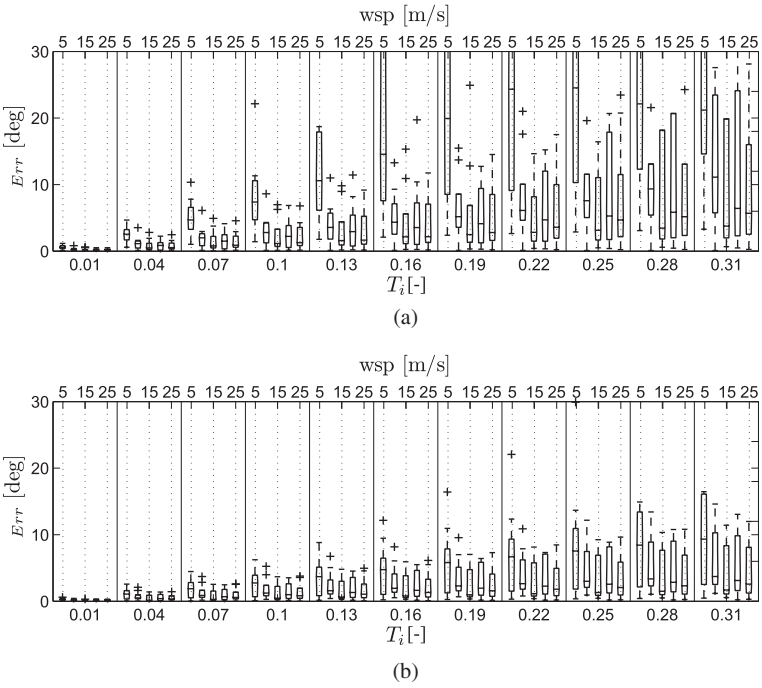

Figure 7. Precision of yaw error estimates using the 2D scan pattern, $\xi_\mathrm{yaw} = 10°$. (a) $\theta_\mathrm{m} = 15$; (b) $\theta_\mathrm{m} = 30$.

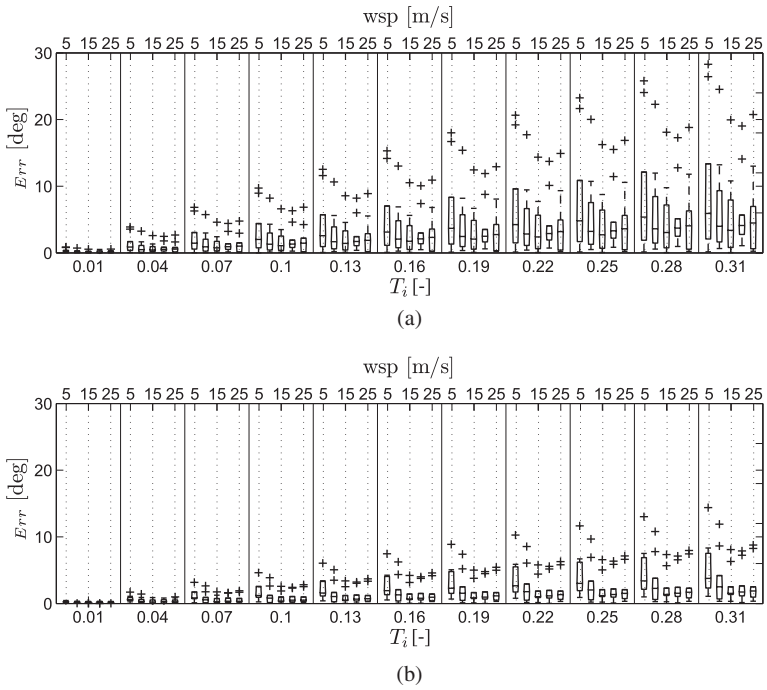

Figure 8. Precision of yaw error estimates using the circular scan pattern, $\xi_{\text{yaw}} = 10°$. (a) $\theta_{\text{m}} = 15$; (b) $\theta_{\text{m}} = 30$.

speeds. For the wide measurement angle, the estimates are more precise, but there is still a large variance in the precisions, especially for the low wind speed cases.

From Figure 8, it is seen that using the circular scan, the precision of the yaw error estimates increases. For the narrow measurement angle, it is seen that the median precision in all case is below 6° and that only a few outliers are above 12°. Furthermore, it is seen that the sensitivity to wind speed seems to be smoothed out compared with the results found using the linear or 2D scan pattern. With the use of the wide measurement angle, it is seen that the median precision in all cases is below 4° and that only a few simulation results are above 6°.

Overall, the results indicate that using the circular scan with the wide measurement angle yields the best estimates of the yaw error. Hence, there seems to be no added benefit of distributing points in the entire rotor plane when estimating the yaw error. However, it should be noted that the expected precisions of the method only relate to the described operating states. Situations with more extreme yaw errors, wake operation and irregular wind shear should be tested to obtain more general conclusions. The results indicate that the LIDAR can be used as a secondary system for fine tuning the yaw, whereas a primary system is needed for extreme direction shifts and during initial alignment of the turbine.

5. APPLICATION TO MEASURED DATA

In the spring of 2009, an experiment was carried out to demonstrate the experimental capabilities of the spinner-based LIDAR.[2,9] During the experiment, a LIDAR was mounted in the spinner of a wind turbine (hub height 59 m). The available data are from a circular scan pattern with a measurement angle of 15°, a sampling frequency of 50 Hz and a rotational frequency of approximately 1 Hz. In Figure 9, the wind speeds measured by the LIDAR during a 2 h period are shown. It is apparent from the figure that a wind shear is present since the measured wind speeds are greatest in the upper part of the measurement circle.

The method for estimating the yaw error based on the circular scan is applied to the measured data. In the simulations, the LIDAR are sampled in the exact same points during each revolution of the LIDAR; this cannot be guaranteed in the experimental case. Therefore, the measurements are binned in azimuth sections of 10°. Temporal averaging is then applied

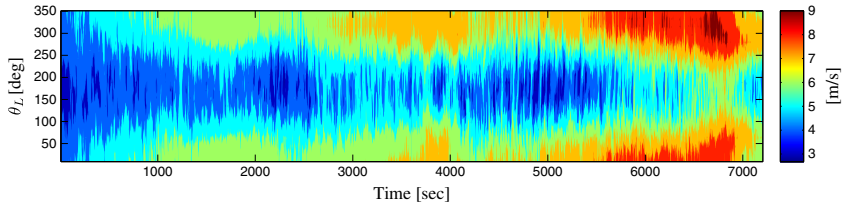

Figure 9. Wind speeds measured by a spinner-mounted light detection and ranging in the spring of 2009; 0° corresponds to the top position of the light detection and ranging.

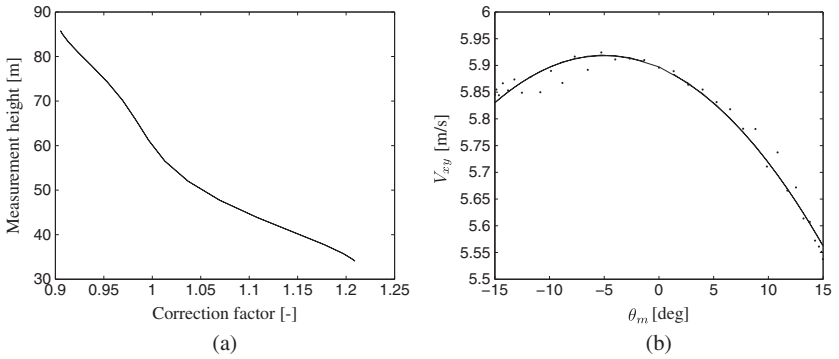

Figure 10. Yaw error estimation method applied to measured data obtained using spinner-based light detection and ranging scanning in a circular pattern. (a) Curve fitted correction factors/estimated wind shear, $\phi(h)$. (b) $\cdots$: $\bar{V}_{\mathrm{xy}}(\theta_{\mathrm{m}})$; —: fitted polynomial.

to the binned velocity measurements according to equation (13), and the shear correction factors are found according to the description in Section 3.1. In Figure 10(a), the shear correction factors found from one specific 10 min averaging period is shown; Figure 10(b) shows the corresponding $\bar{V}_{\mathrm{xy}}(\theta_{\mathrm{m}})$ plot. From Figure 10, it is seen that the measurement points are more scattered than in the simulation study. Figure 11 shows the estimated yaw errors during the 2 h period based on 10, 5 and 2.5 min running averages obtained using the LIDAR measurements and met-mast measurements.

In Kragh *et al.*,[1] poor correlation between the yaw error estimates based on the LIDAR and on the met-mast was observed. Further data analysis revealed an offset error of approximately 17° of the yaw angle sensor system that led to misinterpretation of the dataset. Compensating for the calibration error yielded better correlation; hence, the graphs in Figure 11 are different from the one in Kragh *et al.*[1]

From Figure 11, it is observed that for the slowly varying yaw error estimates, there is good correlation between the estimates based on the LIDAR and on the met-mast. From Figure 11(c), it is seen that the high-frequency yaw error variations estimated using the LIDAR-based method are not correlating with the yaw error estimates from the met-mast. From all three results given in Figure 11, it is seen that even though the results of the two types of yaw error estimates correlated, they differ in magnitude. There can be number of reasons why the poor correlation at high frequency and the offset between the two estimates of the yaw error. First of all, the met-mast is not located at the position of the LIDAR measurements. In addition, the met-mast provides only a point measurement, whereas the LIDAR scans a large area using approximately 50 measurement points per scanning revolution. Finally, if both a horizontal wind shear and a yaw error is present, a bias will be introduced in the yaw error estimate. The influence of different inflow types on the yaw error estimate based on nacelle-mounted LIDARs is the topic of the next section.

6. SHORTCOMINGS OF YAW ERROR ESTIMATION USING SPINNER-BASED LIGHT DETECTION AND RANGING

In the previous sections, it has been shown that a spinner-mounted LIDAR can provide reliable estimates of the yaw error in certain flow conditions. However, the use of a spinner-based LIDAR for yaw error estimation is subject to certain constraints. As stated previously, only situations with varying magnitude of vertical wind shear was considered. However, an

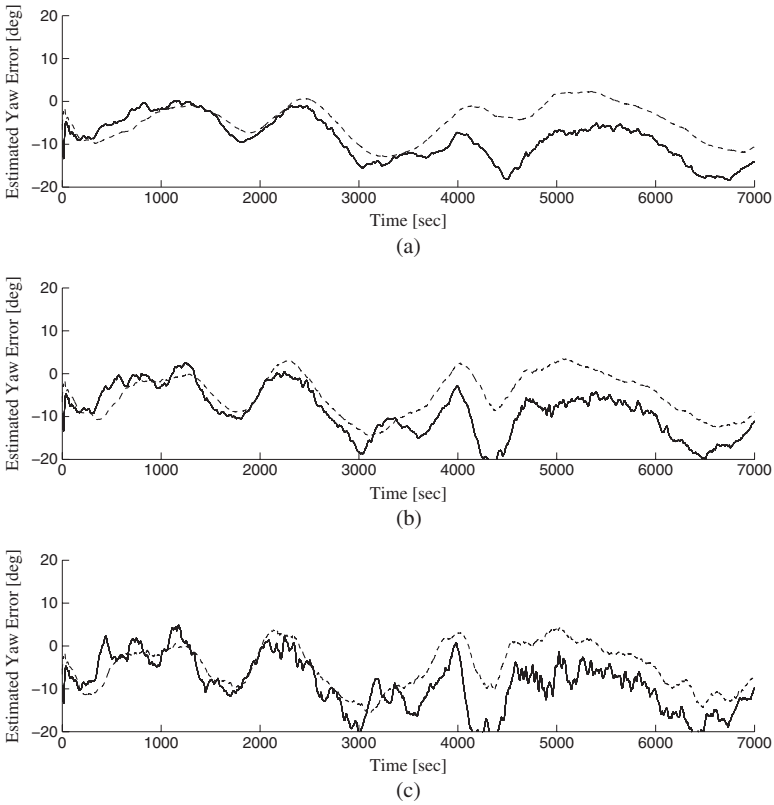

Figure 11. Estimated yaw errors. —: Estimation based on the light detection and ranging measurements. — — —: Estimation based on nacelle yaw angle sensor and met-mast data. The yaw errors are estimated as the average error between the yaw angle and a sensor on the met-mast at 57 m height for averaging periods of (a) 600, (b) 300 and (c) 150 s.

operating turbine might encounter various types of inflow such as a vertical wind shear, a horizontal wind shear, a yawed flow and a sloped inflow; when the turbine is located within a park, wakes might also be present. These types of inflow, of which the first four is the topic of this discussion, will affect the turbine and the LIDAR measurements in different ways.

Figure 12 shows the four different inflow types and the effect of the inflow types on angle of attack, relative velocity, blade root bending moment, true axial velocity and the velocity estimated from the spinner LIDAR measurements. The effects are shown as relative effects; hence, a plus sign in the right half rotor plan indicates that a given parameter has a higher value in the right half rotor plane than in the left half rotor plane and vice versa. The angle of attack and relative velocity are defined as shown in Figure 13.

A yawed inflow will cause a 1P variation in angle of attack and relative velocity that will induce a 1P variation in the blade root bending moment antisymmetric around the horizontal axis of the turbine (cf. Figure 12). The true axial velocity will in this case be constant in the entire rotor plane, whereas the axial velocity estimated from the LIDAR measurements will have a 1P variation antisymmetric around the vertical axis of the rotor.

For a horizontal wind shear, it is again seen from the figure that 1P variations in angle of attack, relative velocity and blade root bending moment arise. This time, however, these variations are antisymmetric around the vertical axis of the rotor. The true axial velocity in this case will have a 1P variation corresponding to the variation in angle of attack, relative velocity and blade root bending moment. The velocity estimated from the LIDAR will have a 1P variation corresponding to variation in the true axial velocity. Recalling that this antisymmetry is similar to the 1P variation expected in the LIDAR measurements for the yawed cases, it is clearly not possible to distinguish between these two inflow types using only the LIDAR measurements. To illustrate the influence of a horizontal wind shear on the yaw error estimates, a series of simulations are performed with increasing horizontal wind shear. In the simulations, it is assumed that the turbine is operating in

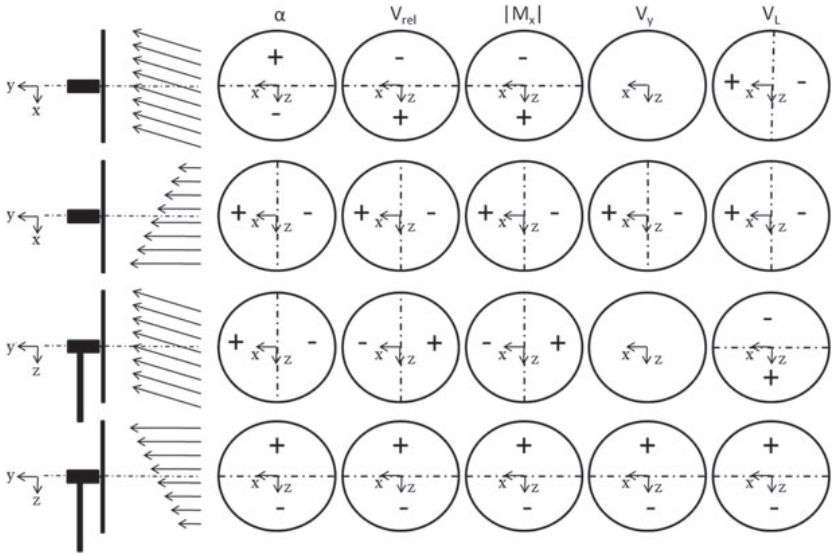

Figure 12. The effects of four types of inflow conditions on angle of attack, relative wind speed, blade root moment, axial velocity and velocity measured by a spinner-based light detection and ranging. From top to bottom: yawed inflow, horizontal wind shear, sloped inflow and vertical wind shear.

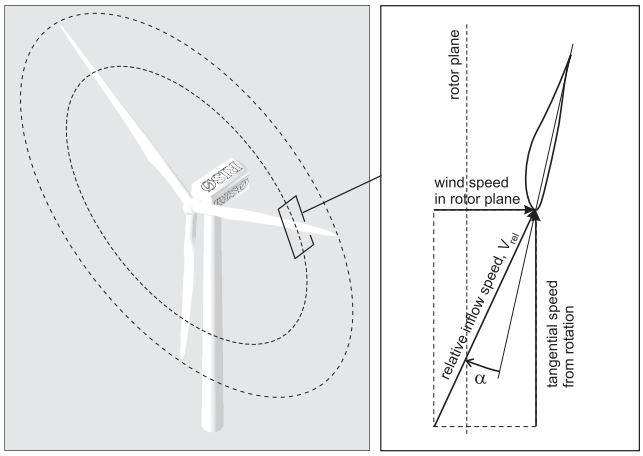

Figure 13. Illustration of the angle of attack and relative velocity at a blade section.

a linear vertical wind shear with a slope of 0.2 m s^{-1} per meter and zero yaw error. A linear horizontal wind shear with a slope from 0–10% of the slope of the vertical shear is gradually applied to the inflow, and the resulting yaw error estimates are plotted in Figure 14. From Figure 14, it is seen that even a small horizontal wind shear compared with the vertical wind shear might corrupt the yaw error estimates. Even though this example is rather academic, it illustrates the problem that might occur if large scale turbulence or nearby objects induce a horizontal wind shear.

For sloped inflow, it is seen that the 1P variations of angle of attack, relative velocity and blade root bending moment are antisymmetric around the vertical axis of the rotor similar to the case with a horizontal shear. Hence, it is not possible

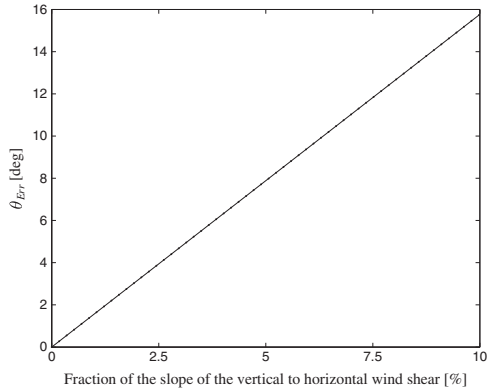

Figure 14. Simulation results from situations with a linear vertical wind shear with a slope of 0.2 m s^{-1} per meter and increasing levels of linear horizontal wind shear. The true yaw error is in all cases zero, and the flow is deterministic. The estimated yaw error is plotted as a function of the fraction between the slope of the horizontal wind shear compared with the vertical wind shear.

to use only the blade root bending moment for distinguishing between horizontal shear and sloped inflow. The true axial velocity in this case is constant in the entire rotor plane, whereas the velocity estimated from the LIDAR measurements has a 1P variation antisymmetric around the horizontal axis.

Finally, for vertical wind shear, the 1P variations in angle of attack, relative velocity and blade root bending moment will be antisymmetric around the horizontal axis. This effect is similar to the one observed for the yawed inflow. Hence, it is not possible to distinguish between a yawed inflow and a wind shear using only the blade root bending moments. The true axial velocity in the case of a wind shear will a have 1P variation antisymmetric around the horizontal axis, as will the velocities estimated using the spinner-based LIDAR. This variation is similar to the one observed for the sloped inflow; thus, it will not be possible to distinguish between a vertical shear and a sloped inflow using only the LIDAR measurements.

As previously stated, it is clear that estimating yaw alignment in complex inflow from either blade root moment or LIDAR measurements alone might lead to erroneous estimates. Similarly, using the LIDAR alone for individual pitch control might be risky since it is not possible to distinguish between the different types of inflow, which requires different types of pitching activity to alleviate loads. A possible solution to the issue could be to combine the LIDAR estimates and blade root bending moment to distinguish between inflow types.

Apart from the aforementioned inflow conditions, also wakes can influence the yaw error estimates and loading on the structure. For situations with wakes, it might be possible to implement an algorithm for wake detection based on the LIDAR measurements and remove the wake effect from the yaw error estimation. Nevertheless, the wake will continue to meander from the point upstream where it was detect until it reaches the rotor. Therefore, the benefits of using information of wakes detected far upstream of the turbine for individual pitch control must be combined with a wake meandering estimator using for example more LIDAR measurement planes.

The previous discussion is based on reflections regarding a spinner-mounted LIDAR scanning in a conical scan pattern using a single beam. A more sophisticated system, e.g. using multiple beam emitted from different positions but with the same focal point, might be able to overcome the aforementioned shortcomings.

7. CONCLUSION

In this study, a method for estimating yaw error developed in previous work was further tested. An extended simulation study was carried out, including higher levels of turbulence intensity. The simulations showed that for all three scan patterns, the widest measurement angle yielded the best results. With the linear and 2D scan pattern, a dependence between wind speed and precision of the estimate was observed. For the circular scan, this dependence was less noticeable. With the use of the widest tested measurement angle, the following median precisions were obtained for the three scan patterns: $< 10°$ for the linear scan pattern but with large variance at low wind speeds, $< 9°$ for the 2D scan pattern but also with large variance at low wind speeds, and $< 4°$ for the circular pattern and with only few outliers above 6°. Hence, no obvious advantages of distributing measurement points in the entire rotor plane was observed for the yaw error estimation. Furthermore, the developed estimation method was applied to data measured on an operating turbine. The results showed a good correlation between yaw errors estimated found using the LIDAR and met-mast data. To develop the method further,

other operating conditions must be tested, a yaw control algorithm developed and experiments with LIDAR-based yaw control performed. Finally, a discussion on the shortcomings of using a spinner-mounted LIDAR for yaw error estimation suggested a number of challenges when applying the method in complex inflow. It was suggested to combine the LIDAR measurements with structural measurements to deal with some of the challenges. All in all, this study gives insights to what can be accomplished in terms of yaw error estimation using spinner-based LIDAR measurement. To assess the potential of implementing a LIDAR-based system for yaw control, more elaborate studies of the current performance of the yaw systems on modern operating turbines must be carried out. Further work will be aimed at assessing the performance of current systems for yaw control.

REFERENCES

1. Kragh KA, Hansen MH, Mikkelsen T. Improving yaw alignment using spinner based LIDAR. In *Proceedings of the 49th AIAA Aerospace Sciences Meeting Including the New Horizons Forum and Aerospace Exposition*. American Institute of Aeronautics and Astronautics, AIAA: Orlando, Fl, USA, 2011.
2. Mikkelsen T, Hansen K, Angelou N, Sjöholm M, Harris M, Hadley P, Scullion R, Ellis G, Vives G. Lidar measurements from a rotating spinner, *Proceedings of EWEC2010*, Warzaw, Poland, 2010. EWEC.
3. Hansen MOL. *Aerodynamics of Wind Turbines*. Earthscan: Oxford, UK, 2000.
4. Burton T, Sharpe D, Jenkins N, Bossanyi E. *Wind Energy Handbook*. John Wiley & Sons, Ltd: Baffins Lane, Chichester, West Sussex, PO191UD, England, 2001.
5. Driggers RG. *Encyclopedia of Optical Engineering—Volume 2 of 3*. CRC: New York, 2003.
6. Mikkelsen T, Mann J, Courtney M, Sjöholm M. Windscanner: 3-D wind and turbulence measurements from three steerable doppler lidars. In *IOP Conference Series: Earth And Environmental Science*, Vol. 1, 2008; U148-U156 (2008). IOP.
7. Laks J, Pao LY, Simley E, Wright AD, Kelley N, Jonkman B. Model predictive control using preview measurements from LIDAR, *49th AIAA Aerospace Sciences Meeting Including The New Horizons Forum And Aerospace Exposition*, Orlando, Fl, USA, 2011.
8. Dunne F, Pao LY, Wright AD, Jonkmann B, Kelley N, Simley E. Adding feedforward blade pitch control for load mitigation in wind turbines: non-causal series expansion, preview control, and optimized FIR filter methods, *49th AIAA Aerospace Sciences Meeting Including The New Horizons Forum And Aerospace Exposition*, Orlando, Fl, USA, 2011.
9. Angelou N, Mikkelsen T, Hansen KH, Sjöholm M, Harris M. LIDAR wind speed measurements from a rotating spinner (spinnerex 2009), 2010. RisøReport, Risø-R-1741(en).
10. Harris M, Bryce DJ, Coffey AS, Smith DA, Birkemeyer J, Knopf U. Advance measurement of gusts by laser anemometry. *Journal of Wind Engineering and Industrial Aerodynamics* 2007; **95**(12): 1637–1647.
11. Larsen TJ. How 2 HAWC2, the user's manual, 2009. RisøReport, Risø-R-1597(ver. 3-9)(en).
12. Mann J. Wind field simulation. *Probabilistic Engineering Mechanics* 1998; **13**(4): 269–282.
13. Pena A, Hasager CB. Remote sensing for wind energy, 2010. RisøReport, Risø-I-3068(EN).
14. Montgomery DC. *Design and Analysis of Experiments*. John Wiley and Sons, Inc.: Hoboken, NJ, 2005.

Appendix B

Potential of Power Gain with Improved Yaw Alignment

WIND ENERGY
Wind Energ. 0000; **00**:1–9
DOI: 10.1002/we

SHORT COMMUNICATION

Potential of Power Gain with Improved Yaw Alignment

Knud A. Kragh, Morten H. Hansen

Department of Wind Energy, Technical University of Denmark, Frederiksborgvej 399, DK-4000 Roskilde, Denmark

ABSTRACT

One of the primary criteria for extracting energy from the wind using horizontal axis upwind wind turbines is the ability to align the rotor axis with the dominating wind direction. The conventional way of estimating the direction of the incoming flow is by using transducers placed atop the nacelle and downwind of the rotor. Recent studies have suggested methods based on advanced upwind measurement technologies for estimating the inflow direction and improving the yaw alignment. In this study, the potential of increased power output with improved yaw alignment is investigated by assessing the performance of a current measurement and yaw control system. The current performance is assessed by analyzing data containing upwind wind speed and direction measurements from a met mast, and yaw angle and power production measurements from an operating offshore wind turbine. The results of the analysis indicate that the turbine is operating with a wind speed dependent yaw error distribution. The theoretical annual energy production loss due to the yaw error distribution of the existing system is estimated to be between 0.1% and 0.2%. Copyright © 0000 John Wiley & Sons, Ltd.

KEYWORDS

Wind turbine; yaw alignment; annual energy production; experimental

Correspondence

knkr@dtu.dk

Received . . .

NOMENCLATURE

$\bar{\theta}_E$	Mean yaw error.
γ	Static calibration of the current system.
ρ	Density of the air.
θ_c	Angular span of the wind directions extracted for the analysis.
$\theta_E^{i,j}$	Yaw error sample from the normal distribution describing the yaw errors at the i'th wind speed bin, $N(\bar{\theta}_E^i, \sigma(\theta_E^i))$.
θ_m	Wind direction measured at hub height at the met mast corrected for the identified calibration error.
θ_t	Measured yaw position of the turbine corrected for the identified calibration error.
θ_E	Yaw error.
θ_{min}^m	The measured wind direction yielding the lowest relative power output of turbine B9.
θ_{min}^t	The measured yaw position of turbine A9 yielding the lowest relative power output of turbine B9.
$\tilde{\theta}_m$	Wind direction measured at hub height at the met mast.
$\tilde{\theta}_t$	Measured yaw position of the turbine.
$\tilde{P}_{max}$	Maximum amount of power available from the wind when a yaw error is present.

A_r	Rotor area.
C_p	Power coefficient.
n_b	Number of wind speed bins.
n_i	Number of segments in each wind speed bin.
P_{A9}	Measured power of turbine A9.
$P_{i,j}$	Sample from the normal distribution describing the power output in the i'th wind speed bin, $N(\bar{P}_i, \sigma(P_i))$.
P_{max}	Maximum amount of power available from the wind.
$Q(V_0^i)$	Probability of wind speed V_0^i.
V_0	Free wind speed.
V_p	Wind speed perpendicular to the rotor.
AEP	Annual energy production.

1. INTRODUCTION

The ability to align the rotor axis with the mean wind direction is crucial when extracting energy from the wind using horizontal axis wind turbines. This alignment is referred to as the yaw alignment, and the rotational movement of the nacelle around the axis of the tower is the yaw of the turbine. For a perfectly aligned wind turbine, the maximum available power that can be extracted from the wind is defined as [1, 2]:

$$P_{max} = \frac{1}{2}\rho A_r V_p^3 C_p, \tag{1}$$

where ρ is the density of the air, A_r is the swept area of the rotor, V_p is the wind speed perpendicular to the rotor, and C_p is the power coefficient. For a perfectly aligned turbine, the perpendicular wind speed is equal to the free wind speed, V_0. If the rotor axis of a turbine is not aligned with the free wind direction, the wind speed perpendicular to the rotor plane is reduced to:

$$V_p = V_0 \cos(\theta_E), \tag{2}$$

where θ_E is the yaw error of the turbine. Hence, the maximum amount of power that can be extracted by a turbine operating with a yaw error, θ_E, is

$$\tilde{P}_{max} = \frac{1}{2}\rho A_r (V_0 \cos(\theta_E))^3 C_p. \tag{3}$$

Thus, the extractable power is reduced by a factor of $\cos^3(\theta_E)$. Experimental results, however, suggest that the actual reduction is proportional to $\cos^2(\theta_E)$ [3], due to changes in the induced velocities of a yawed wake.

Apart from having an impact on the power production, the yaw alignment of a horizontal axis wind turbine also affects the loads induced on the turbine. The blades of a horizontal axis wind turbine operating with a yaw error will experience variations of angles of attack and relative velocities at a frequency corresponding to the rotational frequency of the rotor. The varying inflow gives rise to varying loads on the blades of similar frequency [4]. However, in this study only the effect of yaw error on the power production is analyzed.

The common three bladed upwind wind turbine does not possess the ability to passively align with the dominating wind direction. Hence, a system for active yaw alignment is needed. The performance of a yaw alignment system depends on the measurement system's ability to estimate the direction of the incoming flow relative to the rotor axis. Currently, the inflow direction is estimated using e.g. wind vanes or sonic anemometers placed atop the nacelle and behind the rotor plane. Since these transducers are placed downwind of the rotor, it is suspected that the flow, in which the transducer is placed, is distorted compared to the flow upwind of the rotor. The magnitude and the sign of the distortion of the point wind direction measurement depends on the point of measurement, i.e. the radial position relative to the rotor disk [5]. The results presented in [5] are from 3D computational fluid dynamics (CFD) simulations in below rated wind speeds, where the flow around the blades is attached as the flow around the blades of pitch regulated turbines. In this study, an active stall-regulated turbine is studied, and it is expected that the flow distortions behind a stalled rotor will be even more outspoken

Wind Energ. 0000; **00**:1–9 © 0000 John Wiley & Sons, Ltd.
DOI: 10.1002/we
Prepared using weauth.cls

than for a turbine operating with attached flow. Therefore, the results that are presented in this study indicate a worst-case scenario of what can be accomplished with modern turbines that are primarily operating in un-stalled conditions.

The performances of existing yaw systems are indicated in several studies where advanced measurement systems are applied for a period of time [6, 7, 8, 9, 10]. The results in [6, 7, 8] show that the observed yaw error is varying with some spreading around a mean offset. In [9], it is shown that the mean offset varies with wind speed. In [10], a nacelle mounted LiDAR is used for estimating the yaw error on a well calibrated onshore prototype turbine. It is found that for this particular turbine the static yaw error is small and power capture can primarily be increased by minimizing the dynamic yaw error. Furthermore, a study of the yaw error of an experimental pitch regulated turbine shows that the magnitude of the yaw error depends on the rotor speed [11]. In the investigated rotor speed range, it is shown that the mean yaw error varies from approximately 0 degrees at standstill to approximately 15 degrees at rated rotational speed. Hence, existing studies indicate that significant yaw errors can be observed for operating turbines and that static yaw errors might be eliminated through calibration.

In recent literature, different approaches for improving the inflow direction estimation using advanced measurement technologies have been suggested. It has been shown that upwind wind speed measurements can be obtained from a spinner mounted LiDAR [6, 7]. Different methods for estimating the yaw error from the spinner LiDAR measurements are tested and the shortcomings of such a system are discussed in [8]. It is shown through simulations that for a certain spinner LiDAR configuration, the yaw error can be estimated with a median precision of less than two degrees in low turbulent flow, and less than four degrees in highly turbulent flows. The use of a pulsed LiDAR for yaw error estimation is suggested in [10], and a sonic anemometer mounted on the spinner is suggested in [9] for e.g. improved yaw alignment. The use of a pulsed LiDAR for yaw error estimation and control is tested in [12] on an operating turbine, and increased power production compared to the original unvalidated system is observed.

The above suggested methods for improving yaw alignment require installation of additional equipment resulting in increased cost and system complexity. If the added cost and complexity are justifiable depends on the potential advantages of the advanced measurement systems. The focus of this study is on assessing the potential of increased power production through improved yaw alignment. Advanced measurement systems might also enable advanced speed and pitch/flap control for load alleviation as discussed in several research papers [10, 13, 14, 15, 16]. Hence, the added system cost should be justified by the combined advantages of increased power capture and load reduction.

The objective of this study is to investigate the yaw alignment performance of an offshore mega watt (MW) size, three bladed, upwind turbine, and assess the potential of increasing the power production by improving the yaw alignment. The yaw alignment performance of the case turbine is assessed by analyzing a multi-year dataset including measurements from both the case turbine and a nearby meteorological mast (met mast). Because the present study is only based on data from one particular turbine, the conclusions of this study will only relate to this particular turbine. However, the results will indicate what in general can be accomplished with the existing technology in inflow conditions similar to those of the case turbine. Compared to the studies presented in [6, 7, 8, 9, 10, 11], the analysis carried out in the present study is based on a larger data set covering the entire normal operating range of the turbine and focus is on what can be achieved with the current system, without introducing additional measurement systems.

The paper is laid out as follows: First, the case turbine and available data is presented, then the performance of the current system is presented. Having established the current state, the potential power increase that can be achieved through improved yaw alignment is assessed. Finally, the results are discussed and conclusion are provided.

2. CASE TURBINE

The case turbine that is used for this study is a Siemens 2.3 MW active stall regulated, three bladed, horizontal axis, upwind turbine with 40 meter blades and a rated wind speed of 13m/s. The turbine is located in the ”Nysted Havmølle park” offshore wind farm owned by DONG Energy, Stadtwerke Lübeck and Pension Danmark. A schematic of the park and corresponding met masts is given in Figure 1. The case turbine is in Figure 1 labeled ”A9” and the met mast used in this study is the mast labeled ”Mast 1”. The distance between the case turbine and the met mast is approximately 200 meters. The details of the yaw controller are undisclosed, however, inspections of the yawing signals reveals a slow acting system.

3. AVAILABLE DATA AND DATA SELECTION

Data is available for the turbine and the met mast in a continuous period from 2004 to 2007. Several data channels are available, but only a subset of the channels are used in this study. The following data channels are used: met mast wind speed and direction measured at hub height, and turbine yaw angle, power production and generator speed. The data is sampled at a sampling rate of 1Hz. To ease the data processing, the data is down sampled to 1 min and 10 min averages.

In the present study, the case turbine is considered as a free standing turbine. To ensure that the inflow to the turbine is not affected by the other turbines in the park, only wind directions which are within a 80 deg cone around the met mast are used, see Figure 2.

From the selected data, the wind distribution is estimated, see Figure 2 that shows the distribution of wind speeds in the wake free sector. It is seen that the predominant wind speeds are around 7-10 m/s, but wind speeds in the range from 0 to 27 m/s are present in the data set. The data presented in Figure 2 will in Section 5 be used for calculating the annual energy production (AEP) of the case turbine. Since the selected data only includes wind speeds from a certain range of wind directions, the calculated AEP will not be completely representative of the actual AEP of the turbine. However, the wind distribution will serve as an example for assessing the power loss of the case turbine due to yaw error.

For assessing the power production and yaw performance of the turbine, data is only selected when the turbine is operating in a normal operational state. Abnormal operational states, such as stand-still or down-rated power production, are identified from flags in the original data set and are discarded prior to the analysis. With the data restrictions relating to wind direction and operational state, the available data is reduced to approximately 7.2 months of data, which are used in the remainder of the paper.

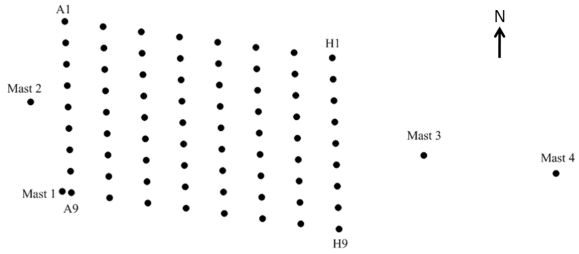

Figure 1. Schematic of the "Nysted Havmølle park" offshore wind farm. The turbines in the park are arranged in a parallelogram where one side is parallel with the north-south direction and the other side with the 277.8 degrees geographical direction. Courtesy of DONG Energy

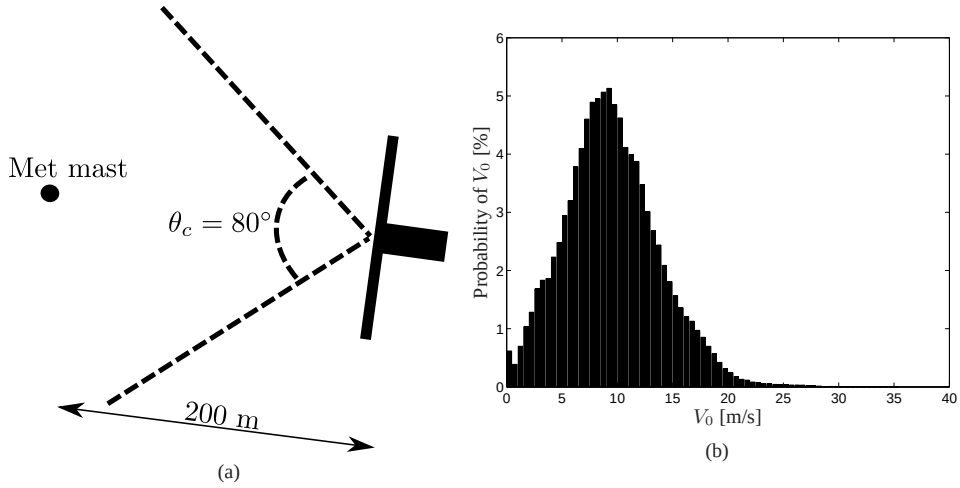

Figure 2. a) Illustration of the wind direction section in which data is collected. The measurement section covers wind directions from 237.5 to 317.5 degrees b) Wind speed distribution calculated from 1 min averages of the selected undisturbed wind speed data from met mast "Mast 1".

Wind Energ. 0000; **00**:1–9 © 0000 John Wiley & Sons, Ltd.
DOI: 10.1002/we
Prepared using weauth.cls

3.1. Calibration of Met Mast Wind Direction and Yaw Position Sensor

The yaw error is estimated using wind direction measurements from a met mast and yaw position measurements from the case turbine. The true mean yaw error can only be found if the static calibrations of the met mast wind direction sensor and the yaw position sensor are known. The calibration errors of the wind direction and yaw position sensor can be estimated from the measured power produced by the B9 turbine which is standing downwind in line with the met mast and the case turbine A9.

The largest difference in power production caused by the wake deficit of one turbine relative to a turbine located further downstream is observed when the free wind direction is parallel to the line connecting the two turbines. This direction is known from the relative locations of the two turbines. The downwind turbine B9 is expected to have the least power output relative to turbine A9 when the free wind direction is 277.8 degrees corresponding to the wind direction parallel to row 9 in the wind farm. The calibration error of the wind direction and yaw position sensor can then be estimated by plotting the power output of turbine B9 relative to turbine A9 as a function of measured wind direction $\tilde{\theta}_m$ and yaw position $\tilde{\theta}_t$, respectively [17]. The power output of turbine B9 relative to turbine A9 is calculated for the 10 min averaged data, and binned in wind and yaw direction bins, see Figure 3(a) and 3(b). The positions of the minimums are found by fitting a 2nd order polynomial to the bin means in the vicinity of the dip in relative power. Hereby, the measured wind direction and yaw position yielding the lowest relative power are:

$$\theta^m_{min} = \arg\min_{\tilde{\theta}_m}(P_{B9}/P_{A9}) = 275.6 \quad \text{deg} \qquad \text{and} \qquad \theta^t_{min} \arg\min_{\tilde{\theta}_t}(P_{B9}/P_{A9}) = 281.9 \quad \text{deg.} \tag{4}$$

It is seen that there is a discrepancy between the calibrations of the two measurement systems. To compensate for the different calibrations, a correction is added to each of the measurements that ensures that the calibrations of both systems are such that zero corresponds to the geographical north. In the remained of the study, only the corrected wind direction and yaw position measurements are used. The corrected wind direction and yaw position measurements are defined as:

$$\theta_m = \tilde{\theta}_m + (277.8 - \theta^m_{min}) \qquad \text{and} \qquad \theta_t = \tilde{\theta}_t - (277.8 + \theta^t_{min}). \tag{5}$$

4. CURRENT PERFORMANCE

The prerequisite for assessing the potential of improving the turbine power production and yaw alignment is knowledge of the existing performance. Figure 4 shows the mean and standard deviation of the 1 min power production data binned according to wind speed. The section of the power curve that can be raised by improved yaw alignment is the section

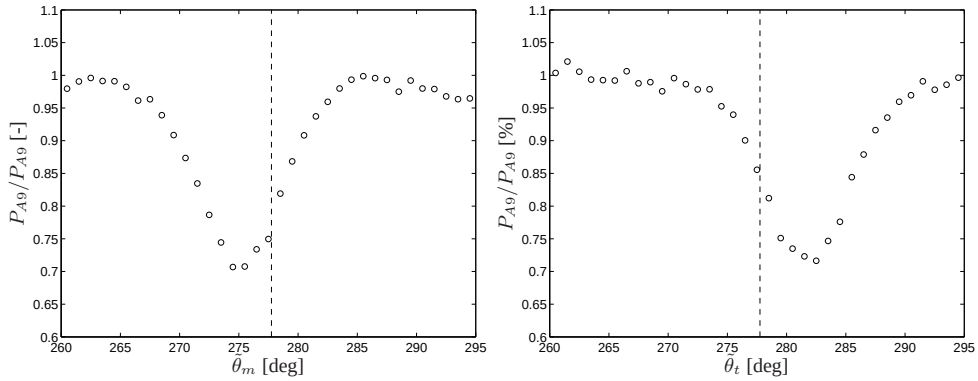

Figure 3. Mean of the 10 minute averaged power production of turbine B9 relative to turbine A9 binned according to met mast wind direction (a) and yaw position (b) in bins of 1 degree widths. – – – indicates the geographical direction from turbine A9 to the met mast, thus the expected position of the minimum.

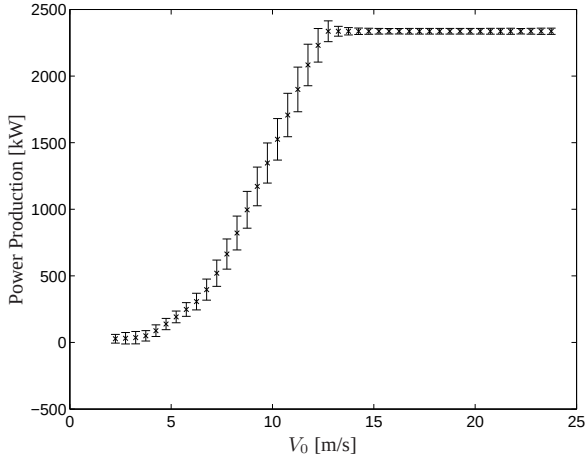

Figure 4. Mean values of the 1 minute averaged power output of the turbine binned according to wind speed. The 1 minute average data is binned in wind speed bins with a width of 0.5 m/s. The error bars represent the standard deviations in the wind speed bins. The presented data is from situations with the turbine operating in a normal operational state and in wind directions within the selected cone, c.f. Figure 2.

below the rated wind speed. At wind speeds above the rated wind speed, the power output is regulated to the rated power and improved yaw alignment will not affect the power output.

The current performance of the yaw alignment system can be assessed by computing the 1 minute averaged yaw error binned on wind speeds. The 1 minute averaged yaw error, θ_E, is estimated as:

$$\theta_E = \theta_m - \theta_t, \tag{6}$$

where it should be noted that the true wind direction in the entire rotor plane is estimated using only a point met mast measurement at hub height. Using wind direction measurements from multiple heights of the met mast would have been favorable, however, wind direction measurements are only available at one height. Figure 5 shows the means and standard deviations of the estimated yaw errors as function of the binned wind speed. The mean yaw error is ranging from -1 deg at 4 m/s to 2 deg at 24 m/s. Zero mean yaw error is achieved at 10 m/s. The standard deviation of the yaw error $\sigma(\theta_E)$ is decreasing with wind speed and is below 5 deg for the operational wind speeds above approximately 5 m/s. Hence, the system is able to keep the turbine aligned around the wind speed dependent mean values, $\bar{\theta}_E(V_0)$. The wind speed dependence of the yaw error observed in Figure 5 is probably due to the swirl of the flow behind the rotor that is expected to depend on both wind speed and rotational speed. BEM theory predicts that the tangentially induced velocities, yielding the swirl, will increase with wind speed below rated and decrease above rated. The wind speed dependency seen in Figure 5 appears similar to the results found for a variable speed turbine in [9], where however the dependency was on both wind speed and rotor speed because the particular turbine operates with variable speed.

5. POTENTIAL OF IMPROVING YAW ALIGNMENT

The aim of this section is to estimate the potential of improving the power production by improving the yaw alignment. The power output of the turbine can be improved in three ways: 1) A static calibration can be added to the yaw controller. This corresponds to moving the curve in the top plot of Figure 5 up and down, thus changing the wind speed at which the turbine has zero mean yaw error. The optimal calibration is expected to depend on the wind speed distribution, and can be found by varying the static calibration and estimating the resulting AEP. 2) The yaw controller can updated with additional sensors for measuring wind direction, e.g. LiDAR, to eliminate the mean yaw error in the entire operating range. 3) The yaw actuation rates can be increased to lower the standard deviation of the yaw error. In the following the potential of the three improvements are estimated based on the estimated wind speed distribution, power curve, and yaw performance.

The AEP of the current system is estimated using the wind speed distribution and the estimated power curve given in Figure 2 and 4, respectively, as:

Wind Energ. 0000; **00**:1–9 © 0000 John Wiley & Sons, Ltd.
DOI: 10.1002/we
Prepared using weauth.cls

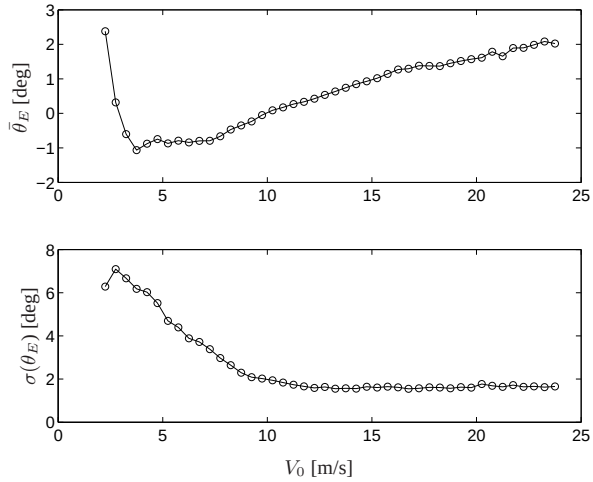

Figure 5. Mean ($\bar{\theta}_E$) and standard deviation ($\sigma(\theta_E)$) of the estimated 1 minute average yaw error of the turbine binned according to wind speed. The data is binned in wind speed bins with a width of 0.5 m/s.

$$AEP = \sum_{i=1}^{n_b} \sum_{j=1}^{n_i} P_{i,j} \tag{7}$$

where n_b is the number of wind speed bins, n_i is the number of 1 minute segments in each wind speed bin, and $P_{i,j}$ are samples from the normal distribution describing the power output in the i'th wind speed bin, $N(\bar{P}_i, \sigma(P_i))$. Hence, it is assumed that the power output in each wind speed bin is normally distributed. The means and standard deviations of the power production in each wind speed bin are found from the data presented in Figure 4. From Figure 4, it is seen that because of the data restriction regarding the operational state of the turbine, no power data is available at very low wind speeds. The power output at wind speeds below the range of the power curve is set to zero. The number of 1 minute segments in each bin is calculated as:

$$n_i = Q(V_0^i)(60 \cdot 24 \cdot 365), \tag{8}$$

where $Q(V_0^i)$ is the probability of the wind speed V_0^i, given by the wind speed distribution presented in Figure 2.

The AEP of the system with zero yaw error across the entire wind speed range is estimated, assuming that the power loss power is proportional to $\cos(\theta_E)^k$, as:

$$AEP^{NL}(\gamma) = \sum_{i=1}^{n_b} \sum_{j=1}^{n_i} \frac{\bar{P}_i}{\cos(\theta_E^{i,j} - \gamma)^k}, \tag{9}$$

where γ is a static calibration of the current yaw controller. Setting $\gamma = 0$ yields the AEP of the current system compensated for the yaw error distribution given in Figure 5. Hence, by varying γ, the AEP of the current system with a static recalibration applied can be estimated. Hereby, the optimal calibration of the yaw controller can be found for the estimated wind speed distribution as the calibration yielding the greatest AEP. It is assumed that the yaw errors in each wind speed bin are normally distributed, and $\theta_E^{i,j}$ are yaw error samples from the normal distribution describing the yaw errors in the i'th wind speed bin, $N(\bar{\theta}_E^i, \sigma(\theta_E^i))$, where $\bar{\theta}_E^i$ and $\sigma(\theta_E^i)$ are given from Figure 5.

For wind speeds above rated, the yaw error is set to zero, because no power output increase is possible above rated wind speeds. In Equation (9), the average power production $\bar{P}_i$ in the i'th bin is used instead of samples from the power production distribution $P_{i,j}$ because it is assumed that the standard deviation of the power production is dependent on the yaw error distribution. In Figure 6, the AEP of the current system relative to the AEP of the system without power loss due to the yaw error distribution is plotted as function of the static recalibration, γ, for $k = 2$ and $k = 3$.

From Figure 6, the potential of the three suggested improvements can be estimated. The potential AEP improvement that can achieved by optimal static calibration of the system can be estimated as difference between the power loss of the current system and the power loss of the optimally calibrated system:

$$\Phi^1 = \max_{\gamma} \left(\frac{AEP}{AEP^{NL}(\gamma)} \right) - \frac{AEP}{AEP^{NL}(0)}. \tag{10}$$

The optimal calibration of the system is estimated by applying a polynomial fit to the data presented in Figure 6. The optimal calibration is estimated to be $\gamma = -0.004$ deg for $k = 2$ and $\gamma = -0.02$ deg for $k = 3$. Thus, it appears that the current static calibration of the system is close to being optimal. Thereby, the theoretical potential of improving the AEP by improving the static calibration is according to Equation (10) $\Phi^1 \cong 0$ for both $k = 2$ and $k = 3$.

The remaining power loss of the system at optimal calibration is then the power loss caused by the wind speed dependence and stochastic variation of the yaw error. Thus, the maximum potential of increasing the power production by removing the wind speed dependence and stochastic variation of the yaw error is:

$$\Phi^{2,3} = 1 - \max_{\gamma} \left(\frac{AEP}{AEP^{NL}(\gamma)} \right). \tag{11}$$

At the optimal static calibration, Equation (11) yields a potential power improvement of 0.1% for $k = 2$ and 0.2% for $k = 3$

In summary, it appears that the yaw system of the case turbine is very well calibrated and that the power output cannot be improved by static recalibration. The results show that the current yaw system is able to keep the rotor closely aligned with the wind direction. This indicates that the implementation of advanced measurement equipment or increased yaw rate can only increase the power capture by a very small amount. Thus, the cost of employing additional measurement equipment should be justified by other benefits of the additional measurement equipment, e.g. pitch control for load alleviation. Finally, it is important to notice that this study is performed on a turbine in offshore and wake-free conditions. For turbines exposed to more complex inflow, the conclusion are likely to be different, and the potential of improving the yaw alignment by used of additional sensors might be greater.

6. CONCLUSIONS

In this study, the current performance of the yaw system of an operating 2.3 MW three bladed upwind offshore wind turbine was analyzed using turbine data and corresponding met mast data. Prior to the analysis, the data was corrected for

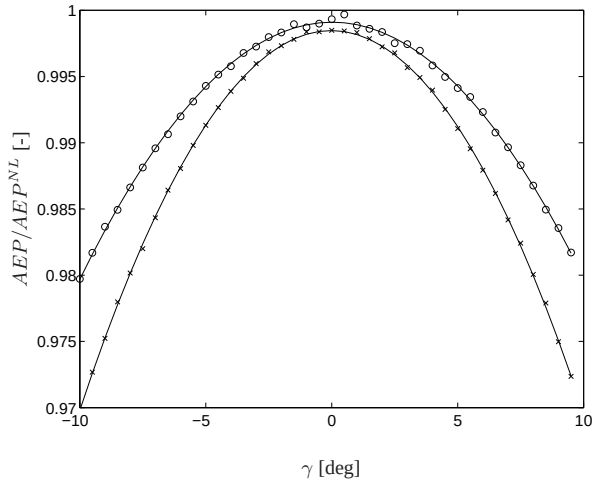

Figure 6. Annual energy production of the current system relative to the annual energy production of the system without yaw error as function of static calibration γ, assuming that the power loss is proportional to $\cos(\theta_E - \gamma)^3$ (x), and $\cos(\theta_E - \gamma)^2$ (o). The solid lines are polynomial fits to the data point.

DOI: 10.1002/we
Prepared using weauth.cls

an identified calibration discrepancy. The results suggest that the turbine is operating in a dynamic yaw error distribution with a slight wind speed dependence. Using the identified yaw error distribution and power curve, an AEP loss of 0.1-0.2% was estimated. The results indicated that the current static calibration of the yaw system is close to optimal. Thus, the majority of the identified AEP loss is due to the wind speed dependent the yaw error distribution. All in all, the study shows that the case turbine is well calibrated, and that the potential of improving the power output beoynd what is possibe with the current system is insignificant.

7. ACKNOWLEDGMENTS

The presented study was made in collaboration with DONG Energy who supplied the data that is the core of the study. Niels Jacob Tarp-Johansen and Leo Enrico Jensen, both employees of DONG energy, are especially acknowledged for their inputs regarding the data processing.

REFERENCES

1. M. O. L. Hansen. *Aerodynamics of Wind Turbines*. James & James, 2000.
2. T. Burton, D. Sharpe, N. Jenkins, and E. Bossanyi. *Wind Energy Handbook*. John Wiley & Sons, Ltd, 2001.
3. H. A. Madsen, N. N. Srensen, and S. Schreck. Yaw aerodynamics analyzed with three codes in comparison with experiment. In *41st Aerospace Sciences Meeting and Exhibit*, 2003.
4. A C Hansen. Yaw dynamics of horizontal axis wind turbines. Technical Report TP-442-4822, National Renewable Enerby Laboratory, 1992.
5. F. Zahle and N.N. Sørensen. Characterization of the unsteady flow in the nacelle region of a modern wind turbine. *Wind Energy*, 14(2):271–283, 2011.
6. T. Mikkelsen, K. Hansen, N. Angelou, M. Sjöholm, M. Harris, P. Hadley, R Scullion, G. Ellis, and G. Vives. Lidar measurements from a rotating spinner. In *Proceedings of EWEC2010*. EWEC, 2010.
7. N. Angelou, T. Mikkelsen, K. H. Hansen, M. Sjöholm, and M. Harris. Lidar wind speed measurements from a rotating spinner (spinnerex 2009). Risø-r-1741(en), Risø-DTU, August 2010.
8. K. A. Kragh, M. H. Hansen, and T. Mikkelsen. Precision and shortcomings of yaw error estimation using spinner based lidar. *Wind Energy*, 2012.
9. T. F. Pedersen, L. Vita, N. N. Sørensen, and P Enevoldsen. Operational experiences with a spinner anemometer on a mw size wind turbine. In *Proceedings of EWEC*, 2008.
10. D Schlipf, S Kapp, J Anger, O Bischoff, M Hofsa, A Rettenmeier, and Martin Kuehn. Prospects of optimization of energy production by lidar assisted control of wind turbines. In *Proceedings of EWEA2011*, 2011.
11. K. A. Kragh and P. Fleming. Rotor speed dependent yaw control of wind turbines based on empirical data. In *Proceedings of the 50th AIAA Aerospace Sciences Meeting including the New Horizons Forum and Aerospace Exposition*, 2012.
12. E. Dakin, M. Priyavadan, and A Hopkins. Catching the wind, an update on improved yaw alignment. In *Proceedings of EWEA*, 2011.
13. F Dunne, L Y Pao, A D Wright, B Jonkman, and N Kelley. Adding feed forward blade pitch control to standard feedback controllers for load mitigation in wind turbines. *Mechatronics*, 21(4):682–690, 2011.
14. J Laks, L Pao, A Wright, N Kelley, and B Jonkman. The use of preview wind measurements for blade pitch control. *Mechatronics*, 21(4):668–681, 2011.
15. E. Bossanyi, B. Savini, M. Iribas, M. Hau, B. Fischer, D. Schlipf, T. van Engelen, M. Rossetti, and C. E. Carcangiu. Advanced controller research for multi-mw wind turbines in the upwind project. *Wind E*, 15:119145, 2012.
16. D Schlipf, S Schuler, P Grau, F Allgower, and M Kuehn. Look-ahead cyclic pitch control using lidar. In *Proceedings of The Science of Making Torque from Wind 2010*, 2010.
17. T. J. Larsen, H. Aa. Madsen, G. Larsen, and K. S. Hansen. Validation of the dynamic wake meander model for loads and power production in the egmond aan zee wind farm. *Journa of Wind Energy*, (Accepted):??, 2012.

Appendix C

Increased Power Capture by Rotor Speed Dependent Yaw Control of Wind Turbines

Increased Power Capture by Rotor Speed Dependent Yaw Control of Wind Turbines

Knud A. Kragh
Ph.D. Student
Department of Wind Energy
Technical University of Denmark
Email: knkr@dtu.dk

Paul A. Fleming
Engineer, Ph.D.
National Renewable Energy Laboratory
Golden, CO, USA
Email: Paul.fleming@nrel.gov

Andrew K. Scholbrock
Engineer
National Renewable Energy Laboratory
Golden, CO, USA

When extracting energy from the wind using upwind horizontal-axis wind turbines, a primary condition for ensuring maximum power yield is the ability to align the rotor axis with the dominating wind direction. Attempts have been made to improve the yaw alignment of wind turbines by applying advanced measurement technologies such as Light Detection and Ranging systems. However, application of advanced measurement equipment is associated with additional costs and increased system complexity. This study is focused on assessing the current performance of an operating turbine and exploring how the yaw alignment can be improved using measurements from the existing standard measurements system. By analyzing data from a case turbine and a corresponding meteorological mast, a correction scheme for the original yaw control system is suggested. The correction scheme is applied to the case turbine and tested. Results show that, with the correction scheme in place, the yaw alignment of the case turbine is improved and the yaw error is reduced to the vicinity of zero degrees. As a result of the improved yaw alignment, an increased power capture is observed for below-rated wind speeds.

Nomenclature

$(\cdot)$	1 minute mean of $(\cdot)$
γ	Power loss of original system compared to corrected system
ω	Rotational speed of the rotor
ρ	Density of atmospheric air
θ^*_{nac}	Wind direction measurement from a nacelle-mounted wind vane corrected for the wind speed dependence
θ_{corr}	Wind direction correction
θ_E	Yaw error
θ^c_E	Median of binned yaw error of the corrected system
θ^{uc}_E	Median of binned yaw error of the uncorrected system
θ_{met}	Wind direction measurement from met-mast at hub height
θ_{nac}	Wind direction measurement from a nacelle-mounted wind vane
θ_{yaw}	Yaw angle of the turbine
ξ	Difference between met-mast and nacelle wind direction measurement
A_r	Swept area of the rotor
C_p	Power coefficient
P_{max}	Maximum amount of power extractable by a turbine
V_0	Free stream wind speed
V_p	Wind speed perpendicular to the rotor plane

1 Introduction

A prerequisite for extracting the maximum possible amount of energy from the wind using horizontal-axis wind turbines is the ability to yaw the turbine, such that the rotor axis is aligned with the dominating wind direction. Hence, accurate measurements of the wind direction must be available to the yaw control system. The present trend of measuring the apparent wind direction on an operating turbine is based on wind vanes or sonic anemometers that are placed atop the nacelle and in the disturbed flow behind the rotor. Transducers that are placed behind the rotor in the disturbed flow, are expected to be significantly affected by rotor-induced flow distortions. Thus, the wind direction measurements are expected to be associated with significant uncertainties. The flow distortions around the nacelle of a wind turbine are studied in [1] using computational fluid dynamics. The study reveals a strong sensitivity of the wind direc-

tion measurement to the transducer position on the nacelle. The effect of the flow distortion has been shown in different field studies. In [2], a study was conducted on an operating 3.6 MW turbine. The study showed that the turbine was operating with a static yaw error of 10 degrees for wind speeds below 20 meters per second (m/s) and 5 degrees for wind speeds above 20 m/s. Yaw errors of similar magnitude were observed in [3, 4], where a 2-MW turbine was studied.

The effect of a yaw error on the power production of a horizontal-axis wind turbine can be assessed by inspecting the expression for the theoretical maximum amount of power that can be extracted from the wind by a turbine. The maximum achievable power is defined in [5] as:

$$P_{max} = \frac{1}{2}\rho A_r V_p^3 C_p, \tag{1}$$

where ρ is the density of the air, A_r is the swept area of the rotor, V_p is the wind speed that is perpendicular to the rotor plane, and C_p is the power coefficient. If a turbine is misaligned by an angle of θ_E, the wind speed that is perpendicular to the rotor plane is reduced to:

$$V_p = V_0 \cos(\theta_E) \tag{2}$$

where V_0 is the free wind speed. Hence, the power that can be extracted by the turbine is reduced by a factor of $\cos^3(\theta_E)$. Experimental results, however, suggest that the power is reduced by a factor of $cos^2(\theta_E)$ [6], which corresponds to a 3% reduction of the power production at a yaw error of 10 degrees.

Apart from affecting the power production, a yaw error will have an effect on the turbine's varying loads. This is especially true for the once-per-revolution (1P) loads.

Different solutions for improving the yaw alignment using advanced measurement techniques have been suggested. In [2], a spinner anemometer, consisting of three sonic sensors is recommended. With a spinner anemometer that is mounted in front of the rotor, the measurements might be less affected by the rotor-induced flow distortion, compared to the measurements from a transducer that is mounted behind the rotor. In [7], different approaches for estimating the yaw error based on a spinner-mounted, continuous-wave Light Detection and Ranging (LiDAR) are explored. Using simulations, the study showed that for a certain spinner LiDAR configuration, the yaw error can be estimated with a median precision of ≤ 4 degrees. In [8], the use of a pulsed LiDAR for yaw error estimation and control was tested on an operating turbine, and researchers observed increased power production caused by the improved measurement system.

The methods suggested in [2, 7, 8] all require installation of additional transducers. However, since [2–4] shows one-sided yaw errors, it might be possible to improve the yaw alignment by applying a correction to the measurements from the existing transducer located on the nacelle. This is the topic of this paper.

The correction scheme is developed by analyzing data from an operating turbine and a nearby meteorological mast (met mast). The case turbine used in this study is the National Renewable Energy Laboratory (NREL) CART3(Controls Advanced Research Turbine 3-Bladed) turbine. The corrections are expected to be correlated with the rotational speed of the rotor. This correlation will be explored and incorporated in a correction scheme for the wind direction measurements from a nacelle-mounted wind direction sensor. In order to test the corrected controller, the CART3 turbine is tested with and without the yaw correction applied to the yaw control system.

The results presented in this paper are an extension of the results presented in [9]. The initial results presented in [9] indicated that the performance of the CART3 turbine was affected by the improved yaw control scheme. However, the amount of data available for the initial analysis was scarce. In this paper, more data is provided along with more definite conclusions. Furthermore, additional analysis was performed to assess the impact of the improved yaw controller on the blade loads.

2 Case Turbine and Site Description

The CART3 turbine is a 600-kilowatt (kW), 3-bladed, variable speed, pitch-controlled, experimental research turbine that is located at NREL's National Wind Technology Center (NWTC) in Boulder, Colorado. The wind rose of the CART3 site is shown in Figure 1 and the turbine is shown in Figure 3. The CART3 was upgraded to include an expanded suite of sensors beyond what a normal commercial turbine would include. Additionally, it uses a custom control system that enables relatively easy software modification for testing experimental controllers [10, 11]. The CART3 began operating in 2011, and will supplement the CART2 in performing controls research. The CART2 is a similar 2-bladed machine that has been used in numerous control studies. A met mast is located approximately 85 meters upstream of the CART3 in the 290 degrees direction that corresponds with the dominating wind direction. The met mast provides wind speed and direction measurements at hub height using a recently calibrated standard cup-anemometer and wind vane. In this study, only hub height measurements of the wind speed and direction were used.

The current yaw control system was designed by Lee Jay Fingersh of NREL. The objective of the yaw controller is to keep the turbine aligned with the dominating wind direction by using periodic corrections of the yaw angle rather than continuous adjustment. The controller is illustrated in Figure 2. The yaw error, which is the difference between the measured wind direction and the yaw angle of the turbine, is measured by a wind vane that is mounted at the rear of the nacelle. The yaw error is filtered by two lowpass filters, one with a time constant of 1 second, and one with a time constant of 60 seconds, thereby producing a fast and slow changing measurement of the yaw error. The fast changing mea-

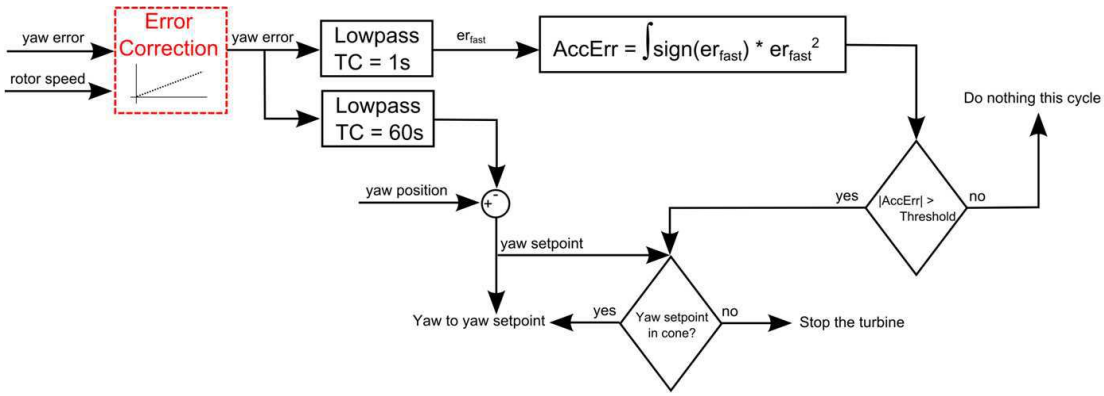

Fig. 2. Schematic of the CART3 yaw controller with rotor speed dependent correction (— — —).

surement of the yaw error is integrated and monitored. When the integrated yaw error (notated AccErr for accumulated error in the figure) reaches a value that corresponds 10 degrees yaw error for 10 minutes (or much less time for larger yaw errors due to the squaring of the error), the yaw angle of the turbine is moved to the location given by the slowly changing measurement of the yaw error. Finally, the CART3 operates within a yaw cone because of difficulties in the yaw system. Hence, prior to yawing, there is a check that the desired location is within the allowable cone. The allowable cone spans from 230 to 360 degrees. In the allowed operating cone, the CART3 is operating free of wakes from other turbines and the met mast is primarily upwind of the turbine.

A schematic of the yaw controller is shown in Figure 2. The correction to the yaw controller that will be described in the following section is indicated in the schematic as a red box.

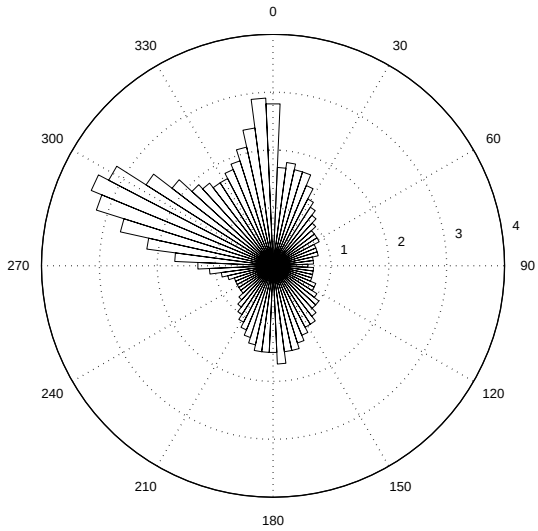

Fig. 1. Wind rose for the CART3 test site. The circles indicate the probability in percent of each wind direction. The predominant wind direction is 292 degrees. The operating cone of the turbine spans from 230 degrees to 360 degrees.

3 Observed Measurement Error

The present yaw controller depends entirely on the wind direction measurements from the nacelle-mounted wind

Fig. 3. CART3 turbine at the NWTC, (NREL Pix no. 18279). The met mast is located approximately 85 meters upwind of the turbine in the 290 degrees direction.

vane. Hence, the performance of the yaw controller is expected to correlate with the accuracy of the wind direction measurements from the wind vane. To assess the performance of the wind direction measurements from the wind vane, measurements from the nacelle wind vane are compared to hub height wind direction measurements from the met mast. The error of the measurements from the nacelle wind vane compared to the met mast measurements is defined as:

$$\xi = \theta_{met} - \theta_{nac}, \tag{3}$$

where θ_{met} is the wind direction measured at the met mast and θ_{nac} is the wind direction measured by the nacelle wind vane. Because this initial assessment is only focused on the performance of the nacelle wind vane, data is extracted from the total pool of data stored for the CART3 independent of underlying turbine controller. Data is extracted for two different types of operation: 1) standstill with a fixed rotor and yaw position, and 2) normal operation. The majority of the available data is around $\omega = 0$ and in the interval $20 \leq \omega \leq 37$ (rpm), with the latter corresponding to the typical operating speeds of the CART3.

To explore the dependence of ξ on the rotor speed, the data is binned in discrete rotor speed bins with widths of 0.5 rpm. The data in each bin is averaged and a linear regression is fitted to the binned data. The binned data and the linear regression is shown in Figure 4. Even though the data is scattered, there is an inclined trend in the binned data, going from approximately 0 degree measurement error at standstill to approximately 15 degrees measurement error at rated rotational speed (37 rpm). Thus, it seems that the turbine anemometer is calibrated at standstill and the inclined trend in the data is likely caused by the rotor-induced swirl of the flow behind the rotor plane. Assuming that the power loss caused by the yaw error is proportional to the observed error at rated speed, the power loss is approximately 6.7% [according to Equation (1) and (2)].

4 Improved Yaw Controller Design

The observed trend in the measurement error of the nacelle mounted wind vane is used for suggesting a rotor speed dependent correction of θ_{nac}. The corrected nacelle wind direction is given as:

$$\theta^*_{nac} = \theta_{nac} - \theta_{corr} \tag{4}$$

where the correction θ_{corr} is defined by the linear regression shown in Figure 4 and given as:

$$\theta_{corr} = -0.67 + 0.43\omega \tag{5}$$

where ω is the rotational speed of the rotor. Equation (4) and (5) constitutes the red box in Figure 2 and has been added to the actual CART3 controller.

5 Experimental Setup and Data Processing

The CART3 turbine is extensively instrumented and data is collected at a sampling rate of 400 hertz (Hz). However, in this study, only a small subset of the available data channels is used. The data used is: yaw position, nacelle wind direction (relative to current yaw position), power output, low speed shaft rotational speed, blade root bending moment of blade number one, and met mast wind speed and direction measured at hub height. To ease data processing, all data is down sampled from 400 to 10 Hz. Since the time constant of the yaw system is well below this value, and the rotational speed of the rotor is less than 0.6 Hz at all times, this down sampling should not remove important information regarding power production, yaw error, or blade root bending moments. To account for the fact that the met mast is located at a distance from the turbine, the available data is split into to 1-minute segments. Hence, it is assumed that the 1-minute average wind speed and direction measured at the met mast represents the wind speed and direction at the turbine. For each 1-minute segment, the mean wind speed, yaw error, rotor speed, power output, and turbulence intensity is calculated. The estimated 1-minute mean yaw error is defined as:

$$\bar{\theta}_E = \bar{\theta}_{met} - \bar{\theta}_{yaw}, \tag{6}$$

where $\bar{\theta}_{met}$ and $\bar{\theta}_{yaw}$ are the 1-minute means of the wind direction measured by the met mast at hub height and the yaw position of the turbine, respectively. Finally, for each 1-minute segment, the 1 Hz damage equivalent blade flap loads

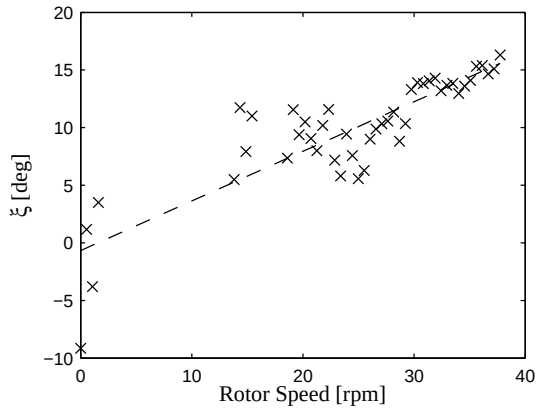

Fig. 4. Observed differences between the nacelle and met mast wind direction measurements as a function of rotor speed. All measurements have been binned in rotor speed bins with a width of 0.5 rpm. x: Binned observations, − − −: Trend line.

(blade DEL) are calculated from the blade root bending moment signal. The damage equivalent loads [12] are calculated using a standard rainflow counting method [13] and a slope of the Wøhler curve of m=10.

Comparing two controllers experimentally is not a trivial task. Ideally, the original and updated yaw controller should be tested in identical inflow conditions. However, since the inflow to a turbine is stochastic, it is not possible to guarantee identical inflow conditions. To overcome the inflow variation challenge, a large amount of data must be gathered and the mean values across the wind speed range must be compared. In this study, the experiment is setup so that the CART3 turbine changes between the original and updated controller every 15 to 30 minutes.

The baseline controller of the CART3 was updated continuously during the commission, leading to changing output and loading characteristics. Thus, since the objective of this study is to assess the effect of improved yaw alignment, only recent data gathered with the current baseline controller is used in the analysis. Because only recent data is used, the amount of data available for the current analysis is small compared to the data used for establishing the correction scheme that contained the total amount of data gathered for the CART3.

An initial analysis of the data collected for the yaw controller comparison revealed that the data collected with the correction in place contained significant parts with high levels of turbulence. Since the data for the uncorrected case did not contain such high levels of turbulence, a direct comparison would not be fair. Therefore, periods with high turbulence intensity ($> 25\%$) have been disgarded. Furthermore, data series with low power production (< 25 kW) have been discarded. The low power production data is removed to ensure that only operating data is analyzed and not standstill or close to standstill data.

The selected 1-minute mean data is sorted in bins according to rotor speed and inflow wind speed. In Figures 5, and 6, the amount of data available in each bin is shown for the cases with and without the correction to the yaw controller applied. The majority of the available data is at a rotational speed around rated (37 rpm). The figures show that only around 10 hours of data is available for the study. This low amount of data is because the CART3 is an experimental turbine that only operates with supervision and is involved in numerous controls studies. Due to the limited amount of data, the conclusions drawn in this study are somewhat uncertain. However, sufficient data is available to indicate the effects of the improved yaw controller on the turbine performance.

The median and standard deviations of the turbulence intensities within each wind speed bin is shown in Figure 7. Even though the average turbulence intensities are not the same for the corrected and uncorrected case, they are within approximately 4% of each other in the entire range.

6 Results

As stated in the introduction, the yaw errors are expected to affect both the power production and the blade loads. Hence, both power production and blade loading data is analyzed in this section. First, however, the corrected controller's ability to align the rotor with the dominating wind direction is assessed.

Figures 8 and 9 show the estimated yaw error as a function of rotor speed and wind speed, respectively. The figures show the medians and standard deviations of the 1-minute segments that are binned in rotor speed and wind speed bins. Using a standard t-test and assuming that the 1-minute segment means are normally distributed and that the means and standard deviations can be estimated using the median and

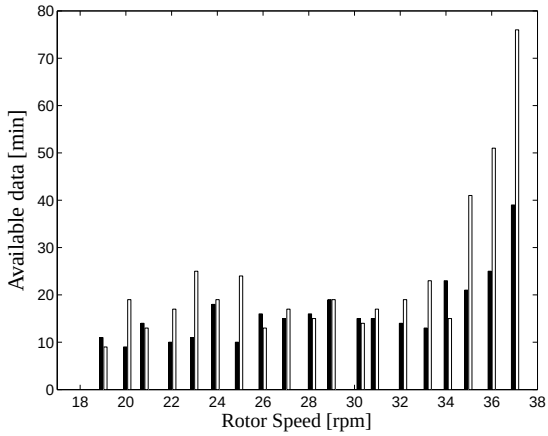

Fig. 5. Amount of data available within each rotor speed bin for the uncorrected yaw controller (black), and the corrected yaw controller (white).

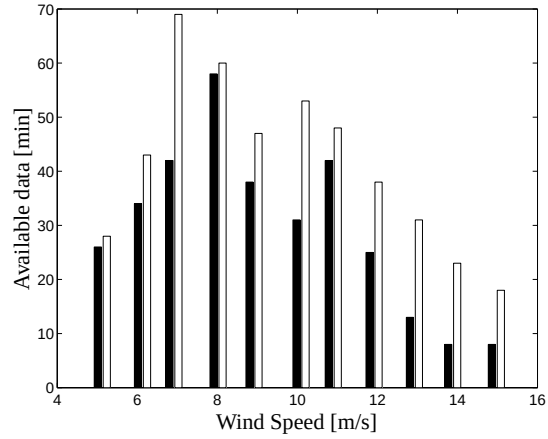

Fig. 6. Amount of data available within each wind speed bin for the uncorrected yaw controller (black), and the corrected yaw controller (white).

standard deviation of each bin, it is tested, for each bin, if the corrected yaw controller yields a significantly lower median yaw error than the uncorrected yaw controller. If an estimated median yaw error at a particular median rotor or wind speed for the corrected controller is significantly lower than the corresponding median yaw error of the uncorrected controller is indicated in the figures. The median is used as an estimate of the true mean of the underlying distribution to decrease the importance of outliers in the data.

In Figure 8, the data covers a range from 18 to 37 rpm. However, the vast majority of the data is collected in the upper part of the range. When comparing Figure 8 to Figure 4, it appears that the median yaw error across the range of Figure 8 is slightly less than what was observed in Figure 4. The rotor speed dependence of the yaw error observed in Figure 4 is not present in the data displayed in Figure 8. However, because most of the data that Figure 8 is based on is located in the upper operating range, it is expected that the slope is less visible. Furthermore, a much larger data set was used to construct Figure 4. In Figure 8, the median yaw errors for the majority of the rotor speeds above 25 rpm are decreased significantly. Without the correction applied, the median yaw error across the rotor speeds was in the range of 10 degrees. With the correction applied, the median yaw error was decreased to below 5 degrees in most of the rotor speed range, and close to zero at rated rotational speed.

In the wind speed domain shown in Figure 9, the median yaw errors are decreased from around 10 degrees across the entire range to around zero in most of the wind speed range when the correction is applied. In the range from 8 to 14 m/s, the median yaw errors are significantly decreased by introducing the corrected yaw controller.

Based on the results observed in Figures 8 and 9, re-

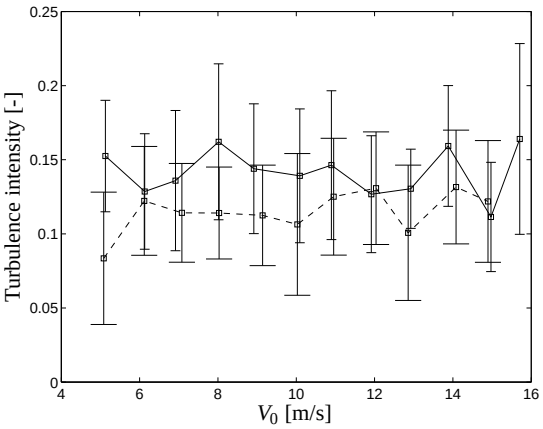

Fig. 7. Median turbulence intensities of the 1-minute segments, binned in bins with a width of 1 m/s for the original yaw controller (− − −), and the corrected yaw controller (—). The whiskers indicate the standard deviation of the turbulence intensities in each bin. Narrow whiskers are for the corrected controller, wide whiskers are for the uncorrected controller.

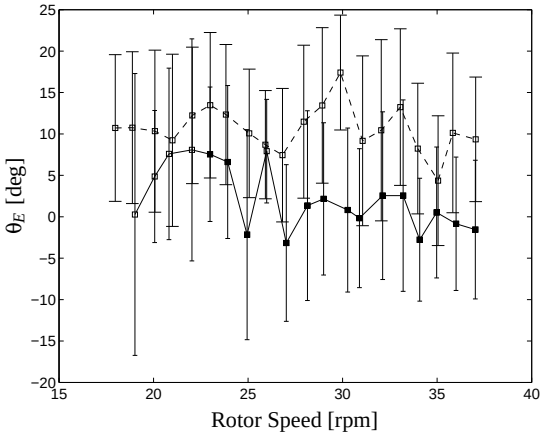

Fig. 8. Medians of the binned 1-minute average yaw errors of the original yaw controller (− − −) and the updated yaw controller (—). Bin widths of 1 rpm. The whiskers indicate the standard deviation of the 1 minute average yaw errors in each bin. The standard deviation is estimated using the median absolute deviation to decrease the influence of outliers. Narrow whiskers are for the corrected controller, wide whiskers are for the uncorrected controller. Solid squares indicate that the value of the corrected controller is significantly lower than the corresponding value of the uncorrected controller—at a level of significance of 95% using the t-distribution.

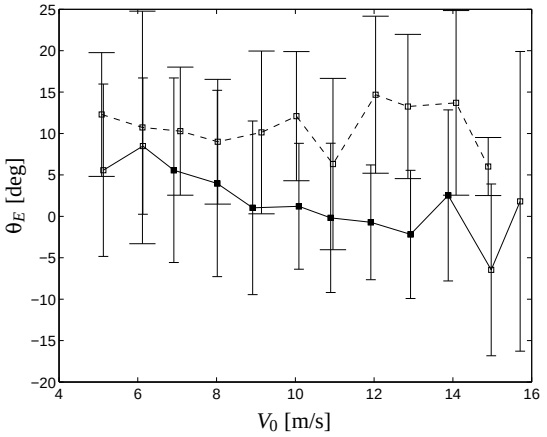

Fig. 9. Medians of the binned 1-minute average yaw errors of the original yaw controller (− − −) and the updated yaw controller (—). Bin widths of 1 m/s. The whiskers indicate the standard deviation of the 1 minute average yaw errors in each bin. The standard deviation is estimated using the median absolute deviation to decrease the influence of outliers. Narrow whiskers are for the corrected controller, wide whiskers are for the uncorrected controller. Solid squares indicate that the value of the corrected controller is significantly lower than the corresponding value of the uncorrected controller—at a level of significance of 95% using the t-distribution.

searchers conclude that the yaw alignment is indeed improved by the corrected yaw controller. Assuming that the power loss that is caused by a yaw error is proportional to $\cos^3(\theta_E)$, the theoretical power loss of the uncorrected controller compared to the corrected controller can be estimated as:

$$\gamma(V_0) = 1 - \cos(|\theta_E^{uc}(V_0)| - |\theta_E^{c}(V_0)|)^3 \qquad (7)$$

where $\theta_E^{uc}(V_0)$ and $\theta_E^{c}(V_0)$ are the median of the binned yaw errors as a function of wind speed for the uncorrected and corrected case, respectively. Figure 10 shows the theoretical median power loss expected of the original system compared to the corrected system; calculated using Equation (7). A power loss of around 3% is expected across the entire wind speed range. However, in the above-rated range, no losses are expected because the turbine in this range is regulated to yield the rated power output.

The true power loss of the original system is assessed by plotting the power output of the corrected and uncorrected controller as a function of wind speed. The data is plotted as the medians and standard deviations of the 1 minute average power output in wind speed bins with a width of 1 m/s. Figure 11 shows the power curves of the corrected and uncorrected controller, respectively. As for the yaw errors, researchers identify the significant power improvements by using a standard t-test and assuming that the 1-minute means are normally distributed. Researchers also assume that the means and standard deviations can be estimated by the medians and standard deviations of the binned values. The power curves presented in Figure 11 indicate that the correction to the yaw controller has a positive effect on the power output. In fact, the median power output at 4 wind speeds is significantly improved with the corrected controller compared to the uncorrected controller.

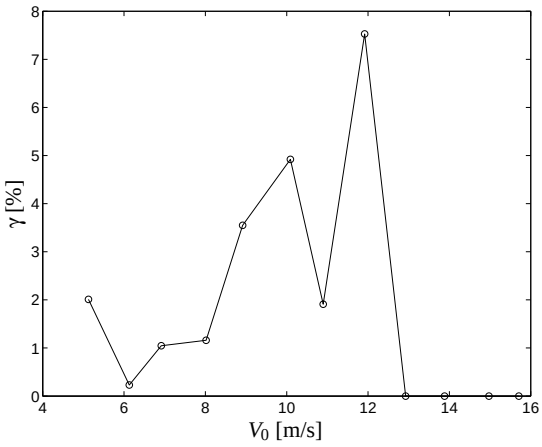

Fig. 10. Theoretical median power loss of the uncorrected system compared to the corrected system in percent, assuming that the power loss caused by the yaw error is proportional to $\cos^3(\theta_E)$.

Figures 10 and 12 show significantly different results. The observed power loss of the original system is much larger that the expected theoretically calculated power loss. The reason for this might because the results presented in Figures 11 and 12 have some uncertainties. For example, the turbulence intensities encountered by the turbine are not exactly the same for the two controllers. In addition, large-scale inflow phenomena might have a significant effect on the power production. The studied wind site is located in an area where extreme wind conditions are common, and because the amount of data is limited, the effects of extreme conditions may not have been completely averaged out. Finally, the wind speeds are only point measurements and might not be representative of the entire rotor plane. Hence, the effective inflow to the rotor might be different than the point measurement. In spite of the uncertainties, the power output is higher for the corrected case than the uncorrected case. Therefore, it is fair to conclude that the correction has a positive effect on the power output. Researchers expect that, with a larger dataset, the observed power loss will converge to the theoretical expectations.

The effect of the correction to the yaw system on the blade loads of the CART3 turbine is assessed by inspecting the 1 Hz damage equivalent blade root loads. Blade root bending moments are usually dominated by 1P variations originating from wind shear, yaw error, and other large turbulence structures. Hence, the variations caused by yaw errors are only one source of the load variations. To assess

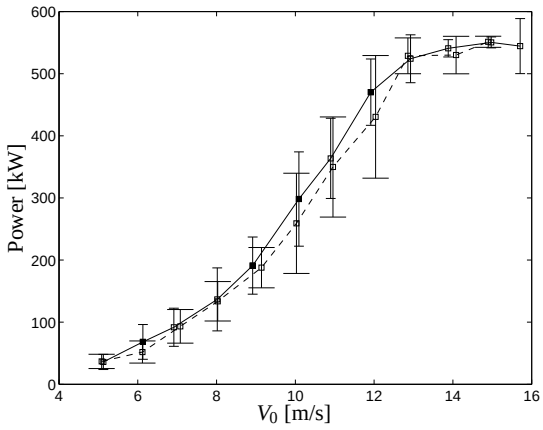

Fig. 11. Medians of the 1-minute average power output in bins with a width of 1 m/s for the original yaw controller (— — —) , and the updated yaw controller (—). The whiskers indicate the standard deviation of the 1 minute average yaw errors in each bin. The standard deviation is estimated using the median absolute deviation to decrease the influence of outliers. Narrow whiskers are for the corrected controller, wide whiskers are for the uncorrected controller. Solid squares indicate that the value of the corrected controller is significantly higher than the corresponding value of the uncorrected controller—at a level of significance of 95% using the t-distribution.

the changes in blade root bending moment variations that are caused by the corrected yaw controller researchers must assume that variations due to other effects such as wind shear are, on average, similar in situations with and without the correction applied. In Figure 13, the median and standard deviation of calculated damage equivalent loads (DELs) in wind speed bins are shown as a function of wind speed. For most wind speeds, the DELs are highest for the corrected controller. This might be explained by the several factors influencing the loads. Because the data has only been sorted to ensure similar turbulence conditions, there is no guarantee that the corrected and uncorrected controller has been tested in the exact same large-scale inflow conditions. Because the blade root load variations are sensitive to the large-scale inflow conditions, such as shear, the results might be corrupted by an uneven distribution of such phenomena for the corrected and uncorrected case. To thoroughly assess the effect of the improved yaw alignment on the load variations, more detailed data must be available for the inflow. With more detailed inflow knowledge, the data could be sorted to yield a comparison of results with more similar inflow conditions.

Another explanation of the increased variations in blade root bending moment below rated might be that the power capture is increased in this range. Increased power capture results in increased thrust on the rotor. Since thrust scales with wind speed, an increase in wind speed across the entire rotor in a situation with wind shear will yield increased thrust variations. Hence, improving yaw alignment in a situation with wind shear might increase the 1P load variations. The increased load variations might not be a problem in below rated operation. However, for above rated operation, it might be beneficial to leave the yaw error uncorrected to keep the load variations down.

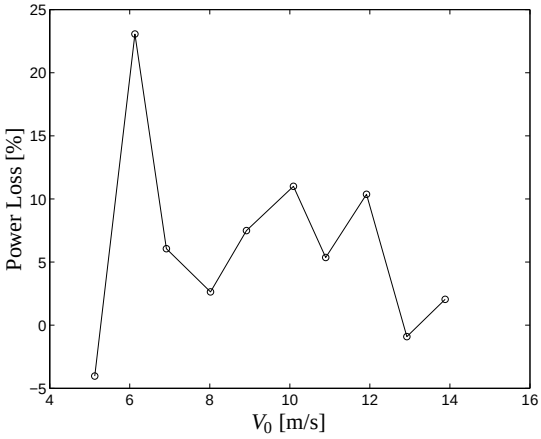

Fig. 12. Observed median power loss of the uncorrected system compared to the corrected system (in percent).

7 Discussion

Based on the results presented in the previous section, the correction of the yaw controller leads to better yaw alignment, which leads to increased power capture. Hence, it has been shown that the yaw alignment and power capture can be improved using only the existing measurement system. Having shown that the median yaw error can be reduced to almost zero using the existing equipment, the potential of achieving substantial improvements by adding additional measurement equipment such as LiDARs would seem limited. However, it is important to note that the presented method relies on recalibration of the existing system using upstream inflow measurements. Such measurements are not generally available for operating turbines. Therefore, if the calibration is applied on operating turbines, researchers must assume that it is the same calibration for all turbines of a similar type. To establish if the calibration holds for other turbines of the same type, more experiments are needed. If upstream measurements (for example from a LiDAR) were used directly in the control system, the described calibration would not be necessary. Finally, it is important to note that advanced measurements, such as LiDAR, can also be used for gust alleviation and improved pitch control. Thus, the benefits of adding additional advance measurement systems are spread across multiple objectives and might be justified by those objectives that are different from improved yaw alignment. A potential drawback of the presented method is wake operation. In this study, only wake-free situations have

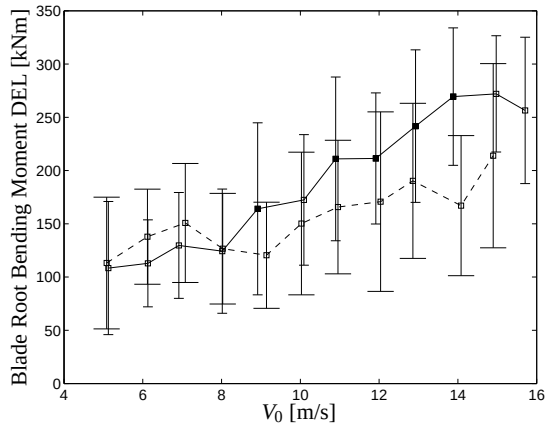

Fig. 13. Median and standard deviation of the 1 Hz damage equivalent blade root bending loads (flapwise) in bins with a width of 1 m/s for the original yaw controller (— — —), and the updated yaw controller (—). The whiskers indicate the standard deviation of the 1 minute average yaw errors in each bin. The standard deviation is estimated using the median absolute deviation to decrease the influence of outliers. Narrow whiskers are for the corrected controller, wide whiskers are for the uncorrected controller. Solid squares indicate that the value of the corrected controller is significantly higher than the corresponding value of the uncorrected controller—at a level of significance of 95% using the t-distribution.

been considered. Hence, if the applied correction is valid in wake operation, has not been established.

The results in this paper indicate power capture increases ranging from -5% to 16%, which differs from the theoretical expectations. It is important to recall the uncertainties related to these results regarding the inflow conditions. With a larger data set, researchers expect that the results will approach the theoretical expectations.

8 Conclusions

In this study, a dataset sampled from the CART3 turbine was analyzed to assess the yaw alignment performance. The data analysis revealed that the turbine was operating in a rotor speed dependent yaw error ranging from 5 to 15 degrees in the operational range of the turbine. Based on the observed yaw alignment performance, a correction scheme was applied to the yaw controller. The performance change caused by the corrected yaw controller was assessed by analyzing data gathered during fall 2011 and spring 2012. The results indicated that, with the correction applied, the power capture could be raised significantly in the below rated domain, at the cost of increased blade root loads.

9 Acknowledgments

Invaluable support for this work was provided by Lee Jay Fingersh, Garth Johnson, Scott Wilde, Mark Murphy, Jerry Hur, Syhoune Thao, and Don Baker of NREL. NREL's contributions to this study were funded by the Wind and Water Power Program, Office of Energy Efficiency and Renewable Energy of the U.S. Department of Energy, under contract No. DE-AC02-05CH11231. The authors are solely responsible for any omission or errors contained herein.

References

[1] Zahle, F., and Sørensen, N., 2011. "Characterization of the unsteady flow in the nacelle region of a modern wind turbine". *Wind Energy*, **14**(2), pp. 271–283.

[2] Pedersen, T. F., Vita, L., Sørensen, N. N., and Enevoldsen, P., 2008. "Operational experiences with a spinner anemometer on a mw size wind turbine". In Proceedings of EWEC.

[3] Mikkelsen, T., Hansen, K., Angelou, N., Sjöholm, M., Harris, M., Hadley, P., Scullion, R., Ellis, G., and Vives, G., 2010. "Lidar measurements from a rotating spinner". In Proceedings of EWEC2010, EWEC.

[4] Angelou, N., Mikkelsen, T., Hansen, K. H., Sjöholm, M., and Harris, M., 2010. Lidar wind speed measurements from a rotating spinner (spinnerex 2009). Risø-r-1741(en), Risø-DTU, Aug.

[5] Hansen, M. O. L., 2000. *Aerodynamics of Wind Turbines*. James & James.

[6] Madsen, H. A., Srensen, N. N., and Schreck, S., 2003. "Yaw aerodynamics analyzed with three codes in comparison with experiment". In 41st Aerospace Sciences Meeting and Exhibit.

[7] Kragh, K. A., Hansen, M. H., and Mikkelsen, T., 2011. "Improving yaw alignment using spinner based lidar". In Proceedings of the 49th AIAA Aerospace Sciences Meeting Including the New Horizons Forum and Aerospace Exposition. American Institute of Aeronautics and Astronautics, AIAA.

[8] Dakin, E., Priyavadan, M., and Hopkins, A., 2011. "Catching the wind, an update on improved yaw alignment". In Proceedings of EWEA.

[9] Kragh, K. A., and Fleming, P., 2012. "Rotor speed dependent yaw control of wind turbines based on empirical data". In Proceedings of the 50th AIAA Aerospace Sciences Meeting including the New Horizons Forum and Aerospace Exposition.

[10] Wright, A., Fleming, P., and van Wingerden, J.-W., 2011. "Refinement and tests of an advanced controller to mitigate fatigue loads in the controls advanced research turbine". In Proceedings of 49th AIAA Aerospace Sciences Meeting including the New Horizons Forum and Aerospace Exposition.

[11] Fleming, P. A., Wright, A. D., Fingersh, L. J., and van Wingerden, J.-W., 2011. "Resonant vibrations resulting from the reengineering of a constant-speed 2-bladed turbine to a variable-speed 3-bladed turbine". In Proceedings of 49th AIAA Aerospace Sciences Meeting including the New Horizons Forum and Aerospace Exposition.

[12] Okamura, H., Sakai, S., and Susuki, I., 1979. "Cumulative fatigue damage under random loads". *Fatigue & Fracture of Engineering Materials & Structures*, **1**, pp. 409–419.

[13] Astm e 1049-85, standard practices for cycle counting in fatigue analysis. In: Annual Book of ASTM Standards, Vol. 03.01. Philadelphia 1999, pp. 710-718.

Appendix D

Load Alleviation of Wind Turbines by Yaw Misalignment

WIND ENERGY
Wind Energ. 2013; **00**:1–12
DOI: 10.1002/we

RESEARCH ARTICLE

Load Alleviation of Wind Turbines by Yaw Misalignment

Knud A. Kragh and Morten H. Hansen

Department of Wind Energy, Technical University of Denmark, Frederiksborgvej 399, DK-4000 Roskilde, Denmark

ABSTRACT

Vertical wind shear is one of the dominating causes of load variations on the blades of a horizontal axis wind turbine. To alleviate the varying blade loads, modern wind turbine control systems have been augmented with sensors and actuators for individual pitch control. However, the loads caused by a vertical wind shear can also be affected through intentional yaw misalignment. Recent studies of yaw control have been focused on improving the yaw alignment to increase the power capture at below rated wind speeds. The focus of this study is on assessing the potential of alleviating blade load variations induced by the wind shear through intentional yaw misalignment at above rated wind speeds. The study is performed through simulations of a reference turbine using the aeroelastic simulation tool HAWC2. The study shows that optimal yaw misalignment angles for minimizing the blade load variations can be identified for both deterministic and turbulent inflows. It is shown that the identified optimal yaw misalignment angles can be applied without power loss for wind speeds above rated wind speed. In deterministic inflow, it is shown that the range of the steady state blade load variations can be reduced by up to 70%. For turbulent inflows, it is shown that the potential blade fatigue load reductions depend on the turbulence level. In inflows with high levels of turbulence, the observed blade fatigue load reductions are small, whereas the blade fatique loads are reduced by 20% at low turbulence levels. For both deterministic and turbulent inflows, it is seen that the blade load reductions are penalized by increased load variations on the non-rotating turbine parts.

KEYWORDS

Wind turbine; load alleviation; yaw misalignment; simulation;individual pitch control

Correspondence

knkr@dtu.dk

Received . . .

NOMENCLATURE

α	Wind shear exponent
λ	Tip-speed-ratio related to the yaw corrected wind speed at hub height $V_h \cos\theta_m$
Ω	Mean rotor speed
ϕ	Inflow angle relative to rotor plane
ψ	Blade azimuthal angle
ρ	Density of the air
θ	Angle of chord to rotor plane including both twist and pitch
θ_m	Yaw misalignment angle
θ_m^{a1}	Cosine variation of yaw misalignment angle, $\theta_m \cos\psi$
θ_m^{b1}	Sine variation of yaw misalignment angle, $\theta_m \sin\psi$
θ_p	Pitch angle

Prepared using weauth.cls [Version: 2010/06/17 v1.00]

c	Chord length
C_D	Drag coefficient
C_L	Lift coefficient
C_u	Coefficient for the influence of relative speed variations on the thrust force variation, in Equation (10)
C_ϕ	Coefficient of Equation (10)
f_a	Local axial thrust force
M_{ff}	Tower bottom fore-aft bending moment
M_{in}	Blade root in-plane bending moment
M_{out}	Blade root out-of-plane bending moment
M_{ss}	Tower bottom side-side bending moment
M_{tilt}	Tilting moment
M_{yaw}	Yawing moment
R	Outer blade radius
r	Radial position of blade section
U	Relative inflow speed
V_h	Wind speed at hub height
z	Vertical distance above ground
z_h	Hub height

1. INTRODUCTION

An increasing demand for competitive renewable energy has lead to the development of increasingly larger wind turbine rotors. Larger rotors yield higher power output, however, larger rotors also yield larger inflow variations in the area swept by the rotor, which increase the load variations. To cope with the increasing load variations on the turbines, controllers are being designed that are focused on load alleviation.

Control systems for horizontal axis upwind turbines have traditionally been based on sensors for measuring the wind speed and direction, rotor speed and power or torque, and actuators for regulating generator torque, yaw angle and collective pitch angle. Using this combination of sensors and actuators, a control scheme for power and speed regulation can be designed [1]. However, generator torque and collective pitch control schemes do not facilitate alleviation of the varying loads induced by azimuth angle dependent inflow conditions, i.e. vertical wind shear. Therefore, some modern wind turbine control systems have been augmented with sensory systems for measuring blade root bending moments to enable individual pitch control for load alleviation [2, 3, 4]. Recent advances within inflow measurement technology, for example Light Detection and Ranging (LiDAR) [5] have even led to the development of inflow measurement based controllers for load alleviation [6, 7, 8]. Individual pitch can efficiently reduce load variations, however, comes at a price of increased pitch actuation rates, and actuator requirements. Therefore, it is relevant to investigate other means of load alleviation that can be applied without increasing the actuator requirements. Load alleviation through modifications of the yaw control system have the potential of decreasing the load variations without increasing the pitch actuation rates, and is the topic of this study.

Previous studies related to yaw control have primarily been focused on increasing the power capture at below rated wind speeds through improved yaw alignment. In [5, 9], large static yaw errors are observed on megawatt (MW) size onshore turbines that indicate a potential for increased power capture by improved yaw alignment. The potential of using LiDAR for improved yaw alignment is discussed in [10], and in [11] active yaw control based on LiDAR measurements is demonstrated through experiments, and increased power capture is observed. In [12], it is shown experimentally that the yaw alignment and power output can be improved by introducing a rotor speed dependent correction to the wind direction measurements. At below rated wind speed, the aim of the yaw controller is to align the rotor axis with the inflow direction. In uniform inflow, maximum power is produced at perfect yaw alignment. In non-uniform inflows, e.g. sheared inflows,

Wind Energ. 2013; **00**:1–12 © 2013 John Wiley & Sons, Ltd.
DOI: 10.1002/we
Prepared using weauth.cls

the optimal yaw direction for power extraction is not necessarily perfect yaw alignment. However, power optimization is beyond the scope of this study. The focus of this study is on load alleviation at above rated wind speeds through yaw misalignment. At above rated wind speeds, a surplus of power is available from the wind and yaw misalignment angles below a certain limit can be introduced without decreasing the power production.

The objective of this study is to assess the potential of reducing the blade load variations using yaw misalignment, and the effect of the yaw misalignment on the loads of the non-rotating turbine parts and the power production. The study is performed through simulations of the NREL 5MW reference turbine [13]. All simulations are performed with the aeroelastic simulation tool HAWC2 [14].

The paper is laid out as follows: First, the method of alleviating blade load variations using yaw misalignment is introduced, then simulation results are presented for both deterministic and turbulent inflows. Finally, the results are discussed and conclusions are provided.

2. METHOD - A SIMPLE ESTIMATION OF OPTIMAL YAW ANGLE

The method is aimed at alleviating the blade load variations that are caused by a vertical wind shear. For a known shape of the vertical shear, it is based on applying a wind speed dependent yaw misalignment angle at above rated wind speeds. In a real application where the wind shear varies with the atmospheric stability and the flow field is affected by turbulence, the method must be based on feed-forward of an estimated wind shear shape, e.g. using a spinner LiDAR; or it must be implemented as feed-back of blade load measurements to the yaw system.

To show the basic mechanism of the method, an exponential vertical shear is assumed as

$$V(z) = V_h \left(\frac{z}{z_h} \right)^{\alpha} \tag{1}$$

where V_h is the wind speed at the hub height z_h, z is the vertical distance above ground (see Figure 1) and the IEC Standard exponent of $\alpha = 0.2$ is assumed.

To obtain a simple estimate of the optimal yaw misalignment angle, the combined effect of a vertical wind shear and the yaw misalignment on the azimuthal variation of the axial blade load is investigated. In this simplified investigation of the optimal yaw misalignment angle, the dynamics of the induced velocities and the turbine are neglected. The axially induced velocities are assumed to be constant over the whole rotor disc, although they will vary due to azimuthal variation in loading and due to the Glauert correction for a yawed rotor. Measuring the azimuth angle ψ from blade upward position, the free wind speed seen by a blade section at radius r in an unyawed flow is therefore given by

$$V(r, \psi) = V_h \left(\frac{z_h + r \cos \psi}{z_h} \right)^{\alpha}, \tag{2}$$

where the wind speed at hub height V_h is assumed to be corrected by the constant axial induction. The small tangential induction is neglected and the turbine and its blades are assumed to be rigid. The tangential relative inflow speed to the blade section due to the rotation in unyawed flow can be written as

$$V_t(r) = r\Omega = V_h \cos \theta_m \lambda \frac{r}{R}, \tag{3}$$

where Ω is the mean rotor speed, R is the blade tip radius, and $\lambda = \Omega R/(V_h \cos \theta_m)$ is the tip-speed-ratio related to the yaw corrected wind speed at hub height $V_h \cos \theta_m$ (including the axial induction), where θ_m is the yaw misalignment angle. The yaw misalignment angle is defined such that positive yaw misalignment angles correspond to situations where the wind is reaching the turbine from the right when see from the turbine (see Figure 1).

The first order effects of wind shear and yaw misalignment on the load at the blade section are determined by the variation of relative inflow angle and speed to the section. Figure 1 shows the different geometrical parameters and the velocity parallelogram for the section at radius r of a blade pointing upwards in a positive yaw misalignment. Assuming zero cone and tilt angles, the sectional velocity vector of the parallelogram related to the free wind is

$$\mathbf{v}_{\text{wind}} = \begin{bmatrix} \cos \theta_m^{a_1} \\ -\sin \theta_m^{a_1} \end{bmatrix} V_h \left(\frac{z_h + r \cos \psi}{z_h} \right)^{\alpha} \cos \theta_m^{b_1}, \tag{4}$$

where $\theta_m^{a_1} \equiv \theta_m \cos \psi$ and $\theta_m^{b_1} \equiv \theta_m \sin \psi$ are the cosine and sine azimuthal variations of the yaw misalignment angle θ_m. The unit-vector $[\cos \theta_m^{a_1} \quad -\sin \theta_m^{a_1}]^T$ describes the axial and tangential components of the wind vector in the sectional plane due to the yaw misalignment, which has a cosine variation over the azimuth with max/min in top and bottom of the rotor plane. The length of the free wind vector given by Equation (2) is reduced by the factor $\cos \theta_m^{b_1}$ due to the fact that the radial component of the wind with max/min at the horizontal blade positions does not contribute to the thrust force.

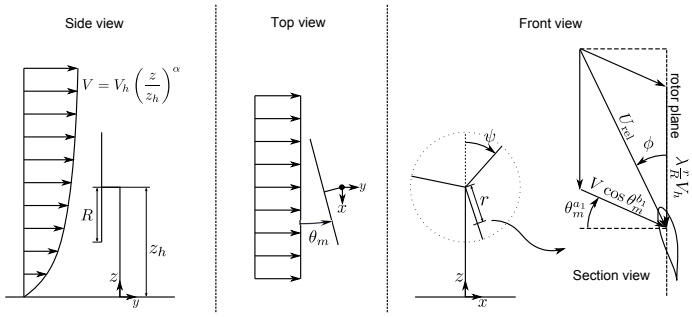

Figure 1. Definitions of geometrical parameters and the velocity parallelogram illustrating the combined effect of wind shear and yaw misalignment given by the angle θ_m on the inflow angle ϕ. Note that the angles $\theta_m^{a_1} = \theta_m \cos\psi$ and $\theta_m^{b_1} = \theta_m \sin\psi$ are the cosine and sine azimuthal variations of the yaw angle.

The sectional velocity vector of the parallelogram related to the blade rotation is $\mathbf{v}_{\text{rot}} = \begin{bmatrix} 0 & V_h \cos\theta_m \lambda \frac{r}{R} \end{bmatrix}^T$. The relative inflow vector can be derived as the sum

$$U \begin{bmatrix} \cos\phi \\ \sin\phi \end{bmatrix} = \mathbf{v}_{\text{wind}} + \mathbf{v}_{\text{rot}}, \tag{5}$$

from which the inflow angle ϕ can be derived as

$$\phi = \tan^{-1}\left(\frac{\left(1 + \frac{r/R\,\cos\psi}{z_h/R}\right)^\alpha \cos\theta_m^{b_1} \cos\theta_m^{a_1}}{\lambda \frac{r}{R} \cos\theta_m - \left(1 + \frac{r/R\,\cos\psi}{z_h/R}\right)^\alpha \cos\theta_m^{b_1} \sin\theta_m^{a_1}} \right), \tag{6}$$

and the normalized relative speed is given as

$$\frac{U}{V_h} = \sqrt{\left(\left(1 + \frac{\frac{r}{R}\cos\psi}{z_h/R}\right)^\alpha \cos\theta_m^{b_1} \cos\theta_m^{a_1}\right)^2 + \left(\lambda \frac{r}{R} \cos\theta_m - \left(1 + \frac{\frac{r}{R}\cos\psi}{z_h/R}\right)^\alpha \cos\theta_m^{b_1} \sin\theta_m^{a_1}\right)^2} \tag{7}$$

Note that the inflow angle and the normalized relative speed depend only on the azimuth angle ψ, the non-dimensional geometric parameters r/R and z_h/R, the yaw corrected tip-speed-ratio $\lambda = \Omega R/(V_h \cos\theta_m)$, and the vertical shear exponent α and the yaw misalignment angle θ_m.

Neglecting second order effects due to unsteady airfoil aerodynamics, the axial blade forces perpendicular to the rotor plane, the thrust force, at a given radial section can modeled as

$$f_a = \tfrac{1}{2}\rho c U^2 \left(C_L\left(\phi - \theta\right)\cos\phi + C_D\left(\phi - \theta\right)\sin\phi\right), \tag{8}$$

where ρ is the density of the air, c is the sectional chord length, U is the relative inflow speed, $C_L\left(\phi - \theta\right)$ and $C_D\left(\phi - \theta\right)$ are the lift and drag coefficients evaluated at the angle of attack $\phi - \theta$ given by the inflow angle ϕ and the total chord rotation θ relative to the rotor plane including the blade twist and pitch.

To investigate how the variations of inflow angle and relative speed affect the blade thrust force, a Taylor expansion of (8) in ϕ and U gives the first order approximation of the thrust variation around the azimuth as

$$\delta f_a(r,\psi) = f_a - f_0 \approx \tfrac{1}{2}\rho c U_0^2 \left(C_u \frac{U - U_0}{U_0} + C_\phi\left(\phi - \phi_0\right)\right), \tag{9}$$

where f_0 is the constant steady state thrust, and the coefficients are

$$\begin{aligned} C_u &= 2C_{L,0}\cos\phi_0 + C_{D,0}\sin\phi_0 \\ C_\phi &= C'_{L,0}\cos\phi_0 - C_{L,0}\sin\phi_0 + C'_{D,0}\sin\phi_0 + C_{D,0}\cos\phi_0, \end{aligned} \tag{10}$$

where $\phi_0 = \tan^{-1}\left(R/(\lambda r)\right)$ and $U_0 = V_h \cos\theta_m \sqrt{1 + \lambda^2 r^2/R^2}$ are the steady state inflow angle and relative speed, $C_{L,0}$ and $C'_{L,0}$ are the lift coefficient and its derivative (lift slope) evaluated at the steady state angle of attack $\phi_0 - \theta$, and similar for the steady state drag coefficient $C_{D,0}$ and its slope $C'_{D,0}$. Note that the thrust variation $\delta f_a(r,\psi)$ is dependent on the yaw misalignment angle θ_m through the dependencies of the inflow angle (6) and relative speed (7).

DOI: 10.1002/we
Prepared using weauth.cls

The optimal yaw misalignment angle that minimizes the azimuthal variation of the flapwise blade root moment can be approximated by solving the minimization problem

$$\theta_{m,opt} \approx \min_{\theta_m} \int_0^{2\pi} \left(\int_0^R \delta f_a(r,\psi) r dr \right)^2 d\psi \tag{11}$$

It should be noticed in Equation (11) that it is the variation of the thrust force that is minimized. In reality, the damage equivalent loads are aim of the minimization, however, calculating damage equivalent loads involves rainflow counting, and no exact mathemetical expression exists for the damage equivalent loads. Therefore, the trust force variations are used. In Section 4, it is shown that the results obtained using thrust force variations correspond to the results of simulation results where the damage equivalent loads are calculated. Because the main contributions to the blade root moment is related to the thrust forces on the outer part of the blade, the minimization problem given by Equation (11) can be simplified to

$$\theta_{m,opt} \approx \min_{\theta_m} \int_0^{2\pi} \left(\delta f_a(r_0,\psi) \right)^2 d\psi, \tag{12}$$

where r_0 is the radius of the dominating blade forces, often selected as the three-quarter radius $r_0 = 3R/4$. The minimization can be further simplified by using that the main variation of the thrust force at this radius and at above rated wind speeds is caused by the variation of the inflow angle. When the blade starts pitching above the rated wind speed, the angles of attack at the outer parts will decrease and the steady state lift coefficients will become small, whereby $C_u \approx 2C_{L,0} << C_\phi \approx C'_{L,0}$ in Equation (10) because the airfoil is operating in attached flow with a lift slope of about 2π. Hence, the optimal yaw misalignment angle is found by minimization of the variation of the inflow angle as:

$$\theta_{m,opt} \approx \min_{\theta_m} \int_0^{2\pi} \left(\phi - \phi_0 \right)^2 d\psi \tag{13}$$

The simplest possible estimate of the optimal yaw misalignment angle can be obtained by requiring that the inflow angle at the blade upward position is the same as the inflow angle when the blade passes through horizontal positions. Solving the equation $\phi = \phi_0$ using (6) for $r = r_0$ and $\psi = 0$ leads to the simple expression:

$$\theta_{m,opt} \approx \tan^{-1}\left(\lambda \frac{r_0}{R} \frac{1 - \left(1 + \frac{r_0/R}{z_h/R}\right)^\alpha}{\left(1 + \frac{r_0/R}{z_h/R}\right)^\alpha} \right), \tag{14}$$

which predicts that the optimal yaw misalignment angle is negative, and that less yaw misalignment is needed as the tip-speed-ratio decreases at higher wind speeds. In the following section the optimal yaw angles are predicted for the NREL 5 MW reference turbine [13] using all four of the above methods.

2.1. Example: NREL 5MW reference turbine

The steady state inflow properties and blade characteristics of the NREL 5 MW reference turbine needed for the computation of the inflow variation (6) and thrust force variation (9) are obtained for above rated wind speeds using the tool HAWCStab2 [15]. These steady state operational conditions for the rotor blades are computed assuming uniform inflow perpendicular to the rotor, and solving the nonlinear equilibrium between the aerodynamic forces obtained from a BEM model and the structural forces obtained from a co-rotational finite beam element model.

Figure 2 shows for different negative yaw angles the azimuthal variation of inflow angle $\phi - \phi_0$ (left plot) and normalized relative speed $(U - U_0)/U_0$ (right plot) at the three-quarter radius section of the NREL 5 MW rotor in the exponential wind shear ($\alpha = 0.2$) with a hub height speed of 15 m/s. Note that in the unyawed flow, the azimuthal variation of relative speed is small, however, this variation become significant when the rotor is yawed due to the added tangential component of the wind (cf. Figure 1). The azimuthal variation of the inflow angle is decreased by the negative yaw, and shows a more 2P variation for the numerical largest yaw angle of -30 deg.

Figure 3 shows the four predictions of the optimal yaw misalignment angle based on the minimization problems in Equations (11–13) and the simple expression in Equation (14) as function of mean wind speeds. The predictions based on the minimizations of the blade root moment and the local thrust force at the three-quarter radius section agree within 5 deg. It is seen that the sign of the optimal yaw misalignment angle differs for wind speeds below and above rated wind speed. The sign change is caused by the different local inflow conditions that characterize operation at below and above rated wind speed. Below and around the rated wind speed, there is a significant mean lift generated on the blade. Thus, the coefficient C_u that quantifies the influence of relative speed variations on the thrust force variation yields large values at below rated wind speeds. Therefore, the largest reductions of the thrust force variations due to the vertical wind shear are achieved by increasing the relative velocity in the bottom part of the rotor while decreasing it at the top. Such adjustments of the

relative velocity can be achieved by introducing positive yaw misalignment. At above rated wind speeds, the lift coefficient is close to zero along the outer part of the blade, and the variation of relative speed becomes less significant. Hence, at above rated wind speeds, the minimum blade load variations are achieved by reducing the angle of attack variations to a mean value close to zero deg. Such a smoothing of the angle of attack variation in a situation with wind shear is achieved through negative yaw misalignment. Finally, it is seen from Figure 3 that the simplified estimations in Equation (13) and Equation (14) only agrees with the more complex estimations at well above rated wind speeds.

3. LOAD BASED ESTIMATION OF OPTIMAL YAW ANGLE - NO TURBULENCE

A series of HAWC2 simulations are performed at varying yaw misalignment angles and mean inflow wind speeds to identify the yaw misalignment angles that yields the largest load reductions in a deterministic inflow without the effect of turbulence. The simulations are performed with a standard speed controller applied that is similar to the one described in [13] and applies collective pitch and generator torque actuation. Two types of vertical wind shear are tested: power law wind shear with an exponent of 0.2, and linear wind shear with a slope of $0.05\ \mathrm{s}^{-1}$. The range of the resulting steady state blade root out-of-plane bending moment ΔM_{out} is used as a measure of the blade load variations. For comparison, the results have been normalized with the range of the steady state load variations when no yaw misalignment is applied. The normalization is defined as:

$$\widetilde{\Delta M_{out}} = \frac{\Delta M_{out}(V_0, \theta_m)}{\Delta M_{out}(V_0, 0)} \tag{15}$$

where (and in the remainder of the paper) $\widetilde{(\cdot)}$ indicates that the result $(\cdot)$ has been normalized with $(\cdot)$ at zero yaw misalignment.

In Figure 4, the results of the simulations are shown as contour plots of $\widetilde{\Delta M_{out}}$ as a function of yaw misalignment angle and wind speed for both the power law and linear wind shear. For both types of wind shear and wind speeds above approximately 13 m/s, the minimum load variations are achieved when a negative yaw misalignment angle is induced. At wind speeds below 13 m/s the minimum load variations are found at positive yaw misalignment angles. The effect of the yaw misalignment on the power production is assessed at the end of the present section. Figure 5 shows the identified yaw misalignment angles yielding the greatest load range reductions as a function of wind speed as well as the corresponding normalized steady state load ranges. The magnitude of the optimal yaw misalignment at above rated wind speeds estimated from the simulated results is similar to the theoretical expectations, and the sign change that was observed in the theoretical predictions is also seen in the simulated results. There is a slight difference in the wind speed at which the sign change of the optimal yaw misalignment is observed for the theoretical and simulated results. This difference is likely due to the added complexity of the simulation model compared to the theoretical model. In the HAWC2 simulations, the blades are flexible and will deflect during rotation. The flexibility of the blades causes a phase shift in the cyclic blade root loads such that maximum and minimum loads are not exactly at the top and bottom position, respectively. At below rated wind speeds, the optimal yaw misalignment angles estimated from the simulations are larger than the theoretical expectations.

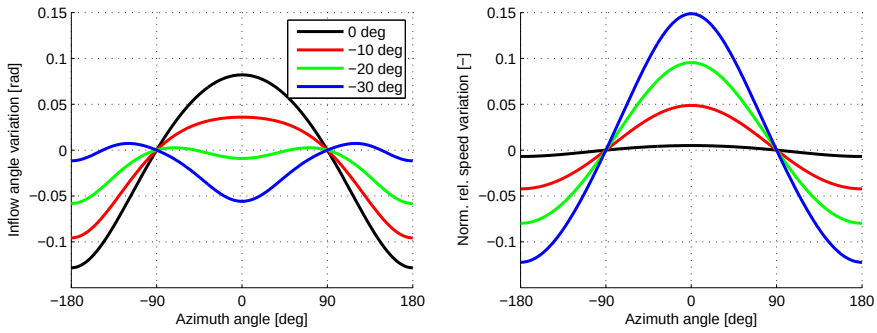

Figure 2. Azimuthal variation of inflow angle $\phi - \phi_0$ (left plot) and normalized relative speed $(U - U_0)/U_0$ (right plot) at the three-quarter radius section of the NREL 5 MW rotor in the exponential wind shear ($\alpha = 0.2$) with a hub height speed of 15 m/s for different negative yaw angles.

DOI: 10.1002/we
Prepared using weauth.cls

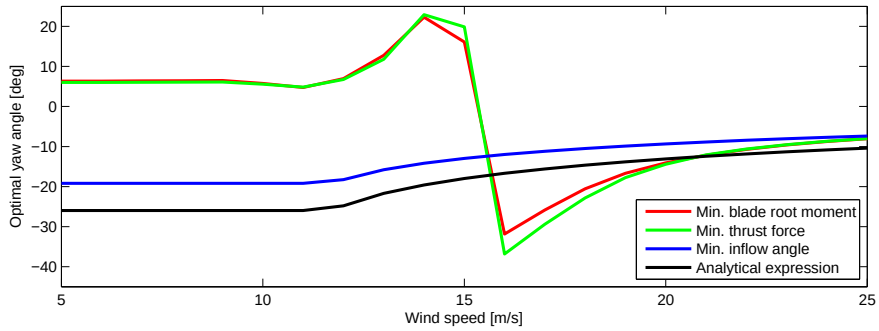

Figure 3. Four predictions of the optimal yaw misalignment angle based on the minimization problems in Equations (11–13) and the simple expression in Equation (14) as function of the above rated mean wind speeds.

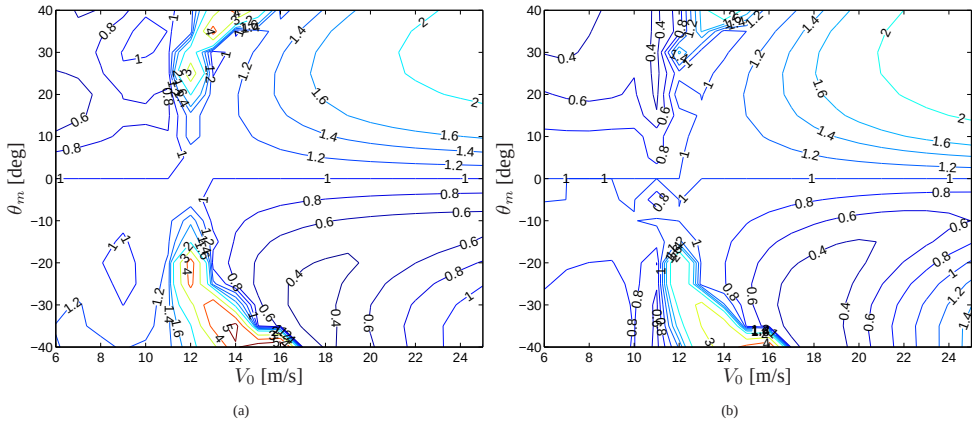

Figure 4. $\widetilde{\Delta M_{out}}$ as a function of wind speed and yaw misalignment angle. a) Power law wind shear with an exponent of 0.2. b) Linear wind shear with a gradient of 0.05 s^{-1}.

Again this is likely due to the added complexity of the numerical model, and because the focus of the study is on above rated operation, this is not explored further.

The power that is available from the wind exceeds the rated power of the turbine at above rate wind speeds. Thus, a yaw misalignment below a certain limit can be introduced at above rated wind speeds without decreasing the power output of the turbine. In Figure 6, the normalized power output is shown as a function of yaw misalignment angle and wind speed. It is seen that the range of yaw misalignment angles that do not decrease the power output is increasing with increasing wind speed. At below rated wind speeds, the maximum power is not achieved at zero yaw error. Investigating this effect further is beyond the scope of this study, but will be part of future studies. To assess how the power output is affected by the optimal yaw misalignment angles identified above, the normalized power output $\widetilde{P}$ at the optimal yaw misalignment angles is plotted as a function of wind speed in Figure 7. The power output is unaffected by the optimal yaw misalignment when the wind speed is above 13 m/s for the power law wind shear. For the linear wind shear, the wind speed must be above 14 m/s for the power output to remain at the rated value. Hence, for the studied turbine, load alleviation using yaw misalignment is generally applicable for wind speeds above 14 m/s.

Above, it was shown that inducing a yaw misalignment can reduce the blade loads. However, it is expected that the introduced yaw misalignment will affect the loading on other parts of the turbine. The range of the steady state load variations on different parts of the turbine is shown as a function of the yaw misalignment in Figure 8 at a mean wind speed of 15 m/s. It is seen that the range of both the in-plane and out-of-plane blade root bending moment is decreasing with negative yaw misalignment angles for both types of wind shear. The effect of the yaw misalignment on the tilt and yaw

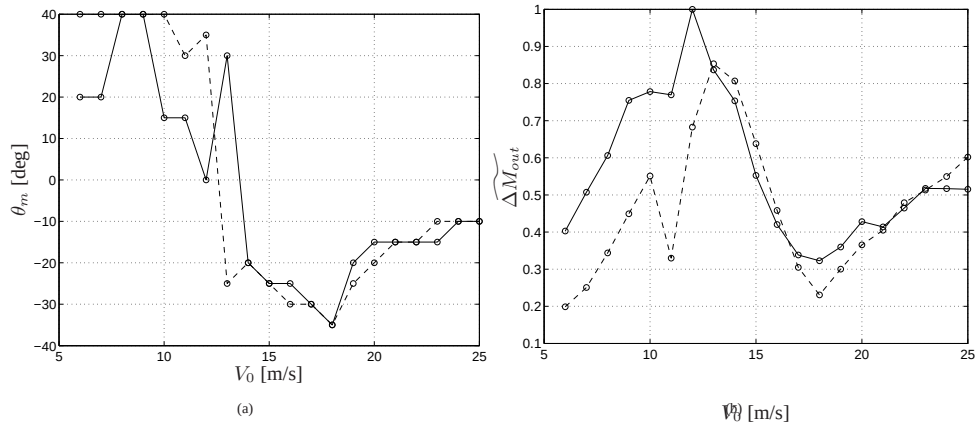

Figure 5. Results of HAWC2 simulations with varying wind speed and yaw misalignment angle. a) Optimal yaw misalignment angle for alleviating blade root out-of-plane bending moment variations as a function of wind speed. b) Normalized load range $\widetilde{\Delta M_{out}}$ with the optimal yaw misalignment angle applied as a function of wind speed for the power law wind shear with an exponent of 0.2 (—), and the linear wind shear with a slope of 0.05 s^{-1} (– – –).

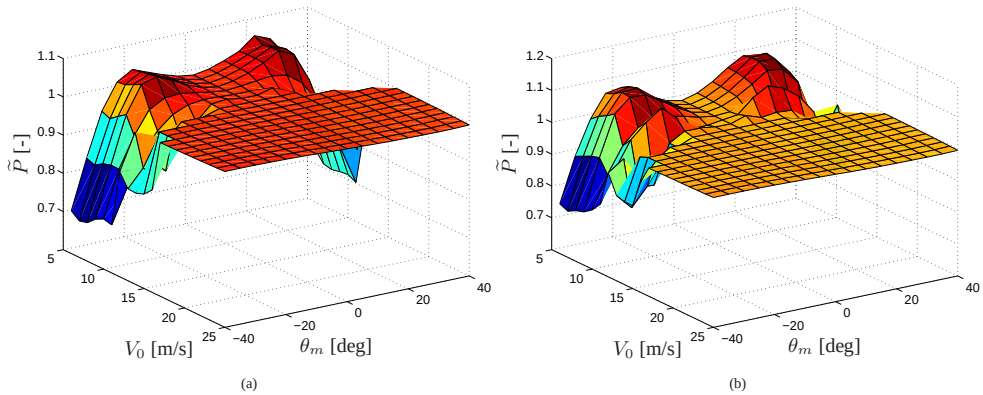

Figure 6. Simulated normalized power output as a function of wind speed and yaw misalignment angle a) Power law wind shear with an exponent of 0.2. b) Linear wind shear with a gradient of 0.05 $s-1$.

loads differs depending on the shear type. For the power law wind shear there is a slight increase in load variation with both positive and negative yaw misalignment angles. For the linear shear, the ranges of the moment variations are decreasing with negative yaw misalignment angles up to a magnitude of -10 deg. Beyond -10 deg yaw misalignment, a rapid increase in the moment range is observed. For the linear wind shear, the range of the tower bottom fore-aft bending moment is decreasing slightly with negative yaw misalignment angles larger than -10 deg. For the power law wind shear, the tower bottom fore-aft bending moment range is increasing with both positive and negative yaw misalignment. The range of the tower bottom side-side bending moment is decreasing slightly with negative yaw misalignment. In summary, it appears that the observed blade load reductions that can be achieved through negative yaw misalignment angles are penalized by increased load variations on the non-rotating parts of the turbine. A full set of design load cases must be calculated and the results related to a cost model to establish if the blade load variation reductions are worth the increased load variations on the non-rotating turbine parts.

Wind Energ. 2013; **00**:1–12 © 2013 John Wiley & Sons, Ltd.
DOI: 10.1002/we
Prepared using weauth.cls

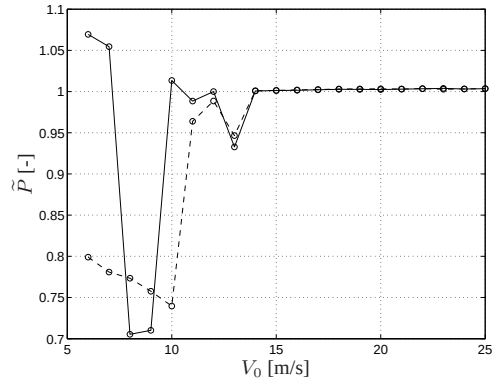

Figure 7. Normalized power output at the identified optimal yaw misalignment angle as a function of wind speed for the power law wind shear with an exponent of 0.2 (—), and the linear wind shear with a slope of 0.05 s^{-1} (– – –).

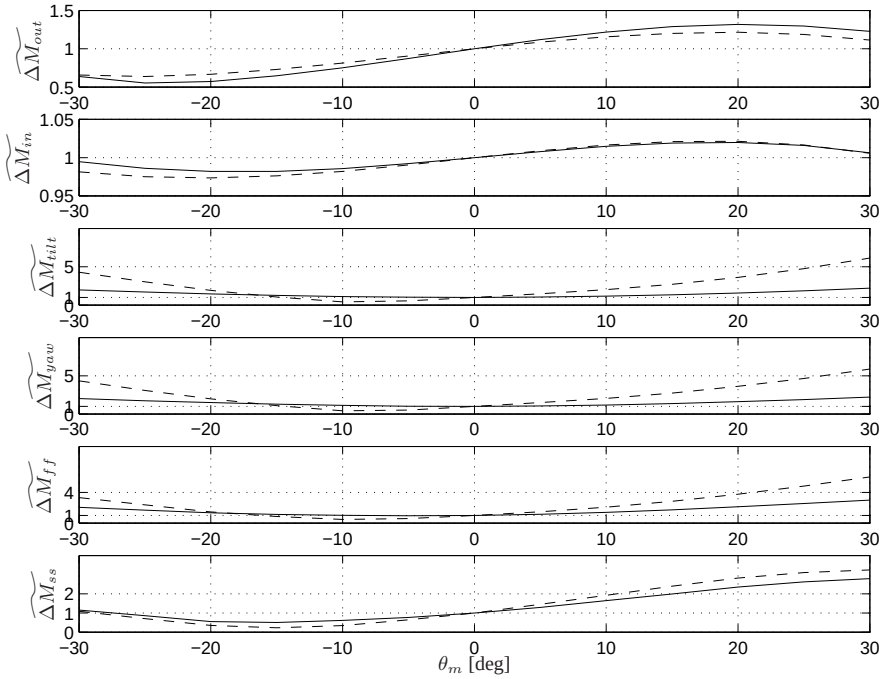

Figure 8. Range of the simulated steady state load variations as a functions of yaw misalignment at 15m/s for the power law wind shear with an exponent of 0.2, (—), and the linear wind shear with a gradient of 0.05 s^{-1} (– – –). All load ranges are normalized by the corresponding load range at zero degree yaw misalignment.

3.1. Sensitivity to Shear Magnitude

In the previous section, the load reductions were only assessed at one particular wind shear magnitude. It is expected that the optimal yaw misalignment will depend on the magnitude of the wind shear. Therefore, simulations are performed at different shear magnitudes and yaw misalignment angles to assess the sensitivity of the optimal yaw misalignment angles on the magnitude of the wind shear. The simulations are performed at three distinct wind speeds; 13, 15 and 18m/s. At

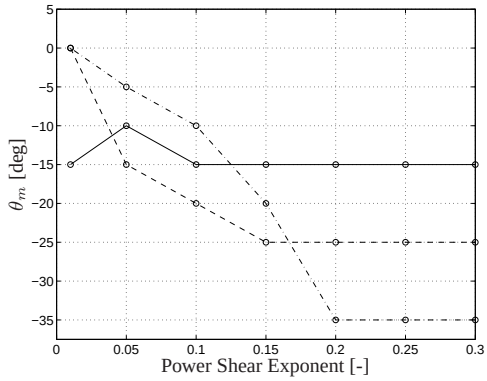

Figure 9. Optimal yaw misalignment angle as a function of wind shear strengths at 3 different wind speeds; 13m/s (—) 15m/s (– – –) and 18m/s (– · –).

each wind speed and wind shear magnitude, the optimal yaw misalignment angle is found from the simulations as the yaw misalignment angle yielding the smallest steady state blade root out-of-plane bending moment range. The identified optimal yaw misalignment angles are shown for all three wind speeds in Figure 9 as a function of the power law wind shear exponent. The optimal yaw misalignment angles are constant for exponents larger than 0.2. Hence, it appears that the optimal yaw misalignment angle is mainly dependent on the mean wind speed for wind shears of magnitudes similar to that defined in the IEC standard (0.2).

4. LOAD BASED ESTIMATION OF OPTIMAL YAW ANGLE - TURBULENCE

The achievable load reductions through intentional yaw misalignment at above rated wind speed with turbulence are assessed through simulations with Cartesian boxes of Mann turbulence [16] as additional inflow variation to the deterministic wind shear. Different turbulence levels ranging from highly turbulent class A inflow to very low turbulent inflow are tested. Six 10 minute time series are generated at each turbulence level with six different seed numbers. The same controller as used for the simulations in deterministic inflow is applied for speed and power regulation.

The load reductions are quantified by the average 1 Hz damage equivalent loads of the six 10 minute simulations, which are shown in Figure 10 as a function of yaw misalignment at four levels of turbulence with a mean inflow speed of 15 m/s and a power law wind shear. The identified optimal yaw misalignment angles and resulting normalized 1 Hz damage equivalent loads are given in Table I. At all tested levels of turbulence, the damage equivalent blade root out-of-plane bending loads decrease with negative yaw misalignment angles to a minimum which is reached at a yaw misalignment angle that is decreasing with decreasing turbulence level. Furthermore, it is seen that the magnitude of the blade root out-of-plane bending load reductions increase with decreasing turbulence intensity. The damage equivalent loads are reduced to 97.5% with class A turbulence (18%), whereas the loads are reduced to 80.6% at a turbulence intensity of 4.5%. The turbulence dependency of the load reductions is not surprising when recalling the effect of yaw misalignment on the load variations. Yaw misalignment will only reduce the load variations caused by a deterministic vertical wind shear. Any turbulence caused loads will not be alleviated by intentionally misaligning the turbine. From Table I it is seen that the tilt loads are slightly decreased at high levels of turbulence and the yaw loads are increased 3% to 7% depending on turbulence intensity. For the tower bottom loads it is seen that the fore-aft load is slightly increased by the yaw misalignment. The increase in tower bottom fore-aft fatique load is around 3-9%. For high levels of turbulence, the damage equivalent tower bottom side-side loads are slightly increased whereas at lower levels of turbulence the loads are decreased. Finally, it is seen that the load reductions observed for the deterministic case are much larger than for the turbulent case, however, the large load reductions of the deterministic case are penalized by significant increases in the fatique loads at the tower top and tower bottom.

Wind Energ. 2013; **00**:1–12 © 2013 John Wiley & Sons, Ltd.
DOI: 10.1002/we
Prepared using weauth.cls

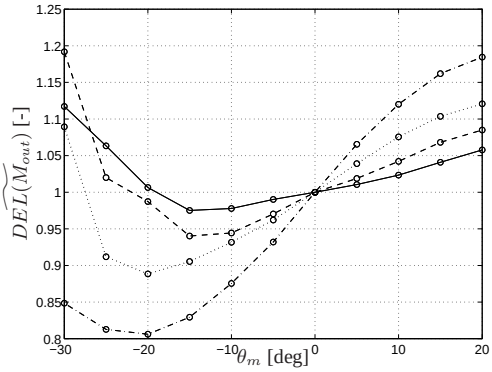

Figure 10. Simulated 1 Hz damage equivalent blade root out-of-plane bending loads as a function of yaw misalignment, normalized with the damage equivalent blade root of plane bending loads at zero yaw misalignment, for four turbulence intensities: 18% (Class A) (—), 13.5% (Class C) (− − −), 9% (· · ·), and 4.5% (−·-). For the blade loads it is assumed that the slope of the Wohler curve is $m = 10$. Mean inflow speed, $V_0 = 15$m/s. Power law wind shear with an exponent of 0.2.

	Turbulence Intensities				
	18%	13.5%	9%	4.5%	0%
θ_m^{opt} [deg]	-15	-15	-20	-20	-25
$\widetilde{DEL}(M_{out})$ [%]	97.5	94.0	88.8	80.6	60.6
$\widetilde{DEL}(M_{in})$ [%]	96.7	97.3	97.2	97.7	98.0
$\widetilde{DEL}(M_{tilt})$ [%]	97.5	98	99	103.3	127.1
$\widetilde{DEL}(M_{yaw})$ [%]	103.5	103.7	105.3	107.5	134.7
$\widetilde{DEL}(M_{ff})$ [%]	106.3	102.7	108.6	106.7	154.9
$\widetilde{DEL}(M_{ss})$ [%]	110.2	95.5	101.6	87.9	122.9

Table I. Identified optimal yaw misalignment angles and estimated normalized 1 Hz damage equivalent loads at the optimal yaw misalignment angle at four turbulence intensities. For the blade loads it is assumed that the slope of the Wohler curve is $m = 10$ and for the remaining loads $m = 3$.

5. CONCLUSIONS AND FUTURE WORK

In this study, the potential of alleviating the once-per-revolution, wind shear induced blade load variations by intentional yaw misalignment was investigated. A simple method for estimating the optimal yaw misalignment angle for blade load alleviation was introduced. The simple method suggested that at above rated wind speed the optimal yaw misalignment angle for minimizing the blade load variations is in the range from $-10 - -30$ deg, depending on wind speed. The potential was further assessed through simulations of the NREL 5MW reference turbine using the aeroelastic simulation tool HAWC2 at varying wind speeds and yaw misalignment angles. Two types of wind shear were tested; power law and linear wind shear. The observed load reductions were similar for both of the tested types of wind shear. For deterministic inflows it was seen that, depending on wind speed, the range of the steady state blade loads can be reduced by up to 70% by introducing a yaw misalignment of approximately -30 deg. It was shown that for wind speeds above approximately 14 m/s (2 m/s above the rated wind speed of the NREL reference turbine), the identified optimal yaw misalignment can be applied without power loss. Results of simulations in turbulent inflow showed that, for highly turbulent inflows, the achievable load reductions are approximately 2.5%. However, the achievable load reductions increases with decreasing turbulence intensity, and at low levels of turbulence, the achievable fatigue load reductions were seen to be approximately 20%. From simulations in both deterministic and turbulent inflow it was seen that the reduction of the blade load variations are penalized by increased load variations on the non-rotating turbine parts.

In future studies, it will be investigated how optimal yaw misalignment can be applied in combination with individual pitch control. Combining individual pitch control and optimal yaw misalignment can potentially lower the pitch actuation rates required by the individual pitch controller because some of the loads are alleviated by the optimal yaw misalignment.

REFERENCES

1. T Burton, D Sharpe, N Jenkins, and E Bossanyi. *Wind Energy Handbook*. John Wiley & Sons, Ltd, 2001.
2. E A Bossanyi. Individual blade pitch control for load reduction. *Journal of Wind Energy*, 6:119–128, 2003.
3. E A Bossanyi. Further load reductions with individual pitch control. *Journal of Wind Energy*, 8:481–485, 2005.
4. E Bossanyi, B Savini, M Iribas, M Hau, B Fischer, D Schlipf, T van Engelen, M Rossetti, and C E Carcangiu. Advanced controller research for multi-mw wind turbines in the upwind project. *Journal of Wind Energy*, 15:119145, 2012.
5. T Mikkelsen, K Hansen, N Angelou, M Sjöholm, M Harris, P Hadley, R Scullion, G Ellis, and G Vives. Lidar measurements from a rotating spinner. In *Proceedings of EWEC2010*, Warzaw, April 2010.
6. F Dunne, L Y Pao, A D Wright, B Jonkman, and N Kelley. Adding feed forward blade pitch control to standard feedback controllers for load mitigation in wind turbines. *Mechatronics*, 21(4):682–690, 2011.
7. J Laks, L Pao, A Wright, N Kelley, and B Jonkman. The use of preview wind measurements for blade pitch control. *Mechatronics*, 21(4):668–681, 2011.
8. K A Kragh and M H Hansen. Individual pitch control based on local and upstream inflow measurements. In *Proceedings of the 50th AIAA Aerospace Sciences Meeting Including the New Horizons Forum and Aerospace Exposition*, Nashville, January 2012.
9. T F Pedersen, L Vita, N N Srensen, and P Enevoldsen. Operational experiences with a spinner anemometer on a mw size wind turbine. In *Proceedings of EWEC2008*, Brussels, April 2008.
10. K A Kragh, M H Hansen, and T Mikkelsen. Precision and shortcomings of yaw error estimation using spinner-based light detection and ranging. *Wind Energy*, pages n/a–n/a, 2012.
11. E Dakin, M Priyavadan, and A Hopkins. Catching the wind, an update on improved yaw alignment. In *Proceedings of EWEA2011*, Brussels , March, 2011.
12. K A Kragh and P A Fleming. Rotor speed dependent yaw control of wind turbines based on empirical data. In *Proceedings of the 50th AIAA Aerospace Sciences Meeting including the New Horizons Forum and Aerospace Exposition*, Nashville, January 2012.
13. J. Jonkman. Nrel 5 mw baseline wind turbine. Technical report, NREL/NWTC, 1617 Cole Boulevard; Golden, CO 80401-3393, USA, 2005.
14. T J Larsen. How 2 hawc2, the user's manual. Risø-r-1597(ver. 3-9)(en), Risø-DTU, September 2009.
15. M H Hansen. Aeroelastic properties of backward swept blades. In *In the Proceedings of 49th AIAA Aerospace Sciences Meeting Including The New Horizons Forum and Aerospace Exposition*, Orlando, January, 2011.
16. J Mann. Wind field simulation. *Probabilistic Engineering Mechanics*, 13(4):269 – 282, 1998.

DOI: 10.1002/we
Prepared using weauth.cls

Appendix E

Sensor Comparison Study for Load Alleviating Wind Turbine Pitch Control

WIND ENERGY
Wind Energ. 2012; **00**:1–14
DOI: 10.1002/we

RESEARCH ARTICLE

Sensor Comparison Study for Load Alleviating Wind Turbine Pitch Control

Knud A. Kragh, Morten H. Hansen and Lars C. Henriksen

Department of Wind Energy, Technical University of Denmark, Frederiksborgvej 399, DK-4000 Roskilde, Denmark

ABSTRACT

With increasing wind turbine sizes, the load alleviating capabilities of modern wind turbines are becoming increasingly important. Load alleviating control schemes have traditionally been based on feed-back from load sensor, however, recent developments of measurement technologies have enabled feed-forward control based on preview measurements of the inflow acquired using e.g. light detection and ranging. The potential of alleviating load variations caused by mean wind speed changes through feed-forward control have demonstrated in several studies, whereas the potential of preview control for alleviating the load variations caused by azimuth dependent inflow variations is less described. Individual pitch is required to alleviate azimuthal load variations, and is traditionally applied through feed-back control of the blade root loads (cyclic pitch control). In this study, the effect of three measurements types on the load alleviating performance of an individual pitch controller is studied. The effect is studied by using a baseline cyclic pitch controller as test bench for assessing the effect of the different measurement types on the controller performance. Hereby, the fundamental differences and limitations of the three measurement types can be identified. The three measurement types considered in this study are: blade root out-of-plane bending moment, on-blade measurements of angle of attack and relative velocity at a radial position of the blades, and upstream inflow measurements from a spinner mounted LiDAR that enables preview of the incoming flow field. The results show that for stationary inflow conditions, the three different measurement types yields similar load reductions, but for varying inflow conditions, the LiDAR based controller yields larger load reductions than the two others. However, the results also show that the performance of the LiDAR based controller is very sensitive to uncertainties relating to the inflow estimation. Copyright © 2012 John Wiley & Sons, Ltd.

KEYWORDS

Wind turbine; Inflow measurements; LiDAR; Cyclic pitch control; Simulation;

Correspondence

knkr@dtu.dk

Received . . .

NOMENCLATURE

α	Angle of attack measured at some position on the blade
$\bar{V_0}$	Average free wind speed
ΔT_d	Time shift of preview time
δ	Estimation error of LiDAR measurement transport velocity
$\Delta\theta_{ff}$	Feed-forward collective pitch increment
$\Delta\theta_i$	Individual pitch increment of blade i
λ^i	Tip speed ratio of blade i
Ω	Rotor speed
ϕ	Cone angle of the LiDAR measurement beam

ρ	Density of the air
τ	Preview time for feed-forward controller
τ_1^i	Time constant for dynamic inflow filter for blade i
θ_L	Azimuthal position of the LiDAR beam
θ_c	Collective pitch command
θ_p	Blade pitch
θ_{ref}	Reference pitch signal
$\tilde{T}_d$	Transport time of LiDAR measurements with estimation uncertainty
$\tilde{V}_0(\theta_L)$	Axial inflow velocity estimated using LiDAR as a function of azimuthal position of LiDAR beam
c	Chord length
$C_d(\alpha)$	Drag coefficient as a function of angle of attack
$C_l(\alpha)$	Lift coefficient as a function of angle of attack
c_t^i	Local thrust coefficient at a section of blade i
$C_t^i(\lambda^i, \theta_p^i)$	Thrust coefficient of blade i
F_i	Out of plane load on blade i
f_t^i	Local thrust force intensity on blade at measurement section
L_p	Distance from LiDAR measurement pattern to rotor
$M_{bx,p}^i$	Blade root bending moment around the x-axis (flap) in pitching coordinate system of blade i
M_{bx}^i	Out-of-plane blade root bending moment of blade i
$M_{by,p}^i$	Blade root bending moment around the y-axis (edge) in pitching coordinate system of blade i
M_{tx}	Tower bottom fore-aft moment
M_{yx}	Nacelle tilting moment
M_{yz}	Nacelle yawing moment
T_d	Time from the LiDAR measures a wind speed till it reaches the rotor
T_s	Sampling time
v_a^i	Axial induced velocity of blade i at radius r
$V_L(\theta_L)$	LiDAR measurement of the free wind speed a radial position as a function of azimuthal position
V_r	Relative inflow speed measured at some position on the blade

Wind Energ. 2012; **00**:1–14 © 2012 John Wiley & Sons, Ltd.
DOI: 10.1002/we
Prepared using weauth.cls

1. INTRODUCTION

Wind turbine control systems have traditionally been based on measurements from conventional sensors for measuring rotor speed and electrical power production or torque, wind vanes or sonic anemometers for wind speed and direction measurements, and strain gauges for load estimation. With these sensors, classical control strategies have been applied for rotor speed regulation and load alleviation [1, 2, 3].

Recently, the development of advanced measurement techniques has catalyzed the development of control schemes that are capable of alleviating more of the varying loads experienced by a turbine, and increase the power output. These technologies include different methods for estimating the incoming flow. The application of pitot tubes on wind turbine blades has been demonstrated in the DANAERO experiment [4, 5, 6], and in [7] a control scheme is proposed that is based on inflow measurements from pitot tubes mounted on the blades. However, especially the light detection and ranging (LiDAR) technology has gained interest. Using LiDAR, it is possible to estimate the inflow to a turbine by measuring the wind speed at a distance upstream of the turbine. The experimental capabilities of LiDARs mounted on wind turbines have been demonstrated in several studies, e.g. [8, 9], and the potential errors associated with LiDAR measurements have been analyzed through simulation [10]. For control purposes, LiDAR has been suggested for both improved yaw and pitch control. Yaw error estimation using a spinner mounted LiDAR and the limitations of a nacelle based LiDAR are discussed in [11], and LiDAR based active yaw control is demonstrated in [12]. The potential of applying LiDAR based collective feed-forward collective pitch control have been demonstrated both through simulations and experiments, [13, 14, 15]. The potential of individual pitch control that applies preview information has been studied through simulation, e.g. in [16, 17, 18, 19, 20, 21].

Many of the studies on applying preview control for load alleviation are focused on one measurement technology and compares the performance of a controller based on that particular technology to a baseline controller based on a different and often simpler control design. Hereby, the comparison is likely to be affected by both the potential advantages of the measurement technology and the improved control design. Thus, it is difficult to distinguish between the improvement introduced by the better measurement technology and the more advanced control design. The objective of this study is to investigate the influence of different sensor types on the controller performance, independent of control design. By keeping the control design the same, the strengths and weaknesses of each of the sensor technologies can be explored by assessing the controller performance for different types of inflow.

In this study, a standard cyclic pitch control design is used as test bench for three different types of measurements eligible for use in control schemes for horizontal axis wind turbines. The following measurements are tested as input to the cyclic pitch controller: blade root out-of-plane bending moment, angle of attack and relative inflow velocity measured at a radial section on the blades, and upstream inflow measurements from a LiDAR mounted in the spinner of the rotor.

True feedback control can accomplished using either the blade root out-of-plane bending moment, or local on-blade measurements of angle of attack and relative inflow velocity, whereas the LiDAR measurements can only be applied in a the cyclic pitch control in combination with a inflow model and by assuming that Taylors hypothesis is valid. By applying Taylors hypothesis, it is assumed that the turbulent structures travels unchanged with the mean free wind speed and direction. In contrast to the on-blade measurements, the upstream measurements of the inflow enables feed-forward pitch control. Hereby, pitch actuation can be initiate prior to the occurrence of a wind speed change.

The study is performed through simulations of the a model of the NREL 5MW reference turbine [22], and the controllers and sensors are tested in both deterministic and turbulent inflows using the aero-servo-elastic simulation tool HAWC2 [23].

The paper is laid out as follows: First, the sensors and controllers are described. Then, simulation results are presented for both deterministic and turbulent cases, and finally the results are discussed and conclusions are given.

2. SENSORS

The three different types of signals that will be tested as inputs to the control system in this study could be acquired using the following sensor technologies: strain gauges mounted at the blade roots, pitot tubes mounted at a selected radial position on each of the blades, and a spinner mounted LiDAR measuring the wind speed at a distance in front of the turbine. Figure 1 illustrates the three measurement systems, and in the following the assumptions made for the simulations relating to each of the sensors are described.

2.1. Blade root bending moment measurements using strain gauges

A strain gauge typically consists of a metallic foil whose the electrical resistance changes with its cross sectional that changes with the longitudinal deformation due to the Poisson effect. Hence, by monitoring the resistance of a strain gauge glued to a structure, the strain of the structure at the position of the strain gauge can be estimated, and the three principal axis strains of a structure can be estimated by using multiple strain gauges. The moments can then be estimated from the

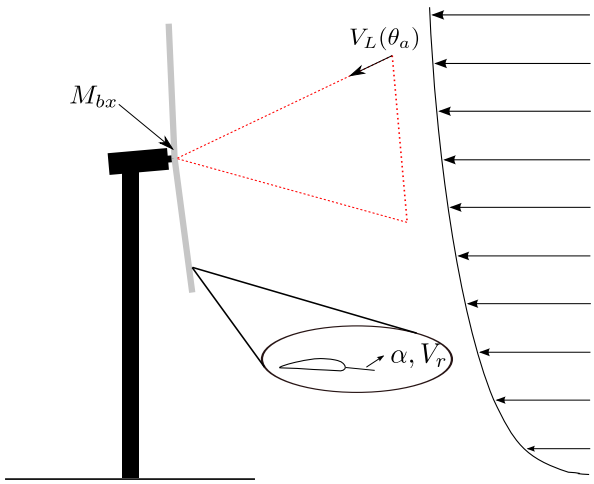

Figure 1. Illustration of the three different measurement types that are simulated in this study.

measured strains by assuming linearity and using calibration. For a wind turbine, strain gauges are typically mounted at the root of the blade from where the blade root bending moments can be estimated. In this study, the out-of-plane blade root bending moment M_{bx} is extracted from the aero-servo-elastic load calculations. In real applications, it is expected that the strain gauges will only provide accurate measurements in a certain frequency range below some cut-off frequency. However, the load variations that are the aim of the this study varies at frequencies around the rotational frequency of the rotor (the 1P frequency), and are well within the range of standard strain gauges. The signals that are extracted from the simulations are low-pass filtered with a 2nd order filter with a cut-off frequency of 10 Hz prior to their use in the controllers to remove high frequency noise.

2.2. Inflow measurements using pitot tubes

Pitot tubes are in essence cylindrical tubes with a distribution of pressure holes, and the flow velocity is estimated from the pressures that are measured at the pressure holes. Both the flow speed and angle can be estimated with a 5 hole pitot tube from the pressure differences between the holes on the well defined tip shaped as a half sphere. For wind turbine applications pitot tubes are typically mounted on the leading edge of the blade pointing forward in the chord wise direction. Hence, the pitot tube measures the local angle of attack, α, and relative inflow velocity V_r at a short distance in front of the blade. Because the measurement is acquired at a small distance in front of the blade, a slight preview of the incoming wind speed is achieved. However, this preview is mostly beneficial for application of flap control, or control based on other localized flow devices because the achievable preview time is very short, and requires very high actuation rates. In this study, the measurements are collected directly from the aero-servo-elastic simulation that provides the angle of attack and relative velocity relative to the 1/4 point. As for the blade root bending moment measurements, the inflow measurements are low-pass filtered before being used by the controller. The measurements are sampled at the 3/4 radial position on the blades, where the force distribution on the blade typically is greatest. Thus, it is expected that measurements collected at 3/4 radial position are the single-point measurements that best represents the overall blade loading. Hence, regulation based on measurements from this position are expected to yield the largest reductions of the overall blade load variations.

2.3. Upstream inflow measurements using a spinner mounted LiDAR

A LiDAR is an optical device that emits laser light at a certain frequency, detects and analyzes the returning light that is reflected by airborne particles, such as dust, aerosols etc. The velocity of the particles is assumed to be equal to the flow velocity, and is estimated from the in and output spectra of the emitted light using Doppler theory. Hereby, the LiDAR provides an estimate of the flow velocity parallel to the emitted laser beam. In this study, the measurements are collected from the HAWC2 simulations using an implemented LiDAR module. The implementation is briefly described in [24] and the theory is described in more general terms in [25]. The LiDAR module is set up to scan in a circular pattern where measurements are sampled on the perimeter of a circle with a diameter corresponding to 3/4 the radius of the rotor as described in [24]. The measurements are sampled approximately 100 meters upstream of the turbine and the wind speeds

DOI: 10.1002/we
Prepared using weauth.cls

that reach the rotor are estimated from the upstream LiDAR measurements under the assumption that the measured wind speed reaches the turbine with a time delay defined as:

$$T_d = \frac{L_p}{\bar{V}_0}, \tag{1}$$

where L_p is the distance from the LiDAR measurement pattern to the rotor, and $\bar{V}_0$ is average free wind speed. In the HAWC2 simulations, the turbulence box is moved through the rotor with a constant velocity, $\bar{V}_0$, and in this study it is assumed that this velocity is known. This is not case in reality where $\bar{V}_0$ has to be estimated from the measurements. The implication of estimating $\bar{V}_0$ is discussed in the Section 4. In summary, the LiDAR provides measurements of the free wind speed projected onto the measurement beam,$V_L(\theta_L)$, as a function of azimuthal position of the LiDAR beam, θ_L and cone angle ϕ. where the cone angle of the LiDAR measurement beam is the angle between the rotor axis and the beam emitted by the LiDAR. The axial inflow to the turbine is estimated as a function of azimuth angle from $V_L(\theta_L)$ as:

$$\tilde{V}_0(\theta_L) = \frac{V_L(\theta_L)}{cos(\phi)}. \tag{2}$$

Equation (2) is valid under the assumption that the actual inflow is parallel to the rotor axis. The limitations of using LiDAR for inflow estimation are discussed in [11].

3. CONTROLLERS

Two types of controllers are involved in this study: a baseline collective pitch controller handling rotor speed regulation, and a cyclic pitch controller aimed at alleviating the 1P varying loads. The baseline collective pitch controller will be active in all simulations, whereas the IPC controller is switched on and off, depending on the test case. A schematic of the control setup is given in Figure 2.

3.1. Collective Pitch Controller

The baseline collective pitch controller that is implemented in this study is similar to the one described for the NREL 5MW reference turbine in [22]. Because the focus in this study is only on load reductions, all simulations are performed in above rated wind speeds. Therefore, only the PI speed control part of the underlying collective pitch controller is active while maintaining constant torque.

3.2. Cyclic Pitch Controller

The cyclic pitch controller is based on the controller described in [2]. The controller is focused at alleviating loads in the non-rotating rotor coordinate system and requires that the out-of-plane loads F_i on the blades $i = 1, 2, 3$ are transformed from the rotating domain to the non-rotating domain. This transformation is achieved using the inverse Coleman transformation defined as [26]:

$$F_0 = \frac{1}{3}\sum_{i=1}^{3} F_i \qquad \begin{bmatrix} F_t \\ F_y \end{bmatrix} = \frac{2}{3}\begin{bmatrix} \cos(\theta_a) & \cos(\theta_a + 2\pi/3) & \cos(\theta_a + 4\pi/3) \\ \sin(\theta_a) & \sin(\theta_a + 2\pi/3) & \sin(\theta_a + 4\pi/3) \end{bmatrix} \begin{bmatrix} F_1 \\ F_2 \\ F_3 \end{bmatrix}, \tag{3}$$

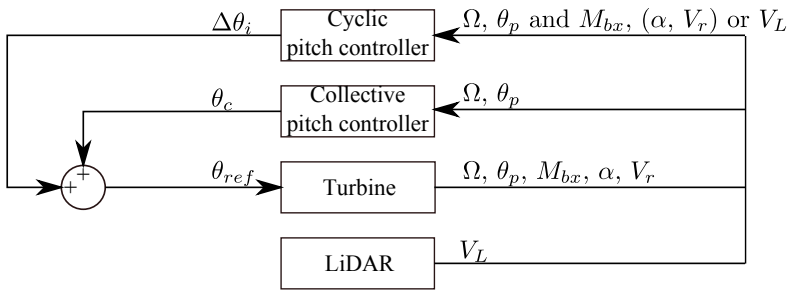

Figure 2. Scematic of the controllers.

where F_0 is the mean thrust on the rotor, F_t and F_y are the tilt and yaw moments on the rotor, and ϕ is the azimuthal angle of blade number 1 that is positive in the rotational direction and with zero deg pointing upwards. To limit the excitation of higher harmonics, F_t and F_y are filtered with a second order filter with at cut-off frequency of 1.5P before two PI controllers are used for calculating the pitch signals, θ_t and θ_y, in the non-rotating domain that will keep F_t and F_y at zero. Finally, the pitch signals are transformed to the rotating domain by applying the Coleman transform:

$$\begin{bmatrix} \Delta\theta_1 \\ \Delta\theta_2 \\ \Delta\theta_3 \end{bmatrix} = \frac{2}{3} \begin{bmatrix} \cos(\phi) & \sin(\phi) \\ \cos(\phi + 2\pi/3) & \sin(\phi + 2\pi/3) \\ \cos(\phi + 4\pi/3) & \sin(\phi + 4\pi/3) \end{bmatrix} \begin{bmatrix} \theta_t \\ \theta_y \end{bmatrix}, \tag{4}$$

where $\Delta\theta_1$, $\Delta\theta_2$ and $\Delta\theta_3$ are the individual pitch increments of blades $i = 1, 2, 3$.

The loads used for each blade in the cyclic pitch controller have only been described in general terms as F_i because the definition of F_i depends on the measurement types. In the following, the specific loads that are used when applying each of the three sensor types are described.

3.2.1. Controller based on blade root bending moments

For the controller that is based on the blade root bending moment measurements, the load F_i is defined as the out-of-plane bending moment at the root of the blade, which is the moment caused by the trust forces on the blades. Usually, the moments are measured on the pitching part of the blade. Hence, the moments are measured in the pitching blade coordinate system, and needs to be transformed to the non-pitching blade root coordinate system. The out-of-plane bending moments of the blades are found as:

$$M^i_{bx} = M^i_{bx,p} \cos(\theta^i_p) + M^i_{by,p} \sin(\theta^i_p), \tag{5}$$

where $M^i_{bx,p}$ and $M^i_{by,p}$ are the blade root bending moment around the x-axis (flap) and y-axis (edge) in the pitching coordinate system of blade i, respectively, and θ^i_p is the pitch angle of blade i. Thus, $F_i = M^i_{bx}$, $i = 1, 2, 3$ when using the blade root bending moment measurements as input to the cyclic pitch controller.

3.2.2. Controller based on local inflow measurements

For the controller based on the local measurements of angle of attack and relative inflow velocity at the 3/4 radius of the blades, it is necessary to combine the two measurements into one load estimate. Such a combination is accomplished by computing the local thrust forces exerted on the blade at the sections where the measurements are made, which can be done by using tabulated airfoil data and pitch angles. First, the local thrust coefficient for each blade section is calculated from the lift and drag coefficients as:

$$c^i_t = C_l(\alpha) \cos(\alpha + \theta^i_p) + C_d(\alpha) \sin(\alpha + \theta^i_p), \tag{6}$$

where $C_l(\alpha)$ and $C_d(\alpha)$ are the lift and drag coefficients that are available from tabulated airfoil data. Then, the local thrust force at the measurement section of each blade is estimated as:

$$f^i_t = \frac{1}{2} \rho c V^i_r c^i_t, \tag{7}$$

where ρ is the density of the air, and c is the chord length at the measurement sections of the blades. Hence, $F_i = f^i_t$, $i = 1, 2, 3$ when using the blade inflow measurements as input to the cyclic pitch controller.

3.2.3. Controller based on spinner LiDAR measurements

The modeled spinner LiDAR provides estimates of the free wind speed that reaches each of the three turbine blades at the 3/4 blade radius. To apply these estimates in a cyclic pitch control scheme, the resulting local inflow to each blade must be estimated. In this study the local inflow is estimated in terms of the angle of attack and relative inflow speed. Hereby, the controller that was described above for the measured local inflow measurements can be applied to the estimated local inflow.

The local inflow to a blade section is illustrated in Figure 3. To estimate the local angle of attack and relative inflow speed, the local axial and tangential induced velocities must also be estimated.

Tabulated steady state induction factors are available from blade element momentum (BEM) calculations as a function of pitch angle, tip speed ration and radial position along the blade. Thus, the induction factors can be estimated when the rotor speed, pitch angles and free wind speed is known. To exploit the LiDARs ability to provide preview measurements, the tip speed ratio of blade i is defined as:

$$\lambda^i = \frac{\Omega R}{\tilde{V}_0(\phi + (i-1)\frac{2\pi}{3} + \tau\Omega)}, \tag{8}$$

Wind Energ. 2012; **00**:1–14 © 2012 John Wiley & Sons, Ltd.
DOI: 10.1002/we
Prepared using weauth.cls

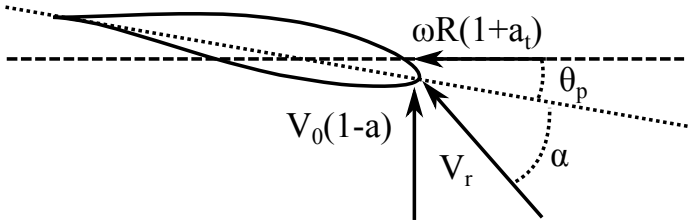

Figure 3. Illustration of the local inflow to a blade section.

where R is the radius of the rotor, Ω is the rotor speed, and τ is the preview time. It is assumed that the tangential induction changes instantaneously, thus, a_t is directly obtained from the tabulated values. Furthermore, it is assumed that the axial induced velocity, v_a^i, at the 3/4 radial position, can be described by a first order filter similar to the one described in [27]:

$$\tau_1^i \dot{v}_a^i + v_a^i = \tilde{V}_0(\phi + (i-1)\frac{2\pi}{3} + \tau\Omega)a(\lambda^i, \theta_p^i), \tag{9}$$

where $a(\lambda^i, \theta_p^i)$ is the steady state axial induction factor at the 3/4 radial position that is available from tabulated BEM calculations and

$$\tau_1^i = \frac{1}{2}\frac{1.1R}{\tilde{V}_0(\phi + (i-1)\frac{2\pi}{3} + \tau\Omega) - 1.3v_a^i}. \tag{10}$$

Using the estimated tangential induction factor and induced axial wind speed, the angle of attack and relative velocity can be estimated for each blade as:

$$\alpha^i = \arctan\left(\frac{\tilde{V}_0(\phi + (i-1)\frac{2\pi}{3} + \tau\Omega) - v_a^i}{\Omega R(1+a_t^i)}\right), \qquad V_r^i = \sqrt{(\tilde{V}_0(\phi + (i-1)\frac{2\pi}{3} + \tau\Omega) - v_a^i)^2 + (\Omega R(1+a_t^i))^2} \tag{11}$$

With the values estimated using Equation (11), the local trust forces can be estimated as described for the controller based on the local on-blade inflow measurements. The preview time for the LiDAR based cyclic pitch controller is set to $\tau = 0.1$s for reasons that are explained in Section 4.1.1.

3.2.4. Tuning of Cyclic Pitch Controller

Because the cyclic pitch controllers in this study are based on three different load measurements, the PI controllers will have three different sets of gains and gain scheduling should be employed to cope with the entire operating range. However, in this study the controllers are only tuned around one operating point, 15 m/s. To be able to perform a fair comparison of the three controllers, the controllers are all tuned in the same manner using an iteratively Ziegler-Nichols method, [28].

4. RESULTS

First, the controllers are simulated in deterministic inflows, and the time series are analyzed to identify fundamental difference between the three systems. Furthermore, the feed-forward controller's sensitivity to uncertainties in the preview time is assessed in deterministic inflow. Finally, simulations are performed with turbulent inflow to evaluated the fatigue load reductions that achievable with each of the controllers. The turbulent inflow is modeled by Cartesian boxes of Mann turbulence [29].

4.1. Deterministic Inflows

Initially, a standard IEC wind shear [30] with a power coefficient of 0.2 is applied and simulations are performed with each of the cyclic pitch controllers and the baseline collective pitch controller applied. Figure 4 shows a section of the resulting steady state time series, and Figure 5 shows the applied steady state pitch actuation as a function of rotor azimuth

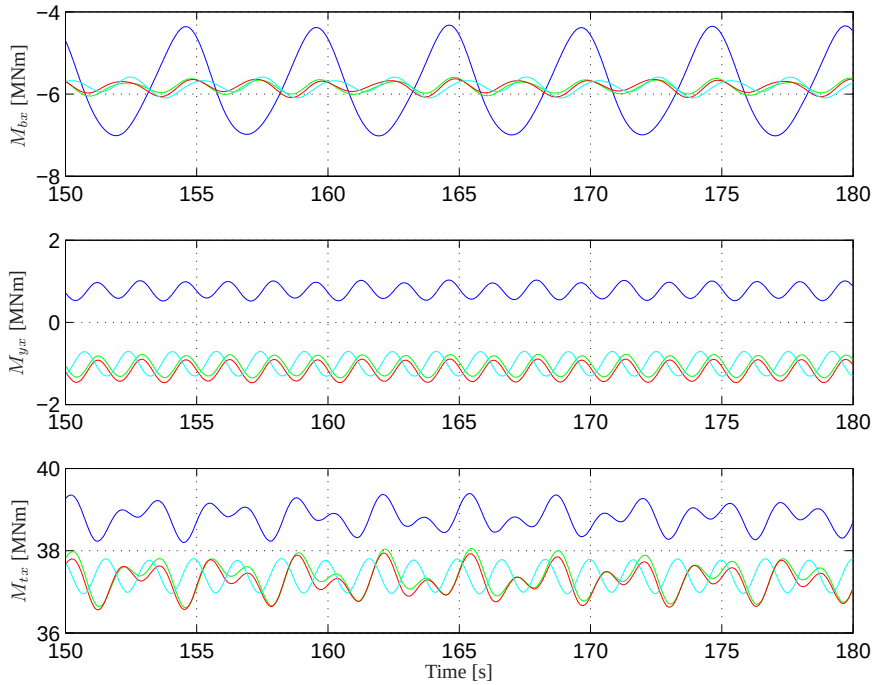

Figure 4. Sample of the steady state time series results of simulations in deterministic inflow with an IEC power law wind shear with the three cyclic pitch controllers and the baseline collective pitch controller applied. Collective pitch controller (blue), cyclic pitch based on blade root moments (green), cyclic pitch based on local inflow measurements (red), and cyclic pitch based on spinner LiDAR measurements (cyan)

angle. All three cyclic pitch controllers significantly decreased the 1P blade root out-of-plane bending moment variations. The remaining moment variations are at frequencies higher than the rotational speed, and beyond the capabilities of the implemented controllers. The range of the remaining loads are similar for all three cyclic pitch controllers. However, whereas the remaining loads are in phase for the controllers based on the on-blade measurements, the remaining loads of the LiDAR based controller have a slight phase shift. This phase shift is likely due to the fact that the blade dynamics is not captured by the LiDAR measurements, and the resulting pitch actuation is only affected by the free inflow variations and does not accommodate any damping of the blade movement. Figure 5 shows that the pitch signal of the LiDAR based controller is shifted in phase compared to the two other cyclic pitch controllers and has slightly less amplitude. The pitch signal of the LiDAR based controller has its minimum almost exactly at the bottom position of the rotor, whereas the signal is slightly shifted for the two other controllers.

Because of the vertical wind shear, the thrust on the rotor is larger in the upper half of the rotor plane than in the bottom half. For the collective pitch controller the uneven thrust distribution creates an overturning tilting moment, which is seen in Figure 4 as a positive mean steady state moment. When cyclic pitch is applied, the thrust distribution is smoothened and is approximately evenly distributed on the rotor. Hereby, the overturning tilting moment is removed and the remaining mean steady state tilting movement is there because of the weight of the rotor that is supported at the tower top.

From the plot of the tower bottom fore-aft moment, it is seen that the variations are slightly increased in magnitude but the mean value is slightly decreased when cyclic pitch is applied. The decreased mean value is caused by the smoothening of the thrust on the rotor.

Based on the results for the stationary and deterministic inflow, it appears that the slight preview, which is possible with the LiDAR, does not increases the controller performance compared to the feed-back controllers. Therefore, simulations are performed with the IEC extreme wind shear [30] to test if the preview can increase the controller performance in more complex situations. Figure 6 shows the free wind speed at the top and bottom of the rotor plane, pitch actuation, blade root out-of-plane bending moment, tilting moment, and tower bottom fore-aft bending moment for simulations with the

DOI: 10.1002/we
Prepared using weauth.cls

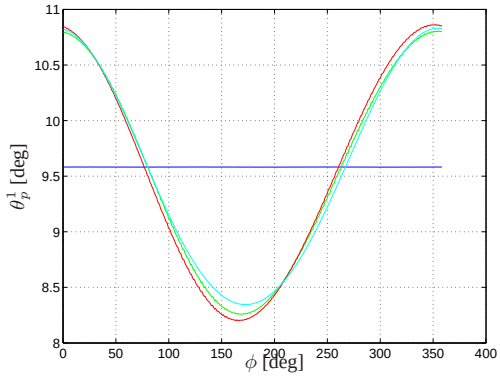

Figure 5. Pitch signal applied in simulation in deterministic inflow with a power law wind shear with the three cyclic pitch controllers and the baseline collective pitch controller applied. Collective pitch controller (blue), cyclic pitch based on blade root moments (green), cyclic pitch based on local inflow measurements (red), and cyclic pitch based on spinner LiDAR measurements (cyan)

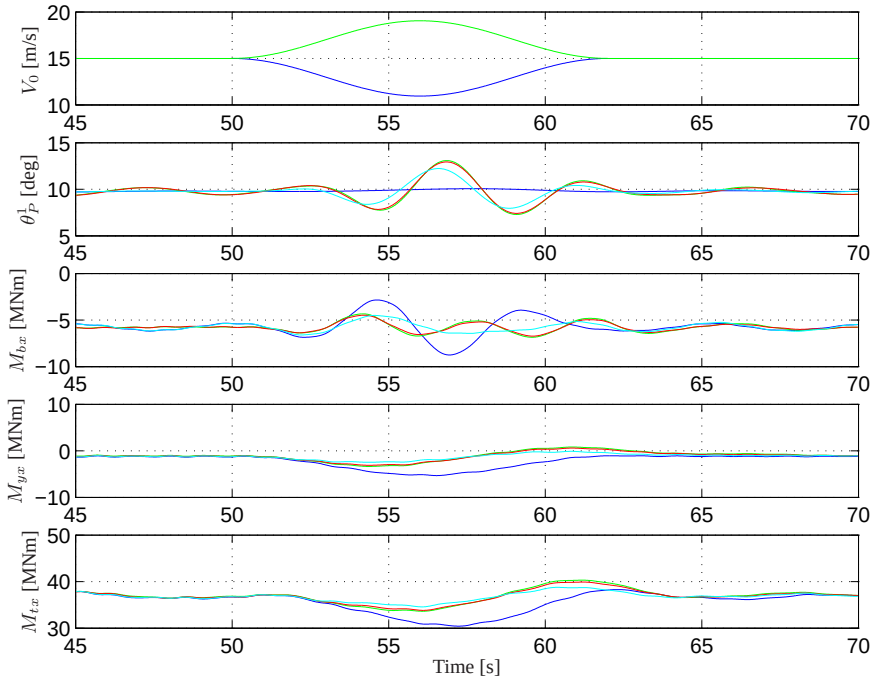

Figure 6. Results of simulations in deterministic inflow with IEC extreme wind shear. In the top plot the wind speed at the rotor top (blue) and bottom (green) is shown. In the remaining plots the performance of the different applied controllers are shown. Collective pitch controller (blue), cyclic pitch based on blade root moments (green), cyclic pitch based on local inflow measurements (red), and cyclic pitch based on spinner LiDAR measurements (cyan)

baseline collective pitch control and cyclic pitch control based on the three different measurement types. With the LiDAR based cyclic pitch controller, pitch actuation is initiated earlier than with any of the other cyclic pitch controllers, and the resulting blade and tower load variations are slightly lower for the LiDAR based controller.

4.1.1. Sensitivity of LiDAR Based Controllers

The results for the LiDAR based controller presented in the previous section were obtained with a preview time of 0.1s. In this section sensitivity of the controller performance to the preview time is explored. The sensitivity is explored through a series of simulations with varying preview time for the LiDAR based controller. The simulations are carried out with both the same extreme wind shear change as above and a standard stationary IEC wind shear. The results for both types of inflow are presented in Figure 7 that shows the range of the steady state blade root out-of-plane bending moments for the standard wind shear, and the range of the extreme blade root out-of-plane bending moments for the extreme wind shear as a function of the preview time. The moment ranges have been normalized with the ranges observed for the baseline collective pitch controller. For comparison, the moment ranges observed using either M_{bx} or the on-blade inflow measurements as input to the cyclic pitch controller are also shown. For the extreme wind shear, the preview that results in the minimum moment range is 0.1s. With this preview time, the range of the extreme loads are decrease slightly more than with any of the other cyclic pitch controllers. However, the performance of the controller appears to be sensitive to changes in preview time. If the preview time is changed $\Delta T_d = \pm 0.1$s from the optimal preview time, the extreme load range is equal to that of the local inflow measurement based controller, $\Delta T_d = \pm 0.3$s will yield a load range equal to that of the blade root bending moment based controller, and $\Delta T_d = \pm 1$s will yield a load range equal to that of the collective pitch controller. The results presented in Figure 7 relies on the assumption that the speed at which a measured wind speed travels towards the turbine is known. Hereby, the specified preview time is always achieved. In a reality, the true transport velocity of a measured wind speed is not know and a more realistic estimate of the transport time could be:

$$\tilde{T}_d = \frac{L_p}{\bar{V}_0 + \delta}, \tag{12}$$

where δ is the estimation error associated with the transport velocity. The estimation error effectively changes the preview time because the wind speeds expected to reach the rotor are shifted in time. The effective preview time is then:

$$\tilde{\tau} = \tau + \Delta T_d, \quad \text{where} \quad \Delta T_d = T_d - \tilde{T}_d. \tag{13}$$

Hereby, the transport velocity error δ causing an effective preview time change ΔT_d is:

$$\delta = \frac{-L_p}{\Delta T_d - \frac{L_p}{\bar{V}_0}} - \bar{V}_0. \tag{14}$$

In Figure 8 δ is plotted as a function of ΔT_d for a mean wind speed of 15 m/s. It is seen that the LiDAR based controller only outperforms the local inflow measurement based controller if the transport velocity error is $-0.2 \leq \delta \leq 0.2$ m/s. To outperform the controller based on the blade root bending moment measurements, the transport velocity error should be $-0.6 \leq \delta \leq 0.7$ m/s. Finally, the error should be $-2.0 \leq \delta \leq 2.6$ m/s for the LiDAR based cyclic pitch controller to outperform the collective pitch controller.

For the standard IEC wind shear, the optimal preview time is identified from Figure 7(b) as 0.1 s. Hence, the same as for the extreme wind shear. The sensitivity of the performance is again seen to be very sensitive to preview time uncertainties. Furthermore, it is seen that even with the optimal preview time, the load reductions of the LiDAR based controller is not as large as with either of the on-blade measurement based controllers.

In summary for the results in deterministic inflow, it appears that the three cyclic pitch controllers yields similar performance for the stationary case, under the assumption that the transport velocities of the LiDAR measurements are known precisely. For the extreme wind shear change, the results showed that the LiDAR based controller yields the largest extreme load reductions, but the magnitude of the reduction is very sensitive to uncertainties relating to the transport velocity of the LiDAR measurements. Finally, the results showed that for the extreme wind shear changes, the cyclic pitch controller based on the local inflow measurements yielded larger load reductions than the controller based on the blade root bending moment. The larger load reduction might might be contributed to the fact that the effect of an inflow change is filtered by both the dynamic inflow model and the blade dynamics before reaching the blade root, and a time lag is hereby introduced. The effect of the inflow change on the local inflow is only filtered by the dynamic inflow model, hence the response of the inflow measurements is faster than the structural response at the blade root. Thus, pitch actuation can be initiated faster by using the local inflow measurement than using the blade root moment.

4.2. Turbulent Inflow

In the previous section, the performances of the controllers were analyzed in deterministic inflow. However, because the real inflow to a turbine is stochastic, the controllers' performance is also assessed in turbulent inflow. Turbulence that fulfills the IEC standards for class A turbulence is generated and simulations are performed with both the collective pitch controller and all of the three types of measurements applied for cyclic pitch control. The simulation results are shown in Figure 9 as plots of the blade root out-of-plane bending moment and tower bottom fore-aft bending moment spectra. It is seen that all the applied cyclic pitch controllers significantly reduces the 1P peak in the blade load spectrum and

DOI: 10.1002/we
Prepared using weauth.cls

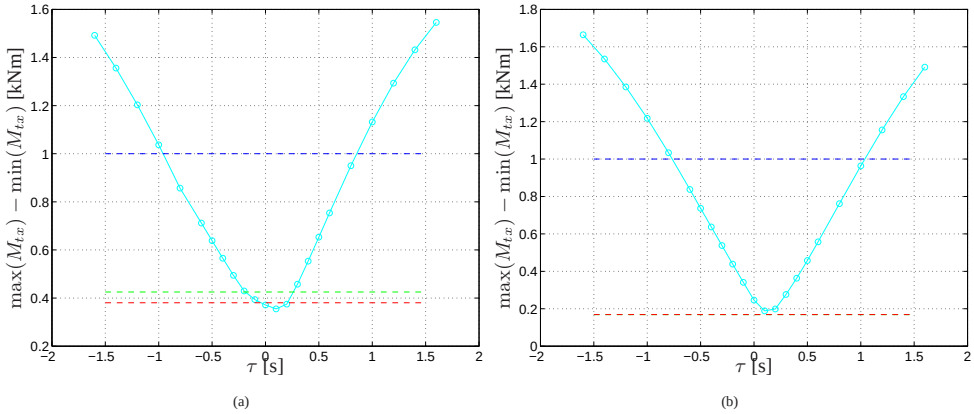

Figure 7. Results of simulations in situations with an IEC extreme wind shear (a) and standard IEC wind shear (b).Range of extreme loads caused by the wind shear as a function of preview time of the Lidar based cyclic pitch (cyan), collective pitch controller (blue), Mbx based cyclic pitch (green), and cyclic pitch based on on-blade inflow measurements (red). The results have been normalized with the moment range observed when the baseline collective pitch controller is applied.

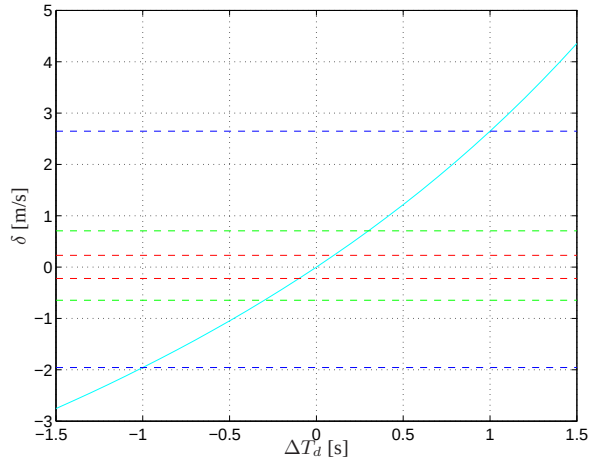

Figure 8. Transport velocity error as a function of preview time shift (cyan). The six horizontal lines indicates the error that decreases the performance of the LiDAR based cyclic pitch controller to the levels of the inflow based IPC (red), blade root bending moment IPC (green), and collective pitch controller (blue), respectively.

leaves the tower bottom load spectrum almost unchanged. The spectra of the blade root bending moment and local inflow measurement based control are almost identical, whereas the spectra of the LiDAR based controller shows higher values in the area around the 1P peak than the other two cyclic pitch controllers. The less load reduction of the LiDAR based controller can be due to the missing blade dynamics, as discussed for the deterministic case, or it can be due to uncertainties with estimating the inflow using a conical scan scan. The uncertainties of using a conical scan are discussed in [11]. It might be possible to improve the performance of the LiDAR based controller through a more sophisticated control design that employs a model of the turbine and blades, or includes blade root bending moment measurements. However, such a controller comes of the price of increased system complexity. In summary, the results in Figure 9 corresponds well to what was observed for simulations in deterministic inflows. Hence, it appears that for a regular inflow with standard turbulence, the cyclic pitch controller based on on-blade measurements outperforms the LiDAR.

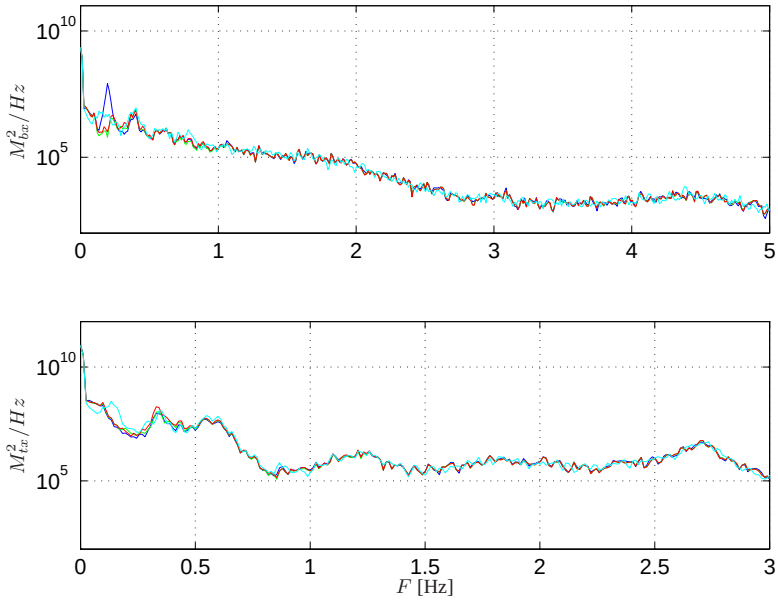

Figure 9. Blade root out-of-plane bending moment (top) and tower bottom fore-aft bending moment (bottom) spectra for 10-min simulations in standard class A turbulence and wind shear with the collective pitch controller (blue), cyclic pitch control based on blade root moments (green), cyclic pitch control based on local inflow measurements (red), and cyclic pitch control based on spinner LiDAR measurements (cyan).

The controller performance is quantified by the 1 Hz damage equivalent loads (DEL) experienced by the turbine when each of the controllers are applied. The damage equivalent blade root out-of-plane and tower bottom fore-aft loads calculated from results of 10 min simulations are summarized in Table I. It is seen that the blade load variation decreases are penalized by slightly increased tower bottom bending moment damage equivalent loads. The increased tower bottom loads might be reduced by a more sophisticated cyclic pitch control design.

5. CONCLUSIONS

In this study, the influence of three different measurement types on the performance of a cyclic pitch controller was investigated. The three different measurements were tested as input to the same cyclic pitch control scheme tuned in a consistent manner, and with identical inflow conditions.

The results showed that, in deterministic inflow with constant wind shear, the three cyclic pitch controllers yielded similar load reductions compared to a standard collective pitch scheme. For situations with changing wind shear the results showed that the LiDAR based controller yielded slightly larger load reductions compared to controllers based on the on-blade measurements. However, for both inflow cases it was observed that the LiDAR based controller is very sensitive to errors in the inflow estimation, and even small errors will deteriorate the performance of the controller.

	Collective pitch	M_{bx} cyclic pitch	Inflow cyclic pitch	LiDAR cyclic pitch
M_{bx}	100%	85.1%	85.8%	90.7%
M_{tx}	100%	103%	108%	110%

Table I. Damage equivalent blade root out-of-plane bending and tower bottom fore-aft bending loads for the collective pitch controller and the three variations of the cyclic pitch controller. The results have all been normalized with the damage equivalent loads of the collective pitch controller.

Wind Energ. 2012; **00**:1–14 © 2012 John Wiley & Sons, Ltd.
DOI: 10.1002/we
Prepared using weauth.cls

Simulations in turbulent inflow showed that using the blade root bending moments as input to the cyclic pitch controller resulted in blade root fatigue load reductions of 15% compared to the baseline collective pitch controller. Using the on-blade inflow measurements the load reductions were 14%, and with the LiDAR measurements the load reductions were 9%. The blade load reductions of all three cyclic pitch controllers came at a price of increased tower bottom loads. The largest increase was observed for the LiDAR based controller.

Overall it has been shown that the uncertainties relating to the time delay of the LiDAR measurement is a significant weakness of the LiDAR based controllers, when used for individual pitch control. It is concluded that for the implemented control schemes the potential of using LiDAR measurement for cyclic pitch control is limit in comparison with using on-blade measurements that does not enable preview.

REFERENCES

1. T. Burton, D. Sharpe, N. Jenkins, and E. Bossanyi. *Wind Energy Handbook*. John Wiley & Sons, Ltd, 2001.
2. E. A. Bossanyi. Individual blade pitch control for load reduction. *Journal of Wind Energy*, 6:119–128, 2003.
3. E. A. Bossanyi. Further load reductions with individual pitch control. *Journal of Wind Energy*, 8:481–485, 2005.
4. H A Madsen and A Fischer. Wind shear and turbulence characteristics from inflow measurements on the rotating blade of a wind turbine rotor. In *Procedings of EWEC2009*, 2009.
5. Christian Bak, Helge A. Madsen, Uwe Schmidt Paulsen, Mac Gaunaa, Peter Fuglsang, Jonas Romblad, Niels A. Olesen, Peder Enevoldsen, Jesper Laursen, and Leo Jensen. Dan-aero mw: Detailed aerodynamic measurements on a full scale mw wind turbine. In *Proceedings of EWEC2010*, 2010.
6. Helge Aagaard Madsen, Christian Bak, Uwe Schmidt Paulsen, Mac Gaunaa, Peter Fuglsang, Jonas Romblad, Niels A. Olesen, Peder Enevoldsen, Jesper Laursen, and Leo Jensen. The dan-aero mw experiments. final report. Ris Report Ris-R-1726(EN), Ris, 2010.
7. TJ Larsen, HA Madsen, and K Thomsen. Active load reduction using individual pitch, based on local blade flow measurements. *Journal of Wind Energy*, 8:67–80, 2005.
8. T. Mikkelsen, K. Hansen, N. Angelou, M. Sjöholm, M. Harris, P. Hadley, R Scullion, G. Ellis, and G. Vives. Lidar measurements from a rotating spinner. In *Proceedings of EWEC2010*. EWEC, 2010.
9. M. Harris, D. J. Bryce, A. S. Coffey, D. A. Smith, J. Birkemeyer, and U. Knopf. Advance measurement of gusts by laser anemometry. *Journal of Wind Engineering and Industrial Aerodynamics*, 95(12):1637 – 1647, 2007.
10. E. Simley, L.Y. Pao, R. Frehlich, B. Jonkman, and N. Kelley. Analysis of wind speed measurements using continuous wave lidar for wind turbine control. 2011.
11. K. A. Kragh, M. H. Hansen, and T. Mikkelsen. Precision and shortcomings of yaw error estimation using spinner based lidar. *Wind Energy*, 2012.
12. E. Dakin, M. Priyavadan, and A Hopkins. Catching the wind, an update on improved yaw alignment. In *Proceedings of EWEA*, 2011.
13. David Schlipf and Martin Kuehn. Prospects of a collective pitch control by means of predictive disturbance compensation assisted by wind speed measurements. In *Proceedings of DEWEK*, 2008.
14. David Schlipf, Simone Schuler, Patrick Grau, Frank Allgwer, and Martin Kuehn. Look-ahead cyclic pitch control using lidar. In *Proceedings of The Science of Making Torque from Wind 2010*, 2010.
15. David Schlipf. Field testing of feedforward collective pitch control on the cart2 using a nacelle-based lidar scanner. In *Proceedings of The Science of Making Torque from Wind 2012*, 2012.
16. F. Dunne, L. Y. Pao, A. D. Wright, B. Jonkmann, N. Kelley, and E. Simley. Adding feedforward blade pitch control for load mitigation in wind turbines: Non-causal series expansion, preview control, and optimized fir filter methods. In *49th AIAA Aerospace Sciences Meeting including the New Horizons Forum and Aerospace Exposition*, 2011.
17. J. Laks, L. Y. Pao, E. Simley, A. D. Wright, N. Kelley, and B. Jonkman. Model predictive control using preview measurements from lidar. In *49th AIAA Aerospace Sciences Meeting including the New Horizons Forum and Aerospace Exposition*, 2011.
18. Knud A. Kragh and Morten H. Hansen. Individual pitch control based on local and upstream inflow measurements. In *Proceedings of the 50th AIAA Aerospace Sciences Meeting Including the New Horizons Forum and Aerospace Exposition*, 2012.
19. Fiona Dunne, David Schlipf, Lucy Y. Pao, Alan D. Wright, Bonnie Jonkman, Neil Kelley, and Eric Simley. Comparison of two independent lidar-based pitch control designs. In *Proceedings of the 50th AIAA Aerospace Sciences Meeting Including the New Horizons Forum and Aerospace Exposition*, 2012.
20. Fiona Dunne, Lucy Y. Pao, Alan D. Wright, Bonnie Jonkman, and Neil Kelley. Adding feed forward blade pitch control to standard feedback controllers for load mitigation in wind turbines. *Mechatronics*, 21(4):682–690, 2011.
21. Jason Laks, Lucy Pao, Alan Wright, Neil Kelley, and Bonnie Jonkman. The use of preview wind measurements for blade pitch control. *Mechatronics*, 21(4):668–681, 2011.

22. J. Jonkman. Nrel 5 mw baseline wind turbine. Technical report, NREL/NWTC, 1617 Cole Boulevard; Golden, CO 80401-3393, USA, 2005.
23. T. J. Larsen. How 2 hawc2, the user's manual. Risø-r-1597(ver. 3-9)(en), Risø-DTU, September 2009.
24. K. A. Kragh, M. H. Hansen, and T. Mikkelsen. Improving yaw alignment using spinner based lidar. In *Proceedings of the 49th AIAA Aerospace Sciences Meeting Including the New Horizons Forum and Aerospace Exposition. American Institute of Aeronautics and Astronautics*. AIAA, 2011.
25. A. Pena and C. B. Hasager. Remote sensing for wind energy. Risø-i-3068(en), Risø-DTU, May 2010.
26. G Bir. Multiblade coordinate transformation and its application to wind turbine analysis. Technical Report CP-500-42553, National Renewable Energy Laboratory, 2008.
27. L.C. Henriksen, M.H. Hansen, and N.K. Poulsen. A simplified dynamic inflow model and its effect on the performance of free mean wind speed estimation. *Wind Energy*, pages n/a–n/a, 2012.
28. J G Ziegler and N B Nichols. Optimum settings for automatic controllers. *Transactions of the ASME*, 64:759768, 1942.
29. J. Mann. Wind field simulation. *Probabilistic Engineering Mechanics*, 13(4):269 – 282, 1998.
30. International Electrotechnical Commission. Iec61400-1(2005) wind turbines.

DOI: 10.1002/we
Prepared using weauth.cls

Appendix F

Individual Pitch Control Based on Local and Upstream Inflow Measurements

Individual Pitch Control Based on Local and Upstream Inflow Measurements

Knud A. Kragh* and Morten H. Hansen†

Risø-DTU, National Laboratory for Sustainable Energy, Roskilde, 4000, Denmark

As wind turbine sizes are increasing, the issue of load alleviation is becoming increasingly important to accommodate design requirements. Load alleviation can be achieved using either local flow devices, such as trailing edge flaps or using individual pitch, the latter being the topic of the present study. In this study, a controller based entirely on inflow measurements is designed. The performance of the controller is tested through simulations in standard operating conditions using two different measurement types; local measurements of angle of attack and relative velocity at a radial position on each blade, and upwind inflow measurements from a spinner mounted LIDAR. The controller is tested both with and without the ability to preview the incoming wind speed. Results show that using either of the tested control strategies the 1P peak in the load spectrum can be removed. It is shown that fatigue load reductions of around 30 percent can be achieved using the local inflow measurements and around 20 percent using the spinner LIDAR measurements.

Nomenclature

α_i	Angle of attack of blade i at a radial position
$\bar{F}_t$	Average thrust coefficient
$\bar{V}_{0,L}$	Mean wind speed estimated using LIDAR
$\Delta C_{t,i}$	Thrust coefficient increment of blade i
λ	Tip speed ratio
ω	Rotational speed of the rotor
ω_s	Sampling frequency
ρ	Density of the air
θ_L	Azimuthal position of LIDAR beam
θ_m	Cone angle of LIDAR measurement cone
$\theta^0_{a,i}$	Current azimuthal position of blade i
$\theta^k_{a,i}$	Preview azimuthal position k of blade i
$\theta_{p,i}$	Pitch angle of blade i
$\tilde{\alpha}$	Angle of attack estimated from LIDAR measurements
$\tilde{V}_r$	Relative velocity estimated from LIDAR measurements
a	Axial induction factor
a_t	Tangential induction factor
c	Chord length
C_d	Drag coefficient
C_l	Lift coefficient
$C_{t,i}$	Local thrust coefficient of blade i at a radial position
$C^{ref}_{t,i}$	Reference thrust coefficient of blade i
$F_{t,i}$	Local thrust force on blade i at a radial position
L_f	Focus length of the LIDAR
N_p	Number of preview samples

*PhD Student, Risø-DTU, National Laboratory for Sustainable Energy, Roskilde, 4000, Denmark
†Senior Scientist, Risø-DTU, National Laboratory for Sustainable Energy, Roskilde, 4000, Denmark

R	Radial position of the blade cross section
t_r	Time at which a measured wind speed reaches the rotor plane
t_s	Sample instance
$V_{0,L}$	Axial velocity estimated using LIDAR
$V_{0,L}^r$	Axial velocity at the rotor plane estimated using LIDAR and assuming frozen turbulence
V_L	Wind speed measured by spinner LIDAR
$V_{r,i}$	Relative velocity of blade i at a radial position

I. Introduction

The dominating sources of the varying loads on wind turbines, except for edgewise gravity loads, are the deterministic and stochastic variations in the wind. As rotor sizes increase, the swept area of the rotor will contain large wind speed and direction variations due to wind shear, veer, turbulence, and wakes from nearby turbines. These variations in the inflow will cause variations in the loads induced on the turbine which can not be alleviated using collective pitch control. Hence, more advanced control techniques are required.

Numerous attempts have been made to develop advanced control schemes for alleviating the varying loads. The suggested methods can be categorized in two categories; lifting surface methods such as trailing edge flaps, and pitch control methods, the latter being the topic of this paper.

Early attempts on implementation of pitch control for load alleviation were based on knowledge from the helicopter technology and is referred to as cyclic pitch control.[1,2] Cyclic pitch is based on applying the multi-blade transformation to blade root bending moment signals. The multi-blade transformation yields non-rotating tilt and yaw moments which can be alleviated using classical PI control schemes. Control actions calculated in the non-rotating frame of reference are transformed back to pitch signals in the rotating frame of reference using the inverse multi-blade transformation.

Recent work on individual pitch control includes further developments of the cyclic pitch methods,[3] gust load reduction using nonlinear estimators to estimate inflow parameters based on blade root bending moments,[4] and methods based on combining LIDAR wind speed measurements with turbine models.[5,6] A more thorough review on methods for load alleviation using both individual pitch and lifting surface methods is given by T. Barlas et al.[7]

The objective of the present study is to develop and test a simple inflow measurement based individual pitch controller. The controller will be based only on inflow measurements and aerodynamic data. Thus, the controller will not depend on structural models of the turbine as many of the advanced controllers do. Because of the simplicity of the controller, the performance of the controller will depend more on the inflow measurements than on modeling issues. Due to the controllers simplicity and its dependence only on inflow measurements, the controller can be used as benchmark controller for testing different inflow measurement types, and assessing the influence of the different measurement distortions on controller performance. Furthermore, a simple controller has the advantage compared to advanced model based controllers that it is less computational intensive and does not require a large number of linearizations of the turbine model which is generally non-linear. The developed inflow measurement based controller is used to assess the load reductions that can be achieved using only inflow measurement and no models of the turbine. Furthermore, the controller will be used to investigate how two different approaches for measuring inflow affects the performance of a inflow measurement based controller. The two measurement approaches that will be tested are: perfect local measurements of angle of attack and relative velocity at a radial position on the blades and wind speed measurements from a spinner mounted LIDAR.[8] The control scheme is tested with and without preview of the incoming wind speed. The individual pitch control scheme developed in this study is based on the ideas in Ref. 9.

II. Control Scheme

In the control scheme suggested by T.J. Larsen et al.,[9] a reference pitch signal is calculated as the difference between the angle of attack at a radial position of one blade and the average angle of attack measured at all blades plus the difference in the corresponding relative velocities multiplied with a gain. The magnitude of the gain is extracted from simulations of a turbine operating in a skew inflow with a cyclic pitch controller, as described in Ref. 9. To remove the dependence on the cyclic pitch controller in the control design, an alternative control scheme is suggested.

The control scheme introduced in this study depends only on inflow measurements and the aerodynamic properties of the blades. It is assumed that the following measurements are available: angle of attack and relative velocity at a certain radial position on the blades, azimuthal position of the rotor, pitch angle and pitch angular velocity of each blade. How the inflow measurements might be obtained is discussed in Section A. Apart from the measurements, it is assumed that the lift, drag and local stationary induction coefficients are available for the blade cross sections at which the inflow measurements are made. The lift and drag coefficient are available through the aerodynamic data of the blades, whereas the induction coefficients are calculated offline using standard blade element momentum theory, c.f. Ref. 10. The calculated induction surfaces are given in Figure 1

The objective of the controller designed in this study is to alleviate the varying thrust loads on the blades. These variations are due to the varying inflow conditions the blades experiences during rotation, caused by wind shear or turbulence. Since inflow measurements are only available at one position on each blade, only the thrust force at one section can be estimated and alleviated. Therefore, the measurements should be positioned at the position where the thrust force intensity is the greatest. The position on the blade, at which the thrust force intensity is the greatest, is typically at the three quarter radius. Hence, in the present study the measurements will be sampled at three quarters of the radius of the blades.

The local thrust forces on a blade, i, at a particular radial position is given as:[10]

$$F_{t,i} = \frac{1}{2}\rho c V_{r,i}^2 C_{t,i}, \tag{1}$$

where ρ is the density of the air, c is the chord length, $V_{r,i}$ is the relative velocity, and $C_{t,i}$ is the local thrust coefficient. The local thrust coefficient for a blade, i, is given as:

$$C_{t,i} = C_l(\alpha_i)\cos(\alpha_i + \theta_{p,i}) + C_d(\alpha_i)\sin(\alpha_i + \theta_{p,i}), \tag{2}$$

where $C_l(\alpha_i)$ and $C_d(\alpha_i)$ are the local lift and drag coefficients as functions of local angle of attack α_i, and $\theta_{p,i}$ is the pitch of blade i. Assuming quasi-stationary conditions, $F_{t,i}$ can be calculated for each blade at each time step using the measurements and Equation (1) and (2). To minimize the variations of the thrust force, $F_{t,i}$ should be equal for all three blades. To ensure that the individual pitch controller does not interfere with the collective pitch controller, the average thrust force of the three blades, $\bar{F}_t$, is chosen as reference. Inspecting Equation (1), it is seen that $F_{t,i}$ is a function of both relative velocity and angle of attack ($C_{t,i}$). The relative velocity can not be changed significantly by pitching, however $C_{t,i}$ can be changed through the angle of attack by pitching. Using Equation (1) and $\bar{F}_t$, a reference thrust coefficient for each blade can be found as:

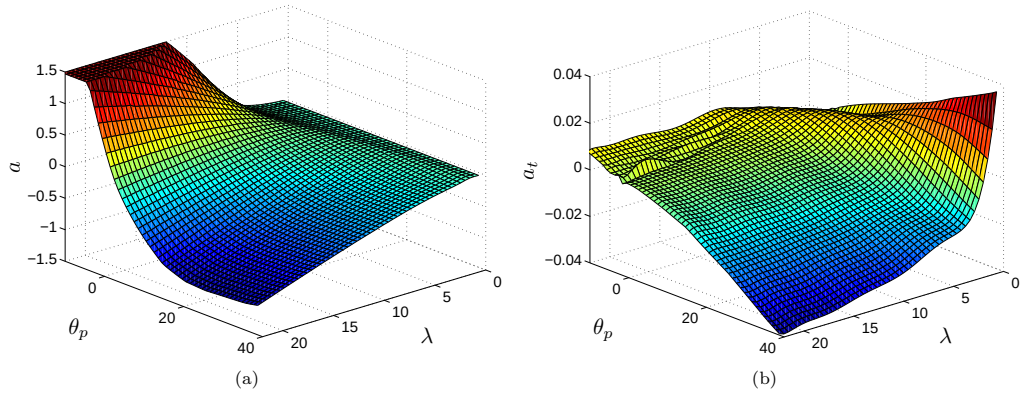

Figure 1. Local induction factors at the three quarter radial position of the blades of the case turbine as a function of tip speed ration, λ, and pitch angle, θ_p. a) Axial induction factors, b) Tangential induction factors.

$$C_{t,i}^{ref} = \frac{\bar{F}_t}{\frac{1}{2}\rho c V_{r,i}^2}. \tag{3}$$

The necessary thrust coefficient increment for each blade is then calculated as:

$$\Delta C_{t,i} = C_{t,i}^{ref} - C_{t,i}. \tag{4}$$

Assuming quasi-stationary inflow, the pitch increment, $\Delta\theta_{p,i}$, giving the desired thrust coefficient increments, $\Delta C_{t,i}$, can be estimated using Equation (2) and a numerical root finding method, e.g. Newton-Rahpson or Bi-section. The individual pitch increment, $\Delta\theta_{p,i}$, is added to the pitch reference of the collective pitch controller and the sum is then the reference which the pitch servo control system should track. The pitch servo is modeled by letting a 2nd order filter describe the transfer function from pitch demand to achieved pitch actuation. The natural frequency and damping ration of the filter is set to 1 Hz and 0.8, respectively.

A. Measurements

There are different possible approaches for obtaining the angle of attack and relative velocities necessary for calculating the reference pitch signals. In this study two different measurement approaches are tested; local inflow measurements and upstream measurements. In reality local inflow measurement could e.g. be obtained using 5-hole pitot tubes mounted at radial positions on the blades. In the DanAero experiment the capabilities of pitot tubes for wind turbine applications were demonstrated.[11] In this study, it is assumed that perfect local measurements of angle of attack and relative velocities are instantaneously available at each time step at each blade at the three quarter radial position. Hence, the performance of the controller based on the local measurement will reflect the upper level of what is achievable with the current controller design. The upwind measurements are assumed to be available from a spinner mounted LIDAR scanning in a circular scan pattern with a radius corresponding to the radial position of the local inflow measurements. An experimental study of such a LIDAR system is found in Ref. 12. The LIDAR system is illustrated in Figure 2.

A more elaborate description of the LIDAR system and how the LIDAR measurements are simulated is found in Ref. 13. The LIDAR provides estimates of the axial inflow velocity based on the measured line of sight velocity (the wind speed projected onto the measurement beam). The estimated axial velocity is defined as:

$$V_{0,L}(\theta_L) = \frac{V_L(\theta_L)}{\cos(\theta_m)}, \tag{5}$$

where V_L is the line of sight wind speed measured by the LIDAR. The estimated axial velocities are associated with uncertainties relating to both geometrical issues and spatial averaging in the laser beam emitted by the

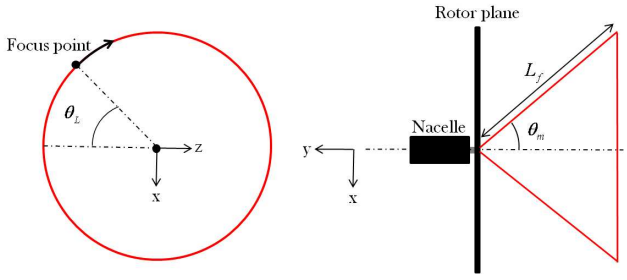

Figure 2. Circular scan pattern. Measurement beam is rotated with a fixed measurement cone angle, θ_m, constant focus length, L_f and constant rotational speed $\dot{\theta}_L$. Right: Top-view, left: View in the direction of the wind.

LIDAR. A thorough analysis of the uncertainties can be found in Ref. 14. To enable usage of the LIDAR measurements for control purposes the wind speed at the rotor must be estimated. The wind speed at the rotor plane is estimated by assuming frozen turbulence. Hence, it is assumed that wind speeds measured at a distance upwind of the turbine will reach the turbine with a time lag depending on the mean wind speed. The time at which the measured wind speed will reach the rotor plane is defined as:

$$t_r = t_s + \frac{L_f \cos(\theta_m)}{\bar{V}_{0,L}} \tag{6}$$

where t_s is the time at which the LIDAR measurement is made and $\bar{V}_{0,L}$ is the mean wind speed in the inflow. How the mean wind speed is estimated and the precision of the estimate will greatly influence the estimation of the inflow at rotor. However, the estimation of the mean wind speed is beyond the scope of this study and will be assessed in further studies. In this study it is assumed that $\bar{V}_{0,L}$ is known. Using the measured wind speed, azimuthal position at which the measurement was made and the time at which the measured wind speed will reach the rotor plane, the free inflow velocities at a radial position r, $V^r_{0,L}$, can be estimated at any time and azimuthal position.

For calculating the reference pitch signal, the angles of attack and relative velocities at the rotor plane has to be estimated. Since only the axial inflow velocity is available from the LIDAR measurements, the local inflow can only be estimated if it is assumed that the tangential velocity is only due to the rotational velocity of the rotor. With this assumption and tabulated values of quasi-stationary axial, a, and tangential, a_t induction factors, the angle of attack and relative velocity at a radial position on the blade can be estimated as:

$$\tilde{\alpha} = \arctan\left(\frac{V^r_{0,L}(1-a)}{\omega R(1+a_t)}\right) - \theta_p \quad \text{and} \quad \tilde{V}_r = \sqrt{(V^r_{0,L}(1-a))^2 + (\omega R(1+a_t))^2}, \tag{7}$$

where ω is the rotational speed of the rotor and R is radial position of the blade cross section at which the angle of attack and relative velocity is estimated. For the control design without preview, the angle of attack and relative velocity is estimated from the LIDAR at the present azimuthal position of the blade. Hence, this estimate is equivalent to the perfect local measurement, however, with all the uncertainties induced by a LIDAR.[8]

1. *Preview measurements*

As mentioned in the introduction, the controller will be tested both with and without preview of the inflow. For the local inflow measurements, the previewed reference pitch of blade i is obtain from measurement of angle of attack, relative velocity and pitch angle of the blade rotating ahead of blade i. The preview for the local inflow measurements is illustrated in Figure 3. From Figure 3, it is seen that the reference pitch signal for blade 1 is calculated using measurements from blade 3. Hence, the reference pitch is known ahead in time as a function of azimuthal position. The azimuthal positions k time steps into the future are estimated assuming that the rotor speed, ω, remains constant in the preview period as:

$$\theta^k_{a,i} = \theta^0_{a,i} + \omega \sum_{j=1}^{k} \omega_s^{-1}, \qquad k = 1...N_p, \tag{8}$$

where $\theta^k_{a,i}$ is the preview azimuthal position k time steps into the future of blade i, $\theta^0_{a,i}$ is current azimuthal position of blade i, ω_s is the sampling frequency, and N_p is the number of preview points. The preview reference pitch obtained from local inflow measurements assumes that the flow is stationary in the 120 degree section separating the blade of a three bladed turbine.

From the LIDAR measurements, the previewed reference pitch is calculating by estimating the free inflow velocity at the blades at future time steps from the stored LIDAR measurements, again assuming constant rotational speed of the rotor in the preview period.

Using preview measurements will enable filtering of the inflow measurements without losing phase. Using filtered inflow measurements will ensure that pitch actuation is only applied in a frequency range that is

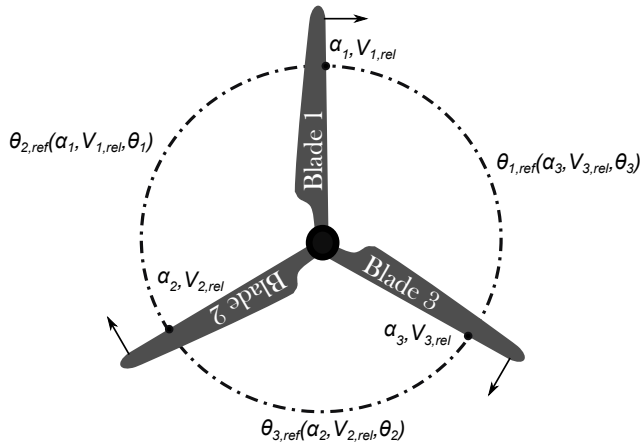

Figure 3. Illustration of the sampling of preview inflow measurements using local measurements. Preview pitch signal for blade i, $\theta_{i,ref}$ is calculated using measurements from the blade leading the rotation.

actually alleviating loads and is not wearing out the pitch system. The cut-off frequency of the filter for the preview measurements is establish after assessing the results of the simulations with the inflow measurement based controller without preview, Section IV.

III. Wind Turbine Model and Simulation Case

In the present study, simulations are performed using the aeroelastic code developed at Risø-DTU, HAWC2.[15] The turbulence is simulated using Cartesian boxes with Mann turbulence.[16] The wind turbine model used for simulations in this study is of a turbine with a hub height of 59 meters, a rated power of 2 MW, and a rated speed of 1.8 rad/s. Simulations are carried out in class A and class C turbulence conditions with a mean wind of 17 m/s and a power law wind shear with a power coefficient of 0.2.

IV. Simulation Results

Simulation results will be presented for situations with and without preview measurements for both class A and class C inflow conditions. First results are presented for the case without preview information, hence pitch actuation is applied in the entire frequency range of the measured and estimated inflow. Then results from simulations with preview measurements are presented. Finally, results are compared in terms of damage equivalent loads.

A. Without Preview

Simulations are performed with the individual pitch controller based on the two types of inflow measurements, using the same turbulence box and collective pitch controller. The duration of the simulations are 600 seconds and in Figure 4 the results of the simulations are summarized. Figure 4 shows a sample of the time series of the pitch signals, power spectral densities of the pitch signals, and the power spectral densities of the non-pitching, out of plan, blade root bending moments. The minimization of the non-pitching bending moment variations is the aim of the controller design. Hence, the performance of the control scheme will be reflected in the spectrum of the non-pitching out of plane bending moment variations. Results are shown for the underlying collective pitch controller as well as for simulations with the individual pitch controller based on either local or upstream measurements added to the collective pitch controller.

From Figure 4, it is seen that the largest peak in the load spectrum of the collective pitch controller is at approximately 0.29 Hz, which corresponds to the rotational frequency of the turbine at rated power (1P). In

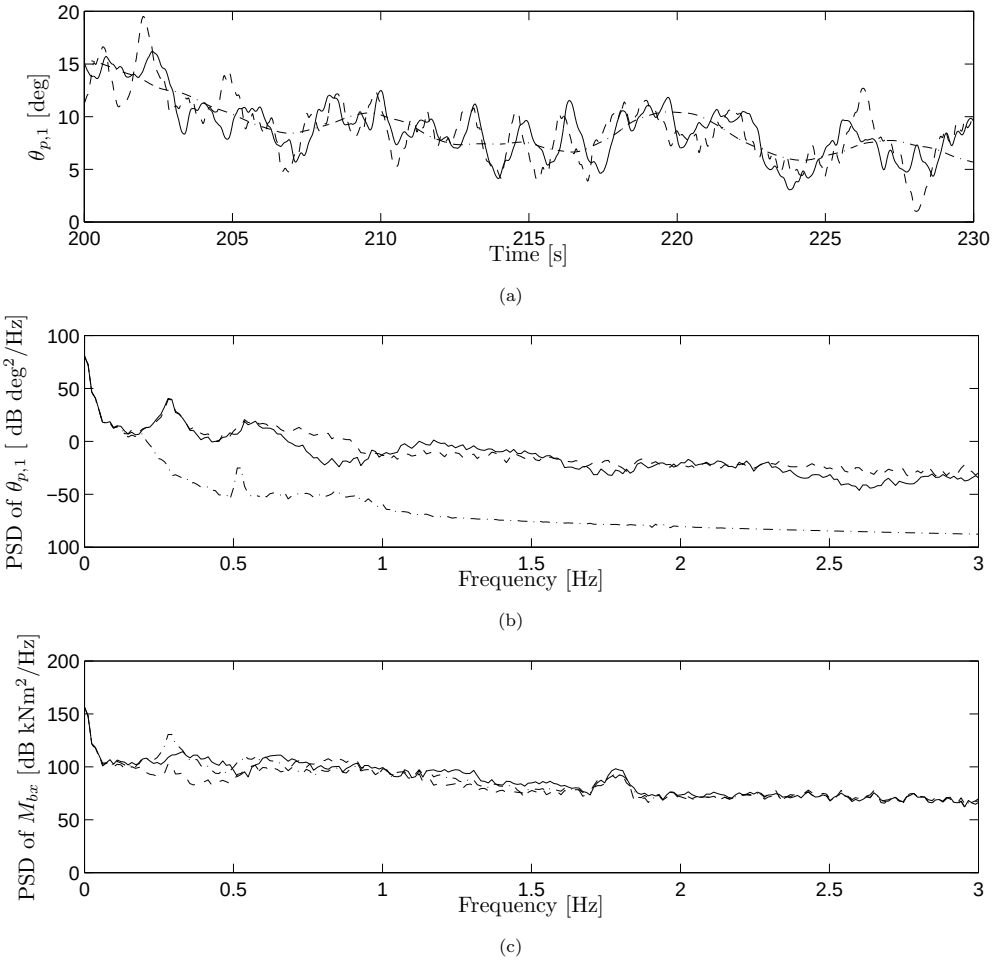

Figure 4. Result of simulations with controllers without preview of inflow at a mean wind speed of 17 m/s and class A wind conditions. a) Sample of the time series of pitch activity b) Power spectral densities of the pitch activity c) Power spectral densities of the non-pitching, out of plan, blade root bending moments, M_{bx}. $-\cdot-$: Collective pitch controller, $---$: Controller based on local measurements, —: Controller based on LIDAR measurements.

Figure 4, it is seen that the 1P spike is removed when the inflow measurement based controllers are applied. However, it is observed that it is only the spectrum in the vicinity of the 1P peak that is reduced. Most of the remaining spectrum is left almost unchanged by the inflow measurement based controller. The largest reduction of the 1P peak is seen when the local inflow measurements are used. The reason that the largest reduction is achieved using the local inflow measurement is probably the fact that the dynamic behavior of the blade is included in the local measurement. Hence, the local inflow measurement will yield a more accurate measurement of the actual inflow a the blade. Inspecting the pitch time series and spectrum it is seen that the pitch spectrum of both the IPC's are very rich and the time series shows very radical pitch actuation. Since only the 1P peak in the load spectrum was lowered by the pitching, it appears that the high frequent pitching is obsolete.

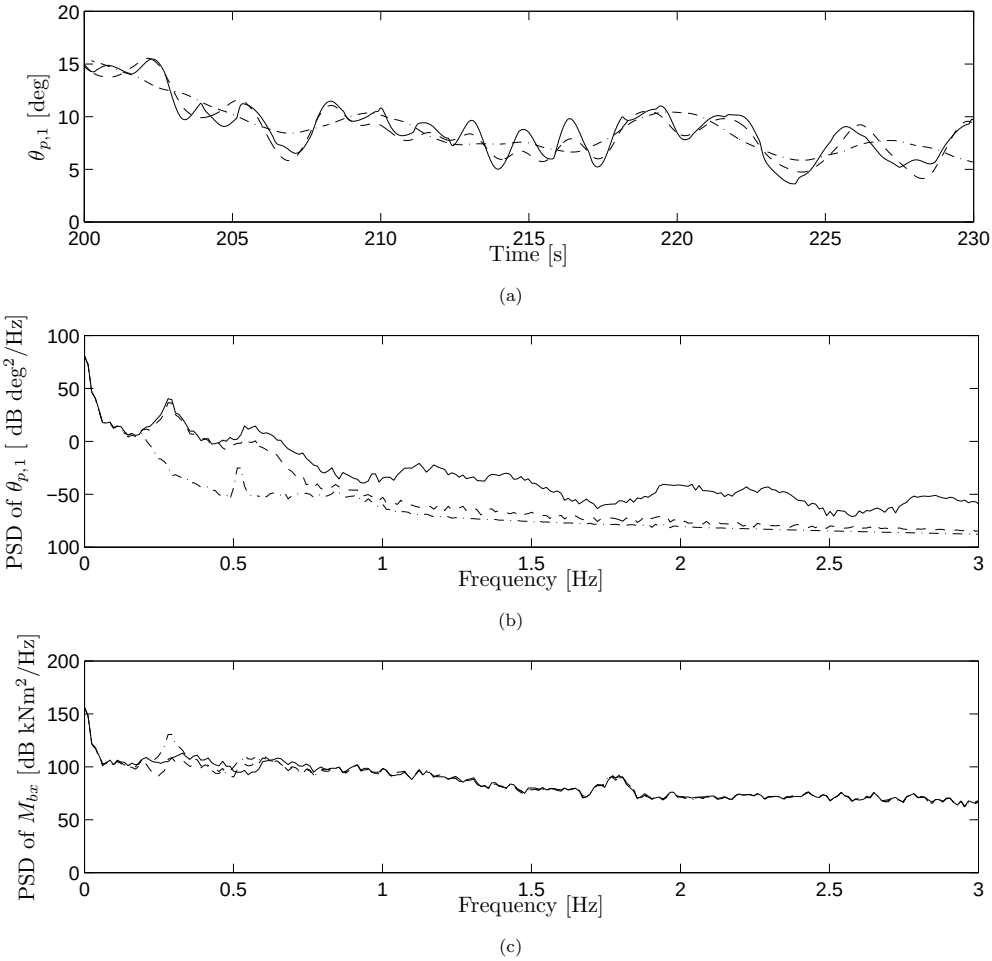

Figure 5. Result of simulations with controllers with preview of inflow at a mean wind speed of 17 m/s and class A wind conditions. a) Sample of the time series of pitch activity b) Power spectral densities of the pitch activity c) Power spectral densities of the non-pitching, out of plan, blade root bending moments, M_{bx}. $-\cdot-$: Collective pitch controller, $- - -$: Controller based on local measurements, —: Controller based on LIDAR measurements.

B. With Preview

From the results above, it was seen that only pitching activity in the frequency range around the 1P frequency change the spectrum of the individual pitch controls compared to the collective pitch control. To avoid excessive pitching, a low pass filter is applied to the preview measurements. Since the filter is only applied to the preview measurements the phase lag introduced by the filter can be compensated for. Both the relative velocity and angle of attack signals are filtered with a low pass filter with a cutoff frequency of 0.5 Hz. The results of the simulations with the filtered preview measurements based on both local and LIDAR measurements are given in Figure 5.

From Figure 5, it is seen that, as for the case without preview, the 1P peak in the spectrum is removed when inflow measurement based IPC is applied. Again it is seen that the largest reduction of the 1P peak is obtained when the local measurements are used. Inspecting the pitch spectrum, it is seen that the

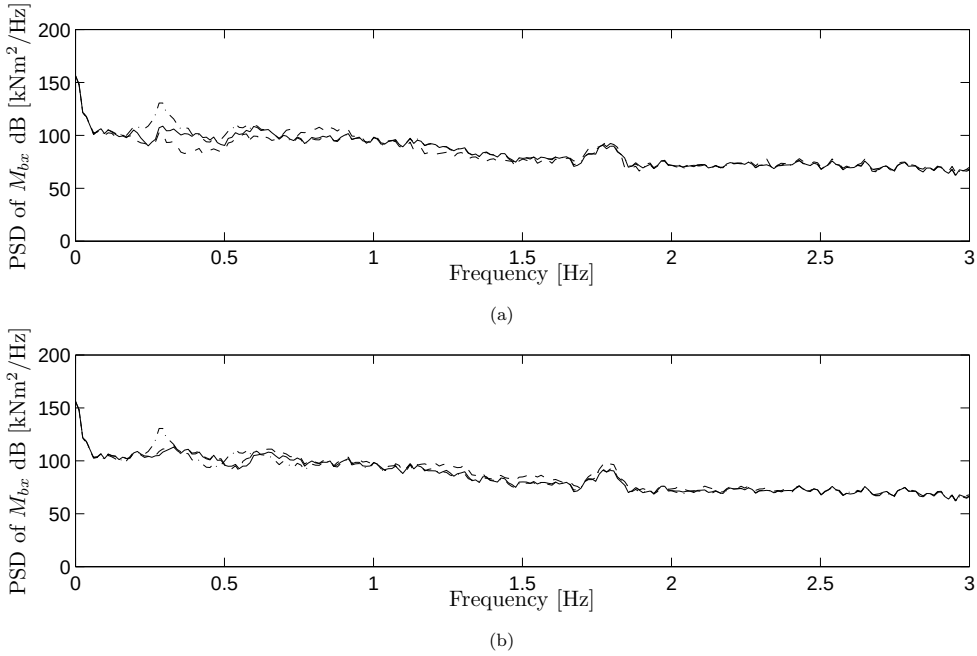

Figure 6. Comparing results from simulation with controllers with and without preview of the inflow at a mean wind speed of 17 m/s and class A wind conditions. a) Controllers based on perfect local inflow measurements, b) Controllers based on spinner LIDAR measurements. – · –: Collective pitch controller, – – –: Controller without preview, —: Controller with preview.

pitch spectrum of the individual pitch controllers are closer to the pitch spectrum of the collective pitch controller compare to the case without preview. Hence, the pitch actuation is less radical when the preview is applied. From the spectrum of the pitching activity it is seen that the spectrum of the case based on local measurements is less rich than the one from the case with spinner LIDAR measurements. The reason for this is the fact that the spinner LIDAR based measurement lacks the tangential component, which is estimated form the rotor speed. The measured rotor speed oscillates because of the torsional flexibility of the shaft. Hence, the tangential velocity estimated from the rotor speed will inherit some of this variation.

In Figure 6 the performance of the controllers with and without preview is compared for both measurement types. It is seen that for the local inflow measurement, the greatest reduction of the 1P peak is observed for the case without preview. However, the large reduction is at the cost of very radical pitching.

For the case with spinner LIDAR measurements, it is seen that controller performance is slightly better when the preview is used in the frequency range above 1P. Hence, it appears that the high frequency contents of the measured inflow upwind of the turbine is not correlating well with the wind speeds actually encounter at the turbine.

From the above results, it appears that the implemented controllers are performing as expected and reduces the blade root bending moments caused by the thrust force variations. To evaluate the value of the controllers, the damage equivalent flap wise bending loads are calculated for all cases and the two inflow classes. The calculated equivalent loads are presented in Figure 7

From Figure 7, it is seen that the largest load reductions are observed when the local, unfiltered measurements are used. When the local unfiltered inflow measurements are used load reductions of 28 and 33 percent compared to the collective pitch controller are achieved for the class A and C inflows, respectively. However, the load reductions are at the cost of very radical pitch actuation. Applying filtering to the local preview measurements decreases the observed fatigue load reductions to 25 and 29 percents. Using the spinner LIDAR measurements, the reductions are 10 and 16 percent for the unfiltered measurements and 17 and 23 percent for the filtered measurements. Hence, it appears that the cost of the assumptions made

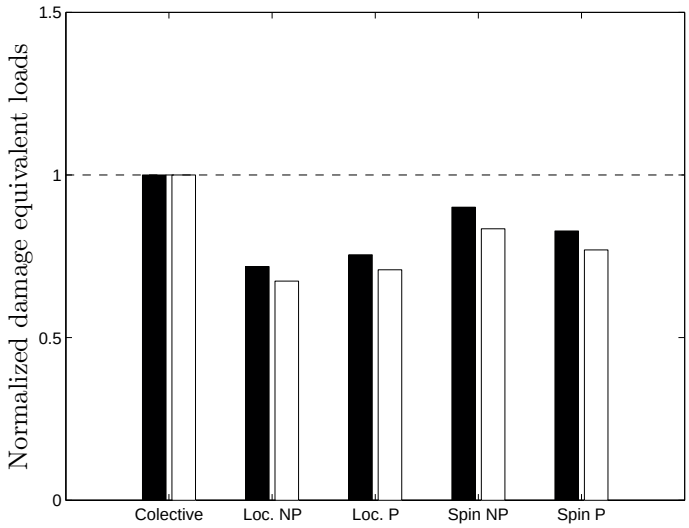

Figure 7. Flap wise damage equivalent blade root loads for all combinations of controllers and measurement type and a mean wind speed of 17 m/s. The loads are normalized with the loads of the collective pitch controller. Black: Class A wind conditions. White: Class C wind conditions. NP: No preview, P: Preview, Loc: local measurements, Spin: Spinner LIDAR measurements.

for enabling usage of the spinner LIDAR measurements in the control scheme is around 10-15 percent. In general it is seen that the largest load reductions are observed in the cases with class C inflow applied, hence, with lowest level of turbulence. The reason the loads are mostly reduced in class C inflow might be that the controller mainly alleviates the 1P variations which are due to deterministic effects such as the wind shear. The deterministic effects are more dominating at low levels of turbulence. Thus, the effect of the wind shear on the fatigue will be largest at low levels of turbulence. Hence, the potential load reductions of alleviating the shear induced load is largest at low levels of turbulence.

From the above results, it appears that the local measurements has the largest potential in terms of load reductions. However, it is important to notice that the above results represent an upper limit on load reductions achievable with the current control design because the results are based on perfect local measurements. Real local measurements of angle of attach and relative velocity will have distortions. Furthermore, the LIDAR measurements has the potential advantage of being able to preview incoming gust better than the local inflow measurements. This potential advantage is not assessed in this study.

In the simulated cases, the inflow measurement based controllers were seen to perform well. Inspecting the range of angle attack measured during the simulations, it is seen that the blade is generally operating at angles of attack where the blade is not expected to stall. Hence, in a range were the thrust coefficients behaves fairly linear, and the thrust coefficients can be increased by pitching. It is expected that the controller performance will decrease in situations where stall will limit the achievable thrust coefficients. Such situations might occur when the turbine is operating partially in the wake of a nearby turbine. In a partial wake operation, radical changes in inflow are encountered by the blades and stall might occur.

V. Conclusions and Future Work

In this study, an inflow measurement based control scheme for individual pitch control was introduced. The control scheme was tested in standard conditions with and without preview of the inflow wind speed, and with two different types of inflow measurements. The two measurement types were: perfect local inflow measurements and spinner LIDAR measurements. Results showed that all combinations of control design and measurement type yielded reductions of the 1P peak in the load spectrum. The largest reduction of the 1P peak was observed for the controller based on local unfiltered measurements. However, using the unfiltered

measurements yielded radical pitch actuation. Using the filtered preview measurements, the pitch actuations was smoothened, at the cost of slightly higher loads. Using the unfiltered local inflow measurements, load reductions of 28 and 33 percent compared to the collective pitch controller were achieved for the class A and C inflows, respectively. Applying filtering to the local preview measurements decreases the observed fatigue load reductions to 25 and 29 percents for the two inflow classes. Using the spinner LIDAR measurements, the reductions were 10 and 16 percent for the unfiltered measurements and 17 and 23 percent for the filtered measurements.

Future work will be aimed at extending the control scheme to take into account dynamic inflow and blade dynamics. Furthermore, the control scheme will be tested in complex inflow containing extreme operating gusts and wakes.

References

[1]Bossanyi, E. A., "Individual Blade Pitch Control for Load Reduction," *Journal of Wind Energy*, Vol. 6, 2003, pp. 119–128.

[2]Bossanyi, E. A., "Further load reductions with individual pitch control," *Journal of Wind Energy*, Vol. 8, 2005, pp. 481–485.

[3]Bossanyi, E. and Witcher, D., "Controller for 5MW reference turbine - Upwind report," Tech. rep., Garrad Hassan and Partners Ltd., 2009.

[4]Kanev, S. and van Engelen, T., "Wind turbine extreme gust control," *Wind Energy*, Vol. 13, No. 1, 2010, pp. 18–35.

[5]Laks, J., Pao, L. Y., Simley, E., Wright, A. D., Kelley, N., and Jonkman, B., "Model Predictive Control Using Preview Measurements From LIDAR," *49th AIAA Aerospace Sciences Meeting including the New Horizons Forum and Aerospace Exposition*, 2011.

[6]Dunne, F., Pao, L. Y., Wright, A. D., Jonkmann, B., Kelley, N., and Simley, E., "Adding Feedforward Blade Pitch Control for Load Mitigation in Wind Turbines: Non-Causal Series Expansion, Preview Control, and Optimized FIR Filter Methods," *49th AIAA Aerospace Sciences Meeting including the New Horizons Forum and Aerospace Exposition*, 2011.

[7]Barlas, T. and van Kuik, G., "Review of state of the art in smart rotor control research for wind turbines," *Progress in Aerospace Sciences*, Vol. 46, No. 1, 2010, pp. 1–27.

[8]Kragh, K. A., Hansen, M. H., and Mikkelsen, T., "Precision and Shortcomings of Yaw Error Estimation Using Spinner Based LIDAR," *Wind Energy (Accepted)*, Vol. ??, 2011, pp. ??

[9]Larsen, T., Madsen, H., and Thomsen, K., "Active load reduction using individual pitch, based on local blade flow measurements," *Journal of Wind Energy*, Vol. 8, 2005, pp. 67–80.

[10]Hansen, M. O. L., *Aerodynamics of Wind Turbines*, James & James, 2000.

[11]Madsen, H. A. and Fischer, A., "Wind shear and turbulence characteristics from inflow measurements on the rotating blade of a wind turbine rotor," *Procedings of EWEC2009*, 2009.

[12]Mikkelsen, T., Hansen, K., Angelou, N., and Sjöholm, M., "LIDAR measurements from a rotating spinner," *Proceedings of EWEC2010*, EWEC, 2010.

[13]Kragh, K. A., Hansen, M. H., and Mikkelsen, T., "Improving Yaw Alignment Using Spinner Based LIDAR," *Proceedings of the 49th AIAA Aerospace Sciences Meeting Including the New Horizons Forum and Aerospace Exposition. American Institute of Aeronautics and Astronautics*, AIAA, 2011.

[14]Simley, E., Pao, L., Frehlich, R., Jonkman, B., and Kelley, N., "Analysis of Wind Speed Measurements using Continuous Wave LIDAR for Wind Turbine Control," 2011.

[15]Larsen, T. J., "How 2 HAWC2, the user's manual," Risø-r-1597(ver. 3-9)(en), Risø-DTU, Sept. 2009.

[16]Mann, J., "Wind field simulation," *Probabilistic Engineering Mechanics*, Vol. 13, No. 4, 1998, pp. 269 – 282.

Appendix G

On the Potential of Pitch Control for Increased Power Capture and Load Alleviation

On the Potential of Pitch Control for Increased Power Capture and Load Alleviation

Knud A. Kragh, Lars C. Henriksen and Morten H. Hansen

Department of Wind Energy, Technical University of Denmark, Frederiksborgvej 399, 4000 Roskilde, Denmark

E-mail: knkr@dtu.dk

Abstract. Wind turbine control is a research area that is gaining increasing interest, and numerous simple and advanced control schemes have been suggested, especially for load alleviation. The performance of such controllers is often compared to the performance of simpler controllers, thus relative to a moving reference. This study is focused on estimating the upper limits of the power increase and load variation alleviation that are achievable through pitch actuation. Knowing these upper limits, the potential of improving existing controllers can be assessed. The achievable power output increase and load variation reduction are estimated through numerical optimization of the pitch and generator torque actuation. Results show that the potential of increased power output at below rated wind speeds through optimized pitch actuation is greatest for inflows that varies with the azimuthal position of the blades. It is shown that at above rated wind speeds, the potential of decreasing the wind shear induced load variations beyond what is possible with a simple cyclic pitch scheme is limited. The results presented in this study are all obtained from simulations with deterministic inflow because the absolute upper limits are sought, and turbulent inflow is assumed to decrease these limits.

1. Introduction

As wind turbines are becoming increasingly larger, the varying loads on the blades due to wind shear, wakes, turbulence etc. are becoming increasingly significant. To accommodate increasingly longer and lighter blades, load alleviation have been applied based on advanced sensors and actuators. Load alleviation can be achieved using for example blade pitch or flap actuation in combination with different types of sensory systems. In this study, the focus is on pitch actuation. Modern, industry standard, load alleviation control schemes include cyclic blade pitching based on blade root bending moment measurements. The performance of cyclic pitch control schemes is well described in the literature, e.g. [1, 2, 3]. Recent developments of advanced measurement systems such as Light Detection and Ranging (LiDAR) systems [4, 5] have lead to the development of control systems that are capable of exploiting preview measurements of the inflow. The performance of preview enabled control systems is indicated in several studies [5, 6, 7, 3, 8]. However, the theoretical potentials of increased power capture and load alleviation by pitching, in general, have not been studied. Because pitching involves turning the entire blade at once, it is expected that not all load variations can be alleviated. Knowing the upper levels of the achievable benefits by pitching will enable an assessment of the value of applying any additional sensors or complex pitch control schemes. For example, if it is found that the upper limits of what is achievable with optimal pitch control are only a few percent above what is

already achieved using industry standard pitch controllers, then the benefits of adding any additional sensors to accommodate more advanced pitch control can only be these few percent.

The objective of this study is to investigate the upper levels of increased power output and load alleviation that are achievable using pitch actuation in deterministic inflow. For below rated wind speeds, the focus is on increasing the power capture, whereas the focus is on load alleviation at above rated wind speeds. The potentials of increased power output and load alleviation are investigated through numerical maximization and minimization of the power output and the loads, respectively, of a reference turbine. The potentials of increased power output and load alleviation are expected to be highly dependent on the inflow conditions. Thus, the maximization and minimization is performed with different types of inflow that contains both temporal variations of the mean inflow speed and azimuth angle dependent inflow variations as in a vertical wind shear. The following inflow types are tested for the power maximization at below rated wind speed: the extreme asymmetric inflow of a half-wake, and the symmetric inflow situation of a square-wave varying mean wind speed. For load minimization at above rated wind speed, the following types of inflows are tested: standard power law vertical wind shear, and the square-wave varying mean wind speed.

All simulations are performed using the aero-servo-elastic simulation tool HAWC2 and a model of the NREL 5MW reference turbine in deterministic inflow. For all optimization cases, except one, a stiff version of the reference turbine is simulated. The stiff turbine is chosen in this initial study because flexibility is assumed to add a complexity to the formulated optimization problem which will lower the achievable upper limits. Further studies will be focused on how the results change when the model complexity is increased by introducing the flexibility of the turbine.

2. Optimization Procedure

The maximization of the power output and the minimization of the loads are performed by solving an optimization problem. The optimization problem differs depending on the inflow type and the objective of the optimization. The two inflow types that are investigated in this study are: temporal variations of the mean wind speed, and azimuth angle dependent inflow. The objectives are: maximization of the power output at below rated wind speed, and minimization of the load variations at above rated wind speeds. The control inputs that are used to fulfill the optimization objectives are: prescribed time variations of collective pitch angle and generator torque for the inflow case of varying mean wind speed, and prescribed azimuthal variation of individual blade pitch angles allowing cyclic pitch variations and prescribed variation of generator torque for the azimuth angle dependent inflow. Because the optimization variables are discrete pitch or generator torque values, the actual control signals applied in the simulation are interpolations of the discrete optimization variables.

The inflow, in the cases of temporal mean wind speed variations, is a number of unit-steps of the wind speed. The time between the steps is adjusted such that the turbine reaches a steady state between the steps, i.e. the wind speed steeps constitutes a number of square-waves. For each square-wave, the same control inputs are applied. Thus, the control inputs are periodic signals with a period corresponding to the length of the square-waves. The resulting power or load variations are averaged for all square-waves to ensure that a periodic solution is obtained.

In the case of the azimuth angle dependent inflow, the inflow to the turbine is either a standard wind shear or a half-wake. A schematic that illustrates the optimizations and the inflow types is given in Figure 1. The optimizations are performed iteratively in MATLAB, letting MATLAB start and post-process the HAWC2 simulations. The actual optimization is performed using an interior point method for the *fmincon* MATLAB routine.

The cost function indicated in Figure 1 differs depending on the inflow type and the objective of the optimization. In the following, the optimization problem is described for each of the

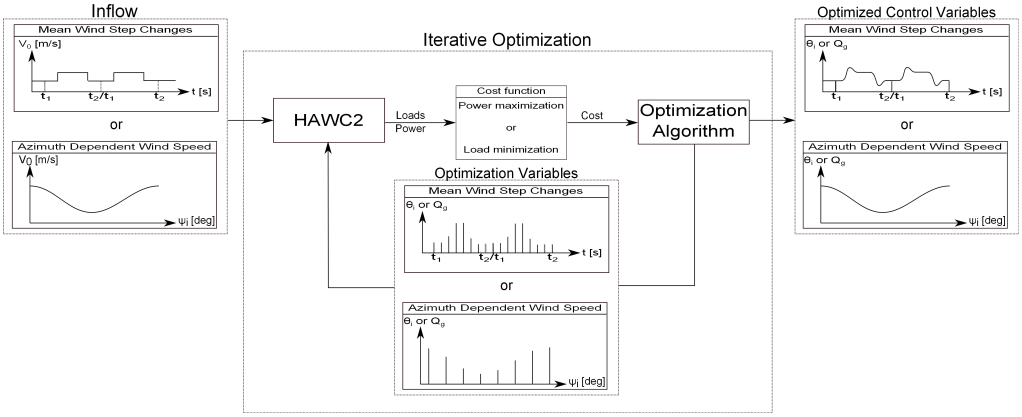

Figure 1. Illustration of the optimization procedure.

optimization cases presented in this study.

2.1. Power Maximization at Below Rated Wind Speed for a Half-Wake Inflow
A standard, partial load control law is implemented for regulating the generator torque. The control law is defined as:

$$Q_g = k\Omega^2, \tag{1}$$

where Ω is the rotor speed and k is a constant. Usually, k is estimated from the aerodynamic characteristics and dimensions of the wind turbine. However, in this study, k is one of the optimization variables. The remaining optimization variables are: two reference pitch values and the azimuthal position of the two reference pitch values (the phase). The pitch values applied in the simulations at the intermediate azimuth angles are obtained by interpolation between the two reference pitch values using a cubic spline. The optimization problem is given as:

$$\max_{\mathbf{u}} \frac{1}{2\pi} \int_{-\pi}^{\pi} P(\psi_i) \frac{\bar{\Omega}}{\Omega(\psi_i)} d\psi_i \tag{2}$$

where $\mathbf{u} = (\theta(\psi_1), \theta(\psi_2), k)$ are the optimization variables, $\theta(\psi_i)$ is the pitch angle at the azimuth angle ψ_i, $P(\psi_i)$ is the obtained azimuth angle dependent power output, $\bar{\Omega}$ is the average steady state rotor speed and $\Omega(\psi_i)$ is the azimuth angle dependent rotor speed. Thus, the potential load increases are neglected.

2.2. Power Maximization at Below Rated Wind Speed for a Square-Wave Inflow
Two types of optimizations are performed for the case of step changes of the mean wind speed; one where optimized constant pitch and k values for the partial load controller are found, and one where optimal periodic collective pitch and generator torque signals prescribed by two linear interpolations each described by 20 points are sought. The optimization problem is given as:

$$\max_{\mathbf{u}} \frac{1}{T} \int_{t}^{t+T} P(t) dt \tag{3}$$

where $\mathbf{u} = (\theta, k)$ and $\mathbf{u} = (\theta(t_i), Q_g(t_i)), i = 1...20$ for the two optimization cases (Q_g is the applied generator torque), t_i is time of the i'th input sample.

2.3. Load Minimization at Above Rated Wind Speed for a Standard Wind Shear
In contrast to the optimizations presented above, the optimizations at above rated wind speed are only focused on pitch angles because the generator torque is kept constant for above rated operation. The applied inflow is an IEC standard power law wind shear. The optimization variables are a number of azimuthally distributed pitch angles that are added to a collective pitch signal, and the azimuth positions of the added individual pitch changes. The collective pitch signal ensures that the rotor speed is kept at the rated value using a standard PI speed controller. The optimization is aimed at minimizing the standard deviation of the blade root, out-of-plane bending moment, and the optimization problem is given as:

$$\min_{\mathbf{u}} \sqrt{\frac{1}{TF_s - 1} \sum_{i=1}^{TF_s} (M_{bx,i} - \bar{M}_{bx})^2} \tag{4}$$

where $\mathbf{u} = \theta(\psi_i), i = 1...n$, $\theta(\psi_i)$ is a vector containing the discrete pitch angles for the n azimuthally distributed optimization point, ψ_i is the azimuth angle of the i'th optimization point, T is the steady state simulation time, F_s is the sampling frequency, $M_{bx,i}$ is the blade root out-of-plane bending moment at time step i of one of the blades, and $\bar{M}_{bx}$ is the mean steady state blade root out-of-plane bending moment.

2.4. Load Minimization at Above Rated Wind Speed for a Square-Wave Inflow
A square-wave mean inflow is applied and optimization of collective pitch angles is carried out for minimizing the load variations. The optimization problem for the load minimization is defined as:

$$\min_{\mathbf{u}} \frac{1}{T} \int_t^{t+T} |P(t) - P_r| + |\tilde{M}_{bx}| dt \tag{5}$$

where P_r is the rated power of the turbine, $\tilde{M}_{bx}$ is the high-pass filtered blade root out-of-plane bending moment signal, and $\mathbf{u} = \theta(t_i), i = 1...20$ is the vector containing the optimization variables, which are 20 periodic pitch angles that are repeated for each square-wave. The actual pitch angles applied in the simulations are linear interpolations between the 20 optimization points. Thus, both power and blade load variations are penalized. It is necessary to penalized the power output because deviations from the rated value caused by sudden collective pitch angle changes are unwanted. Static changes of the blade root bending moment cannot be avoided when the wind speed changes and the power is to be kept constant. Using the high-pass filtered blade root out-of-plane bending moment signal, variations, e.g. extreme loads, are penalized without affecting the static change. Hereby, the load variation minimization does not interfere with the objective to keep the power at rated.

3. Results of Power Maximization at Below Rated Wind Speed

In this section, the optimal power outputs at below rated wind speed are presented based on simulations of a stiff version of the reference turbine. First, the results for the half-wake inflow situation, then the results for a inflow with step changes of the mean wind speed are presented.

3.1. Half-Wake Inflow
The inflow to the turbine is shown in the top-plot of Figure 2. This inflow represents an extreme situation where the wind speed is significantly higher in one half of the rotor plane than in the other. The applied inflow is an idealization of what is expected for a turbine in a wind farm. In a real wind farm, the wake would meander and not remain constant in one half-plane [9]. The results of the power maximization are presented in Figure 2 that shows the results of two types

of optimizations regarding the pitch angles; one where a constant pitch angle and one where the optimal individual pitch variations defined from two pitch angles and phase angles are found. In both optimizations, the constant k is also found. The two optimization cases reflect an optimized collective pitch and an optimized 1P individual pitch controller. In Figure 2, it is seen that by applying the optimized cyclic pitch signal, the power output is raised compared to when only k and the collective pitch angle is optimized. With the optimized cyclic pitch signal, the power integrated over one period is raised approximately 3.6%. However, the increased power output is penalized by increased load variations. Especially, the blade root load variations are increased.

3.2. Square-Wave Inflow

The time series of the applied inflow is shown in the top-plot of Figure 3. The square wave represents a very extreme situation that is not seen in real operating conditions. This type of inflow is chosen because it represents a very severe challenge for a turbine control system and the results represent a first attempt of estimating the maximum potential of applying power maximization using collective pitch control. Such a control scheme could for example be based on preview of the inflow provided by a LiDAR. The results of the optimization are presented in

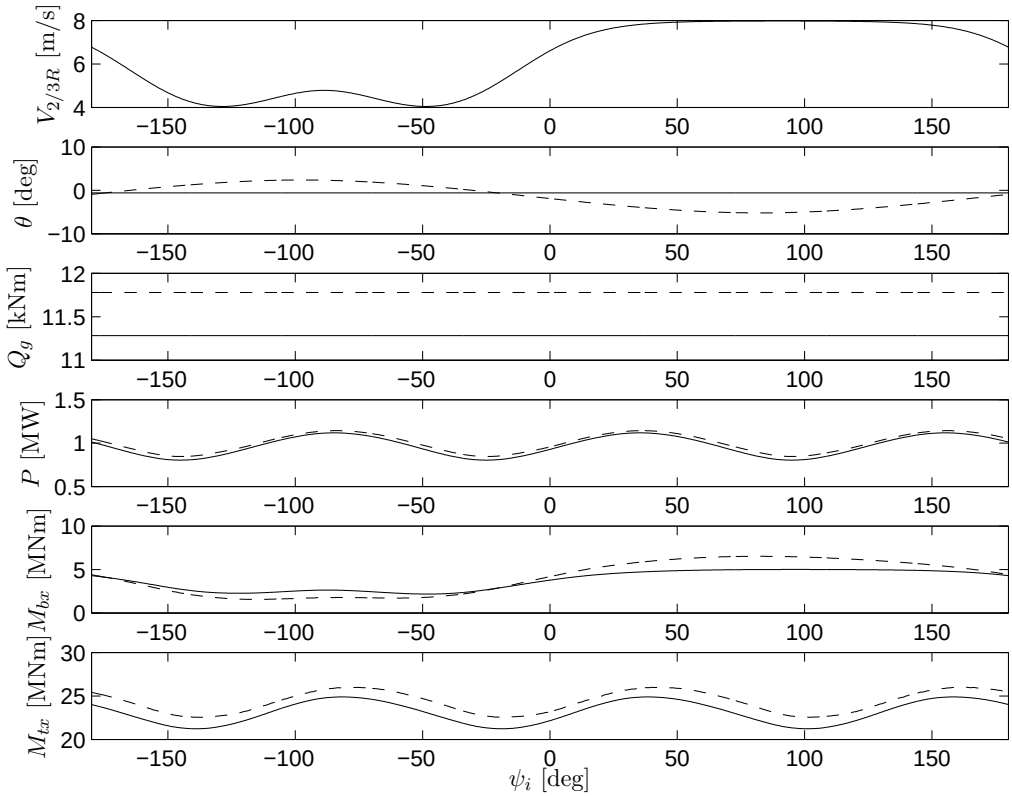

Figure 2. Results of the power maximization at below rated wind speeds in half-wake operation. Optimized constant pitch and k (—), optimized k and pitch values for cyclic pitch (− − −). From the top and down: Free wind speed at the two-thirds radius of the rotor, pitch angle, generator torque, power output, blade root out-of-plane bending moment and tower bottom fore-aft bending moment.

Figure 3. For the case with optimized pitch and generator torque, the actuations are applied slightly before the wind speed change occurs. However, it is seen that the actuations have very limited effect on the power output, and the observed increase in integrated power output is negligible (0.04%).

4. Results of Load Minimization at Above Rated Wind Speed

In this section, the focus is on minimizing the loads for above rated operation. First, results are presented for a standard vertical wind shear and optimization of azimuth angle dependent pitch values. Then, results are presented for a inflow containing step-changes of the mean wind speed and temporal optimization of periodic pitch angles. For the standard vertical wind shear, results are presented for both a stiff and a flexible version of the reference turbine. For the inflow with step-changes of the mean wind speed, results are only presented for a stiff turbine because optimization studies of the flexible turbine are ongoing.

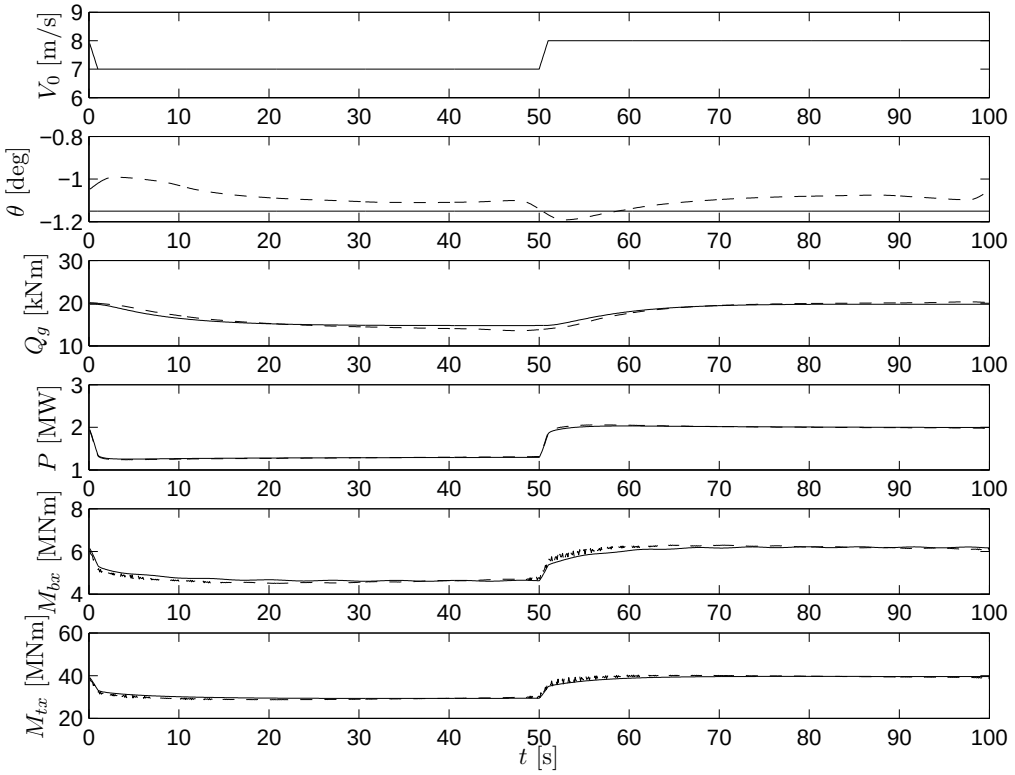

Figure 3. Results of the power maximization at below rated wind speeds and step changes of the collective wind speed. Optimized constant pitch and k (—), optimized periodic pitch and generator torque actuations (– – –). From the top and down: Free wind speed, pitch angle, generator torque, power output, blade root out-of-plane bending moment and tower bottom fore-aft bending moment.

4.1. Standard Vertical Wind Shear

Figure 4 and 5 shows the results of the blade load minimization of a stiff version of the reference turbine. Figure 4 shows the results of the optimization normalized with results obtained with a standard collective pitch controller. For comparison, the figure also shows results obtained with a simple cyclic pitch controller [1]. Figure 5 shows the optimized azimuth angle dependent pitch signals. For all the optimizations, the power output is unaffected. The blade load variations for a resolution of two azimuthal optimization points are similar to those of the simple cyclic pitch controller; as expected because the two pitch optimization points only allows for a 1P varying pitch signal. With additional optimization points, the optimized pitch signal tries to alleviate the loads caused by the tower shadow and the load variations decrease slightly. Inspecting the tower bottom load variations, it is seen that these are smallest when four optimization points are applied, thus, it appears that applying a very complex pitch signal is not beneficial.

In Figure 6 and 7, the results of the load minimization with a flexible version of the reference turbine are shown. As for the stiff turbine, similar load variations are experienced for the simple cyclic pitch controller and the two point optimization, and the blade load variations are decreased slightly more when a more complex pitch signal is applied. In contrast to the stiff turbine, for the flexible turbine, the tower bottom load variations are significantly decreased when a complex pitch signal is applied.

4.2. Square Wave Inflow

The results of the optimization are summarized in Figure 8. It is seen that with the optimized signal applied, the pitch actuation is initiated prior to the wind speed change. Hereby, both the

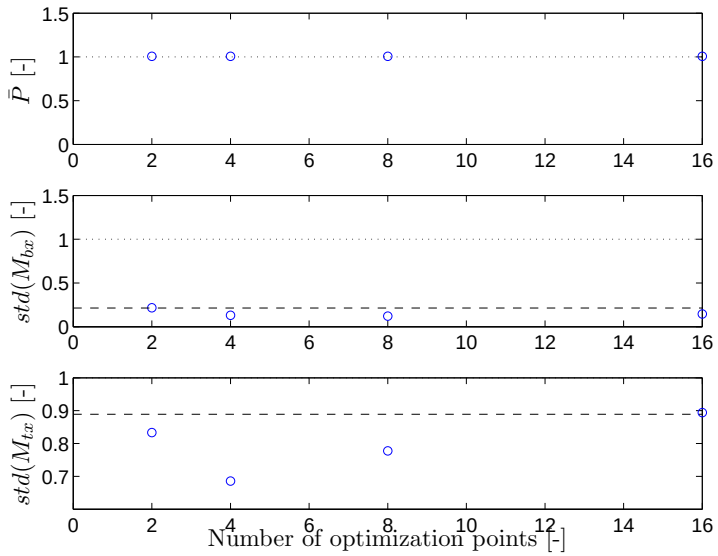

Figure 4. Results of the load variation minimization at above rated wind speed (15 m/s and power law vertical wind shear) for the stiff turbine. From the top and down, mean steady state power output, steady state standard deviation of the blade root out-of-plane bending moment, and steady state standard deviation of the tower bottom fore-aft bending moment. All results have been normalized with the results of a simulation with a standard collective pitch controller applied. Results obtained with a simple cyclic pitch controller are shown for comparison (– – –).

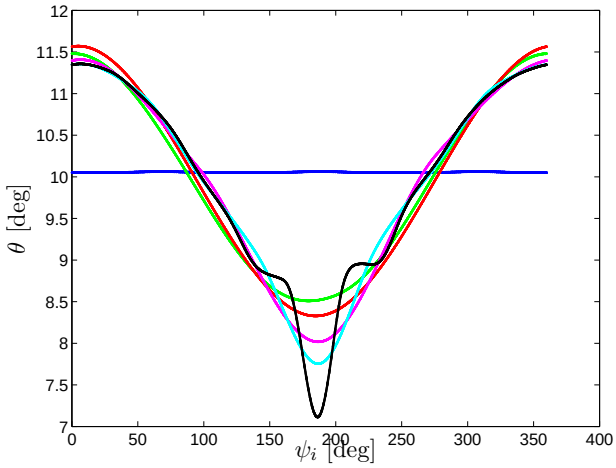

Figure 5. The applied steady state pitch signals for the stiff turbine. Blue: collective pitch control, green: simple cyclic pitch control, red: 2 optimized pitch angles, magenta: 4 optimized pitch angles, cyan: 8 optimized pitch angles, and black: 16 optimized pitch angles.

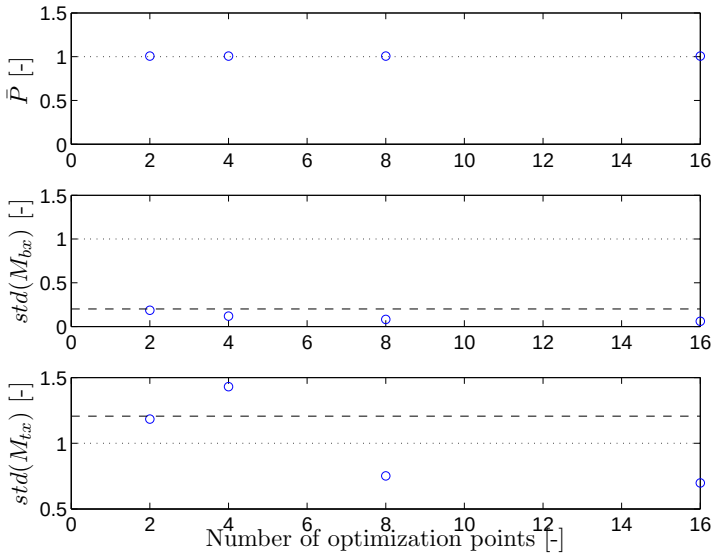

Figure 6. Results of the load variation minimization at above rated wind speed (15 m/s and power law vertical wind shear) for the flexible turbine. From the top and down, mean steady state power output, steady state standard deviation of the blade root out-of-plane bending moment, and steady state standard deviation of the tower bottom fore-aft bending moment. All results have been normalized with the results of a simulation with a standard collective pitch controller applied. Results obtained with a simple cyclic pitch controller are shown for comparison (– – –).

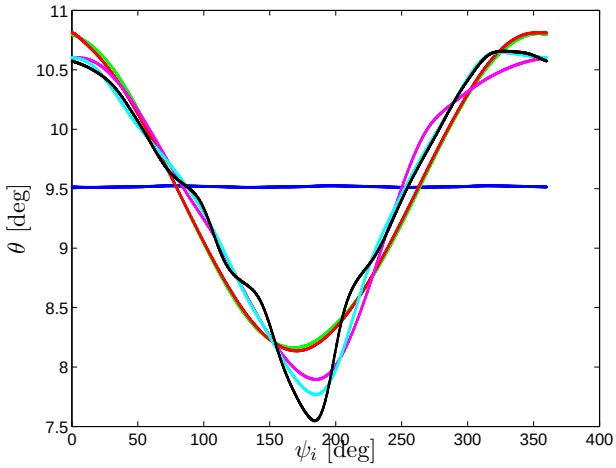

Figure 7. The applied steady state pitch signals for the flexible turbine. Blue: collective pitch control, green: simple cyclic pitch control, red: 2 optimized pitch increments, magenta: 4 optimized pitch increments, cyan: 8 optimized pitch increments, and black: 16 optimized pitch increments.

power and load variations are decreased compared to the results with the standard collective pitch controller. Furthermore, it is observed that even with the optimized pitch signal applied, some discontinuous load and power changes are observed in the results. These discontinuities are expected because the wind speed changes are discontinuous, and the applied pitch signal is continuous.

5. Conclusions and Further Work

In this study, an approach was presented for estimating the upper limits of power maximization and load variation minimization using pitch actuation. It was shown that, for below rated operation, the greatest potential of increased power output by pitch actuation is for situations with azimuth angle dependent inflow. For the tested half-wake situation, an averaged power output increase of approximately 3.5% was observed compare to an optimized collective pitch controller. For above rated operation, it was shown that the majority of the wind shear induced load variations can be alleviated using a simple 1P pitch signal, and only limited additional blade load alleviation was observed when a more complex pitch signal is applied. For stepwise mean wind speed changes it was shown that pitch actuation prior to an extreme event can significantly decrease the load and power variations. In summary, the study indicates that there is a potential for power maximization at below rated wind speed, and that preview measurements would allow significant alleviation of extreme loads. However, the potential of decreasing the wind shear induced blade load variations more than what is possible with a simple cyclic pitch controller is limited. Further work should be aimed at increasing the complexity of the turbine and performing optimizations for cases that more resembles a real turbine operating in common inflow.

References

[1] E. A. Bossanyi. Individual blade pitch control for load reduction. *Journal of Wind Energy*, 6:119–128, 2003.
[2] E. A. Bossanyi. Further load reductions with individual pitch control. *Journal of Wind Energy*, 8:481–485, 2005.

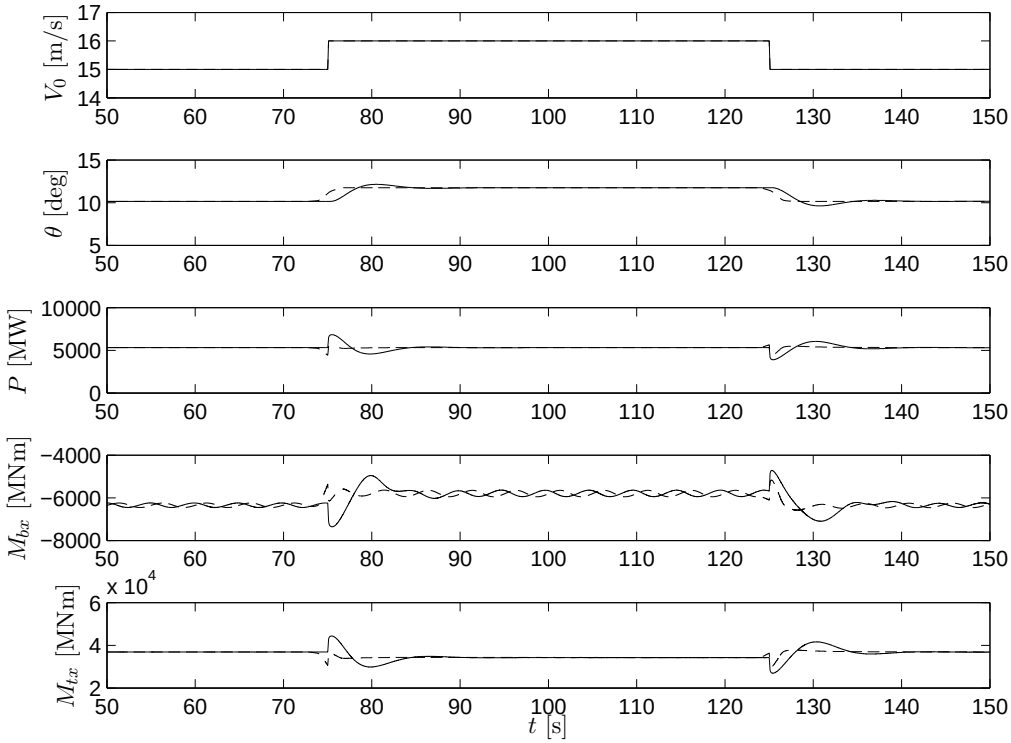

Figure 8. Results of the load variation minimization at above rated wind speeds and step changes of the mean wind speed. Standard collective pitch control (—), optimized periodic pitch values (– – –). From the top and down: Free wind speed, pitch angle, power output, blade root out-of-plane bending moment and tower bottom fore-aft bending moment.

[3] E. Bossanyi, B. Savini, M. Iribas, M. Hau, B. Fischer, D. Schlipf, T. van Engelen, M. Rossetti, and C. E. Carcangiu. Advanced controller research for multi-mw wind turbines in the upwind project. *Wind E*, 15:119145, 2012.

[4] T. Mikkelsen, K. Hansen, N. Angelou, M. Sjöholm, M. Harris, P. Hadley, R Scullion, G. Ellis, and G. Vives. Lidar measurements from a rotating spinner. In *Proceedings of EWEC2010*. EWEC, 2010.

[5] D Schlipf, S Kapp, J Anger, O Bischoff, M Hofsa, A Rettenmeier, and Martin Kuehn. Prospects of optimization of energy production by lidar assisted control of wind turbines. In *Proceedings of EWEA2011*, 2011.

[6] F Dunne, L Y Pao, A D Wright, B Jonkman, and N Kelley. Adding feed forward blade pitch control to standard feedback controllers for load mitigation in wind turbines. *Mechatronics*, 21(4):682–690, 2011.

[7] J Laks, L Pao, A Wright, N Kelley, and B Jonkman. The use of preview wind measurements for blade pitch control. *Mechatronics*, 21(4):668–681, 2011.

[8] D Schlipf, S Schuler, P Grau, F Allgower, and M Kuehn. Look-ahead cyclic pitch control using lidar. In *Proceedings of The Science of Making Torque from Wind 2010*, 2010.

[9] Gunner C. Larsen, Helge Aa. Madsen, Ferhat Bingl, Jakob Mann, Sren Ott, Jens N. Srensen, Valery Okulov, Niels Troldborg, Morten Nielsen, Kenneth Thomsen, Torben J. Larsen, , and Robert Mikkelsen. Dynamic wake meandering modeling. Technical Report Ris-R-1607(EN), Ris, 2007.

Technical University of Denmark
DTU Vindenergi

info@vindenergi.dtu.dk
www.vindenergi.dtu.dk